U.PORTO
FEUP FACULDADE DE ENGENHARIA
UNIVERSIDADE DO PORTO

INSTITUTO DE CIÊNCIAS BIOMÉDICAS ABEL SALAZAR
UNIVERSIDADE DO PORTO

# Antimicrobial Biomaterials for use as Dialysis Catheters

Inês Silva Borges

Integrated Master in Bioengineering

Branch of Molecular Biotechnology

Supervisor: Dr Inês Gonçalves (i3S)
Co-supervisor: Dr Fernão Magalhães (LEPABE-FEUP)

September 2016

**The work described in this thesis was conducted at:**

I3S/INEB - Instituto de Investigação e Inovação em Saúde; Universidade do Porto

LEPABE/FEUP - Laboratório de Engenharia de Processos, Ambiente, Biotecnologia e Energia; Universidade do Porto

**The work described in this thesis was financially supported by:**

Project POCI-01-0145-FEDER-007274 (Institute for Research and Innovation in Health Sciences); Project POCI-01-0145-FEDER-006939 - Laboratory for Process Engineering, Environment, Biotechnology and Energy – LEPABE and NORTE-01-0145-FEDER-000005 – LEPABE-2-ECO-INNOVATION, funded by FEDER funds through COMPETE2020 - Programa Operacional Competitividade e Internacionalização (POCI) and Programa Operacional Regional do Norte (NORTE2020), and by national funds through FCT - Fundação para a Ciência e a Tecnologia; and Project PTDC/CTM-Bio/4033/2014 (NewCat - New biomaterials to prevent infection associated with dialysis catheters), funded by FEDER funds through COMPETE2020 - Programa Operacional Competitividade e Internacionalização (POCI) – and by national funds through FCT - Fundação para a Ciência e a Tecnologia.

*Se podes olhar, vê.*
*Se podes ver, repara.*

José Saramago

# Acknowledgments

Acabam assim 5 anos de muitas aventuras, muitas aprendizagens, muitas descobertas, muitos encontros e desencontros. Enfim, um período cheio de muitos, de demasiados e de q.bs. Um período muito rico. Rico essencialmente de pessoas. E é a essas pessoas que tenho que agradecer. Obrigada principalmente aos "amores que ficam para a vida", sem vocês isto não tinha piada nenhuma. São essencialmente vocês que ficam, e ficam para sempre.

Tenho que agradecer aos meus orientadores, Dr Inês Gonçalves e Dr Fernão Magalhães, a quem devo este trabalho e todo o apoio e disponibilidade demonstrados. Obrigada pela oportunidade. Em especial à minha orientadora, à fantástica Inês Gonçalves. Se eu já a admirava antes, esse sentimento só se multiplicou nestes últimos meses.

Um grande obrigado ao Artur Pinto que me ensinou tudo. À Patrícia Henriques, à Diana Paiva que contribuíram diretamente e me ajudaram imenso.

Aos meninos do E-146 que tornaram muito mais divertido trabalhar naquele laboratório, obrigada pelas risadas e boa disposição.

Um agradecimento especial a toda a equipa do nBTT- Nanobiomaterials to control infection and thrombus formation. Obrigada Fabíola, Cláudia, Catarina, Maura por se mostrarem sempre disponíveis e por terem de aturar as minhas dúvidas. Aos coleguinhas mais novos e com quem partilhei tantas frustrações, tantas risadas, foi muito bom termo-nos uns aos outros. Micaela, Diana e Luís, muito obrigada! Obrigada especialmente na ajuda com as experiências megalómanas. Desejo-vos o melhor no vosso futuro, vai correr tudo bem! A verdade é que tudo se torna mais fácil quando estamos rodeados pelas pessoas certas e eu tive imensa sorte, porque conheci e trabalhei com pessoas espetaculares.

Obrigada às minhas karatecas por também terem de levar com as minhas frustrações e me ajudarem a livrar de energias negativas e estar sempre no meu melhor.

Finalmente, um grande obrigado à minha família. Só sou o que sou hoje graças ao vosso apoio, compreensão e acompanhamento. Pai, mãe e Miguel, vocês são essenciais e imprescindíveis para eu dar o melhor de mim e procurar ultrapassar-me a cada obstáculo.

# Abstract

End-stage renal disease is a worldwide public health problem with an increasing incidence and prevalence. The population affected needs to perform kidney transplant or, in most of the cases, dialysis for the rest of their lives as a process to remove waste and excess water from the blood. Dialysis catheters are an immediate and effective lifeline for dialysis patients however they are associated with a greater risk of infection and hospitalization. Dialysis catheter-related infections are a serious public health issue that can result in endocarditis or peritonitis, which can lead to sepsis and death.

So far, the existing strategies to convey antibacterial properties to catheter materials are not fully effective or present significant disadvantages. Therefore and since the number of dialyzed patients and bacteria resistance to antibiotics are increasing, catheter-related infections will became an even more alarming problem in the near future. As such, the design of a new biomaterial for the development of antimicrobial catheters is a striking need.

Since graphene discovery, graphene-based materials (GBMs) have excited researchers from several different areas. Biocompatibility and antimicrobial properties are particular goals when it comes to the biomedical and biological applications of GBMs and materials containing GBMs.

This work focused on the antibacterial potential of GBMs, in particular graphene nanoplatelets, for the development of a material for catheter production to prevent the infections that occur due to bacteria adhesion and growth on the catheter surface. Polyurethane (PU) is the polymer most commonly used for catheter manufacture and the modification of its surface was therefore studied on the course of this work. Specifically, a commercially available form of graphene nanoplatelets grade M (GNP-M) was investigated for the first time to confer antibacterial properties to PU. The effect of nanoplatelets size and oxidation was also studied, using GNP with two different sizes: GNP-M5 and GNP-M15, which have 5 µm and 15 µm average lateral size, respectively. For biomaterials development, two different strategies were explored: i) polyurethane composites with GNP as nanofillers and ii) GNP-containing coatings on PU. The antibacterial properties of the produced materials, namely non-oxidized and oxidized GNPs powders, PU/GNP composites and PU/GNP coatings, were tested towards *Staphylococcus epidermidis* bacteria.

Oxidation of GNP was successfully performed and antimicrobial studies showed that oxidized GNPs have stronger antibacterial activity than non-oxidized GNPs and that smaller particle size improves the antibacterial properties. PU/GNP composites produced by melt-blending showed a good dispersion of GNPs in the polyurethane matrix but no significant modification of the surface, with few GNPs exposed in a planar orientation and mostly covered with polymer. Antibacterial assessment confirmed that the GNPs present at the surface of the composites were not sufficient to effectively contact bacteria and no effects were detected on bacteria attachment, metabolic activity or viability. Finally, GNP-containing coatings were produced by dip coating and different GNP concentrations and PU:GNP ratios were tested. It was demonstrated that good dispersions and solvent evaporation are critical factors to fabricate uniform and homogeneous coatings. The PU/GNP-M and PU/GNP-Mox coatings produced showed increased GNPs exposure at the surface comparing with the melt-blending composites. Oxidized GNP induced higher antibacterial effect towards *S. epidermidis* than

non-oxidized forms, either through anti-adhesive or bactericidal activity, depending on the GNP concentration used.

Overall, this work demonstrates the potential of using GBMs as nanomaterials to confer antibacterial properties to PU, and hence as a promising strategy to produce a biomaterial for catheter production with reduced risk of infection.

# Table of contents

# Figure List

# Table List

# Abbreviations and Symbols

**AVF -** arteriovenous fistula
**AVG -** arteriovenous graft
**BB -** brilliant blue
**BP -** benzylpenicillin
**BSA -** bovine serum albumin
**CD -** β-cyclodextrin
**CF -** carbon foam
**CFUs -** colony-forming units
**CRB -** catheter-related bacteremia
**CS -** chitosan
**CVD -** chemical vapor deposition
**DI -** deionized water
**DMF -** dimethylformamide
**EDS -** energy-dispersive X-ray spectroscopy
**FGO -** functionalized GO
**FGt -** functionalized few-layered graphite
**FLG -** few-layer graphene
**G -** graphene
**GBMs -** graphene based materials
**GNPox -** oxidized graphene nanoplatelets
**GNPs -** graphene nanoplatelets
**GNs -** graphene nanosheets
**GO -** graphene oxide
**GSH -** glutathione
**Gt -** graphite
**HD -** hemodialysis
**IONPs -** iron oxide nanoparticles
**IPA -** isopropanol
**LB -** Langmuir–Blodgett
**MBC -** Minimal Bactericidal Concentration
**MDG -** methanol derived graphene
**MHM -** modified Hummers method
**MIC -** Minimal Inhibitory Concentration
**NLf -** native lactoferrin
**NPs -** nanoparticles
**NRC -** nanorod composite
**NWs -** nanowires
**PBS -** phosphate-buffered saline
**PD -** peritoneal dialysis
**PDDA -** poly (diallyldimethylammonium chloride)
**PE -** poly(ethylene)
**PEG -** polyethylene glycol
**PEI -** polyethyleneimine
**PET -** polyethylene terephthalate
**PHGC -** polyhexamethylene guanidine hydrochloride
**PI -** propidium iodide
**PLA -** poly (lactic acid)
**PLL -** poly-L-lysine
**PNIPAM -** poly(N-isopropylacrylamide)
**PP -** polypropylene
**PPC -** poly(propylene carbonate)
**PS -** polystyrene
**PU -** polyurethane
**PVA -** poly(vinyl alcohol)
**PVDF -** polyvinylidene fluoride
**PVK -** polyvinyl-N-carbazole
**PVP -** polyvinyl pyrrolidone
**RFUs -** relative fluorescence units
**rGO -** reduced graphene oxide
**ROS -** reactive oxygen species
**SEM -** Scanning electron microscopy
**SOD -** superoxide dismutase
**TCC -** tunneled cuffed catheter
**TCF -** transparent conductive film (TCF)
**TGA -** Thermogravimetric analysis
**THF -** tetrahydrofuran
**TSA -** Trypticase Soy Agar
**TSB -** Trypticase Soy Broth
**TTP -** tetradecyl triphenyl phosphonium bromide
**TWEEN -** polyoxyethylene sorbitan laurate
**XPS -** X-ray photoelectron spectroscopy

# CHAPTER I:
# Motivation and Aim

## 1. Motivation and Aim

Hemodialysis (HD) represents the most widely adopted therapy for patients with end-stage kidney disease. However, hemodialysis patients suffer from higher rates of morbidity and mortality, particularly due to vascular access-related problems. The challenge for the dialysis catheters is to find strategies to face its essential problems, involving infection and thrombosis. This has been subject of extensive research and developments have been made but research community has not achieved the so desirable goal, yet. Several strategies are currently being adopted but the results are still far for us to say that a solution has been created.

Meanwhile, since its recently discovery in 2004, graphene has changed the way we look to materials and has been conquering numerous fields. Is has blown away scientist with its outstanding properties. From batteries to solar panels, from clothes to sensors, from new composite materials to DNA transporters, from drug delivery to antimicrobial surfaces, everything can be improved with the use of graphene. Is seems that it can lead us to where we dare to go and to what our imagination makes us dream about. The interaction between graphene, or more generally graphene-based materials (GBMs), and biological systems is being intensively studied to give insights to the effects of GBMs on bacteria, mammalian cells, animals, and plants. In 2010 the antibacterial properties of GBMs were explored for the first time and since then a growing number of reports have described GBMs as antimicrobial nanomaterials. Several factors affect their activity such as the materials' concentration, physical and chemical properties, and there is still a lot of controversy on the mechanisms of action. As materials with low mammalian cell cytotoxicity, increased antimicrobial properties and low cost caused by the cheap raw material, GBMs may become an ideal material in biomedical applications, namely biomedical devices and implants.

GBMs have been thought as a straightforward and economic approach to confer bactericidal properties to the most commonly used dialysis catheters. Thereby, incorporation of GBMs on the polymer used for catheter construction can improve the antimicrobial properties of dialysis catheters and consequently, GBMs may prevent catheter-associated infections. This was the purpose of this investigation and the motivation to access whether GBMs really represent a new revolution in the antimicrobial materials field as it has been verified in so many and distinct areas.

The objectives of this study were to prepare polymer surfaces containing GBMs and evaluate their antibacterial properties. The polymer used was polyurethane, since it is the material most commonly used for catheter production, and the GBMs used were commercial graphene nanoplatelets (GNPs). The effect of nanoplatelets size and oxidation was also studied, using GNP with two different sizes: GNP-M5 and GNP-M15. GNPs dispersions were also evaluated in terms of antibacterial properties. As it was known from the start this was not a straightforward study. Several difficulties were found and had to be overcome, and different strategies were assessed to reach a solution that had the potential to effectively work as an antibacterial material for catheter development.

## 2. Structure of the Dissertation

Chapter II – Literature Review aims to contextualize the problem assessed, including social and economic problems related to hemodialysis, as well as a more detailed review on catheter development, materials and manufacturing. There is also information on catheter-related infection and the microorganisms more associated to this health problem. The chapter ends with an extensive review on the state of art on graphene-based materials (GBMs) directed to their antimicrobial application and studies with bacteria.

In Chapter III - Materials and Methods the materials used and the experimental procedures are described in detail. It includes production, characterization techniques and biologic testing of the different materials produced. Starting from GNPs oxidation and antibacterial assessment of the powders aqueous dispersions. Followed by the two different approaches conducted for polymer modification: first the production of PU/GNP composites by melt-blending, in which GNPs are physically embedded in a PU matrix, and secondly the application of a GNP containing coating onto PU surfaces by dip-coating. In particular it was known that the orientation and exposure of the nanosheets was an important aspect on surfaces, being an essential factor for the bacterial toxicity of GBMs. Thereby, the material production methods were evaluated to optimize the exposure of GNPs on the polyurethane surface.

Results obtained and their consecutive discussion can be found in Chapter IV – Results and Discussion. This chapter is divided by the different materials produced: powders, composites and coatings. And in each section, the results from the characterization techniques and the antibacterial activity assessments performed for each type of material are described and discussed.

Finally, in the last chapter, Chapter V, the conclusions taken from this work are described and future work is also discussed.

# CHAPTER II:
# Literature Review

## 1. Dialysis Catheters: an Overview

Chronic kidney disease is a worldwide public health problem with an increasing incidence and prevalence, poor outcomes, and high cost [10]. The number of patients with end-stage renal disease is growing worldwide and the mortality of this patients is 10-20 times higher than that in the general population [11]. Renal replacement therapy is essential for maintenance of life for those with end-stage renal disease, which can be performed in two different modalities: dialysis and kidney transplantation [12].

Dialysis is the process to remove waste and excess water from the blood. There are two types of dialysis: hemodialysis (HD) and peritoneal dialysis (PD). While HD filters the blood outside the body allowing it to flow through a dialyzer, PD uses the lining or peritoneum of the abdominal cavity to filter blood inside the body through a draining process [13]. The most common is hemodialysis, but peritoneal dialysis is also performed and regarded as very promising since patients can benefit from the treatment at home without the need to travel to a healthcare center[14]. Catheters are soft tubes used in both types of dialysis[6]. As such, dialysis catheters are an immediate and effective lifeline for dialysis patients and their use is steadily increasing. In HD, the site from where the blood is removed and returned is called the vascular access. HD differs in the type of vascular access which include the arteriovenous (AV) fistula (AVF, a connection between an artery and a vein) and the AV graft (AVG, a looped plastic tube that connects an artery to a vein) both more appropriate for long-term use; and the central venous catheter, which can be either temporary or a permanent tunneled catheter (Figure

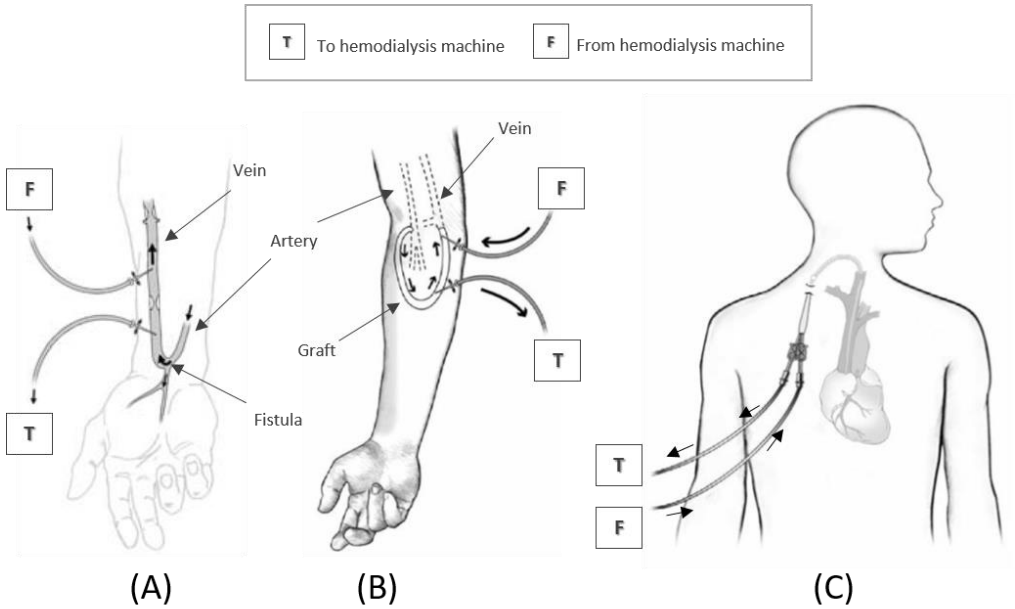


**Figure 1.** The three types of vascular access: arteriovenous fistula (A), arteriovenous graft (B) and venous catheter (C).The arrows illustrate the direction of the blood flow. In the first case (A), needles and tubes are inserted in the AV fistula, while in the second case (B) they are inserted in the tube that connects the vein with the artery. Adapted from Diseases, 2014[8].

1)[15]. The type of vascular access seems to have a significant influence on survival and studies

report AVF having the highest long-term patency and the lowest infection and complication rates [16; 17; 18].

The HD catheter is tunneled since it is placed under the skin instead of directly inserted into the vein. Most catheters have one or two cuffs, which are intended to stabilize catheter placement and minimize bacterial migration through the skin into the body. Non-cuffed tunneled catheters are used for emergencies and for short periods (up to 3 weeks) and are responsible for 90% of catheter-related bloodstream infections[19]. Tunneled cuffed catheters (TCC) (Figure 2) are recommended for long-term, when an AV fistula or graft has been placed but is not yet ready for use, or when there are no other options for permanent access (such as when a patient's blood vessels are not strong enough for a fistula or graft)[20], and their use is associated with a substantially greater risk of infection, hospitalization and mortality compared to the use of an AVF[17]. Tunneled catheters induce a risk of bacteremia in patients 10 times higher than when AV fistulas or grafts are used[21]. Up to 30% of hospital admissions in hemodialysis patients are related to vascular access complications, and include infection and thrombotic occlusion[17; 22]. These complications result in the removal or replacement of up to 50% of all catheters, contributing to the substantial medical costs attributable to vascular access[23]. Therefore, the existence of a dialysis catheter that minimizes these complications can yield many patient and social benefits[20].

## 2. Catheter-Related Infection

Catheter-related infections have as source the patient's own skin flora and, can be introduced extraluminally via skin or intraluminally via the catheter hub[19]. Epidermal commensal bacteria can migrate along the external surface of the catheter, starting from the skin insertion or, alternatively, inside the catheter lumen and spread further along the subcutaneous tunnel to the inner cuff and, subsequently, to the peritoneum or the endocardia (depending on the place of catheter insertion), resulting in tunnel infection and peritonitis or endocarditis, respectively [24]. Bacteria can also adhere to the catheter material itself, forming a protective glycocalix biofilm and possibly causing luminal infections which are far more severe and difficult to treat [25; 26]. Biofilms are frequently observed on PD catheters, with *Staphylococci* and *Pseudomonas spp.* being the most frequently recovered Gram-positive and Gram-negative species, while fungi are rarely observed[25].

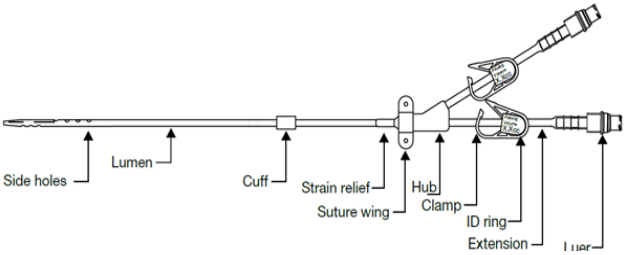


**Figure 2.** Structure of an hemodialysis catheter[6].

Catheter-related bacteremia (CRB) is associated mostly to Gram-positive organisms (52–84%)[27], with *Staphylococcus epidermidis* being responsible for 40-50% of the episodes, followed by *Staphylococcus aureus* (10-20%). Gram-negative species, especially *Pseudomonas aeruginosa, Stenotrophomonas* sp., and *Acinetobacter baumannii*, are recovered in one-third of the cases. While fungus, in particular *Candida* sp., are less common (≤10% of the cases)[27; 28; 29]. Bacteremia is the most alarming and clinically relevant event in the setting of catheter-related infections, because of its rate of occurrence and its potential to lead to sepsis[26]. Thus, there is an urgent need to develop a catheter surface more resistant to microbial colonization

and hence with improved antimicrobial properties. Amongst the different strategies that are being tested, up to now only antiseptic-impregnated dressings and catheters, and catheter coatings such as antibiotics, have been proven efficient to prevent catheter related infections[19; 20; 28; 30]. However, antiseptics and antibiotics can induce bacteria resistance as a consequence of their prolonged use[26] and loose efficiency along time due to leaching[28]. Nanomaterials emerge as a strategy with interesting opportunities to overcome those problems. Apart from scalability, low cost, and versatility, such materials offer advantages related to resistance, lower toxicity to the environment than traditional antibiotics, as well as longer duration[31]. As such, a common approach to prevent the attachment and proliferation of microbes on surfaces has been to functionalize or coat the surface with antimicrobial nanomaterials, such as silver nanoparticles (Ag NPs)[32], titanium oxide ($TiO_2$) NPs[33] and carbon nanotubes (CNTs)[34]. In particular, graphene and graphene-based materials (GBMs) are nanomaterials with increasing interest and potential in its antimicrobial properties[31].

## 2.1 Staphylococcus epidermidis

As mentioned, Gram-positive bacteria are responsible for most of the catheter-related infections, with *Staphylococcus epidermidis* on the lead, justifying the use of this species as the bacterial model of the present work. *S. epidermidis* is a Gram-positive biofilm-forming bacteria, producing extracellular polysaccharides (also known as glycocalix, capsule or slime) when growing on a surface[35]. It belongs to the genus of *Staphylococci* characterized by cluster-forming cocci, usually forming grape-like clusters (Figure 3)[5]. And, as member of the coagulase-negative *Staphylococci* group, differentiates from other species, such as *S.aureus*, due to its inability to produce the exoenzyme coagulase (enzyme that converts fibrinogen to fibrin and leads to the coagulation of blood plasma)[36]. Coagulase-negative *Staphylococci* are microorganisms that naturally habit on human skin and mucous membranes and represent therefore part of our endogenous flora[37].

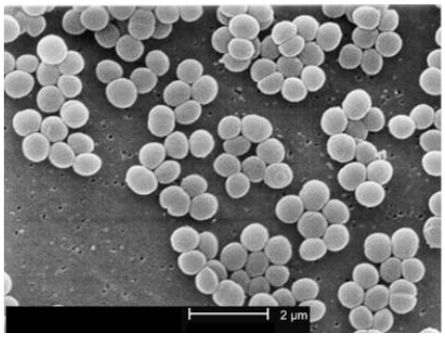

**Figure 3.** *Staphylococcus* clusters[5].

*S. epidermidis* is the most common cause of nosocomial infections and also the main responsible for many coagulase-negative infections developed outside a hospital environment[37]. Moreover, the most important group of infections caused by this bacteria are infections on foreign bodies, such as catheters and any implanted devices[36; 38]. It is responsible for 22% of the intravenous catheters infections in the USA[39]. Besides, its naturally high resistance to antimicrobials make them subject of great concern when it comes to medical device infections, particularly when they form biofilms. This microorganism develops biofilm in two stages: initially through cell-surface interactions, followed by the formation of the biofilm which involves cell-cell interactions plus cell aggregates formation[35; 40]. *S. epidermidis* invasiveness ca be explained by the high level of genetic diversity between its strains[40; 41]. The main parameters that governs bacterial adhesion to surfaces, such as catheters, is the hydrophobicity of the bacterial cell surface together with the electrostatic interactions and Van der Waal's forces between the bacteria and the material's surface[36; 40].

# 3. Hemodialysis catheters: materials and manufacturing

Catheters are made of medical grade materials, which means that the materials have been approved for use in medical applications[42]. The catheter material must not promote blood plasma coagulation, damage proteins, enzymes or any of the blood cells, cause hemolysis or initiate platelet release reaction[38; 43]. For this application, and for a number of other biomedical applications, the biomaterial is polymeric. The most commonly used polymers are polyurethane (PU) and silicone. Silicone was for a long time the standard material for catheter construction because of its biocompatibility and because it is soft and flexible[6; 38]. However it has too low stiffness and limited tensile strength[44]. Silicone catheters have also a higher risk of infection due to various factors, including its rougher surface topography compared to PU, which leads to more bacterial adhesion[45]. With the development of biomaterials technology PU has taken over silicone in catheter production.

Polyurethane is a thermoplastic elastomer and the ability to manipulate its characteristics during the manufacture process makes it a very interesting material in the medical device industry. Thermoplastics are made by the copolymerization of two or more monomers: one providing the hard (crystalline) polymer segment that acts as a thermally stable component and determines the plastic properties, and the second monomer providing the elastomeric or "elastic" properties[44]. In particular, PU is the reaction product of three components: diisocyanates, long-chain polyols (generally a polyester or polyether) and short-chain diols (called the chain extenders). The hard polymer segment consists on the combination of diisocyanate with short-chain diol, and the soft segment consists on the polyols[44; 46].

PU is a tough elastomer, flexible and with very good blood-compatible properties[38]. It has much higher tensile strength than silicone (3-10 times higher) and it's easier extruded. Catheters made of PU can be designed to have very thin walls, making it possible to have catheters with increasing inner lumen while maintaining the outer diameter and, thus, increasing blood flow rates[42]. A very interesting and useful characteristic of PU is that it is rigid at room temperature, making easier the catheter insertion, and when inserted inside the body the temperature is higher and the material softens, minimizing the risk of perforations[42; 47].

The typical PUs used in the manufacturing of medical device are the Pelletane® and Tecothane®. In these polymers' synthesis the diisocyanate is an aromatic isocyanate, the 4,4-methylene bisphenyl diisocyanate (MDI), the polyol is a polyether, the polytetramethylene oxide (PTMO), and the chain extender is 1,4-butanediol (BD)[7; 46]. Thus, they are composed by an aromatic hard segment and a polyether soft segment (Figure 4). In the present investigation PU was used as the model for catheter material and the series used was Tecothane®.

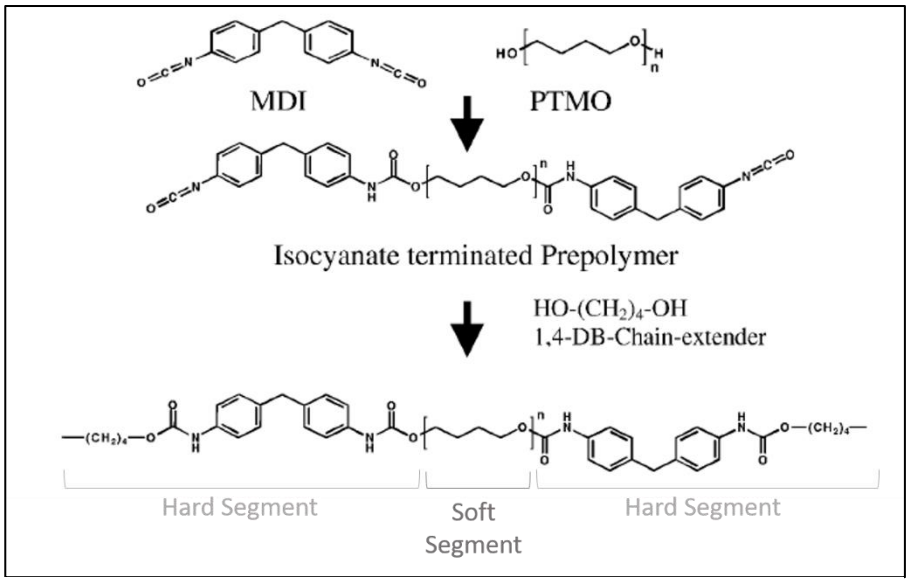


**Figure 4.** Synthesis of polyether-based polyurethanes Pelletane® and Tecothane®. Adapted from Ma et al.[7].

The manufacturing processes for catheter production include: injection molding, extrusion, tipping, bonding and printing[6]. In injection molding the polymer granules or pellets (Figure 5) are melted and injected into a mould at controlled temperature, pressure and flowrate. After, the material cools down and takes the shape of the mould. Extrusion is performed for tube construction and consists in melting the polymer and then forcing it through a die. Tipping and bonding are processes used for the manufacture of the catheter luer and tip and its side holes (Figure 2).The last process, printing, serves only to print useful information on the catheter surface[6; 46].

**Figure 5.** Tecothane® thermoplastic polyurethane (TPU) pellets.

# 4. Graphene-based materials (GBMs)

Graphene is the most recently discovered member of the nanocarbon family but has already attracted enormous interest. Its discovery in 2004 at the UK's University of Manchester gave the physicists Andre Geim and Konstantin Novoselov the Nobel Prize in Physics in 2010[48].

The graphene-based materials (GBMs) include graphite (Gt), few-layer graphene (FLG) (also referred as graphene nanoplatelets (GNPs) or graphene nanosheets (GNs)), graphene (G), graphene oxide (GO) and reduced graphene oxide (rGO). These GBMs vary in layer number, lateral dimension, surface chemistry, defect density, and composition or purity, all properties relevant for their biological effects[49]. Single-layer graphene (G) is an one-atom-thick planar sheet composed of carbon atoms densely packed in a honeycomb crystal lattice with hybridized $sp^2$ bonding. It presents very unique features, namely high area/thickness ratio, mechanical strength and stability, as well as exceptional electronic and optoelectronic properties. One issue with graphene is its hydrophobicity that can cause it to restack irreversibly[50]. Few-layer graphene (FLG) or graphene nanoplatelets (GNPs) have 2 to 10 layers of such two-dimensional sheets. Graphite consists on more than 10 graphene sheets and is not

considered a nanomaterial. Graphene oxide (GO) is similar to graphene, but presents oxygen-containing functional groups such as carbonyls, carboxyls and hydroxyls, making it more hydrophilic. These polar and reactive groups reduce the thermal stability but may be important to promote interaction and compatibility with polar solvents or with a particular polymer matrix[51]. The synthesis methods control GBM's structure and properties, and a variety of processing techniques are used by researchers[50; 52]. Top-down strategies are the most frequently used methods to synthesize graphene and, together with the different types of GBMs, are represented in Scheme 1.

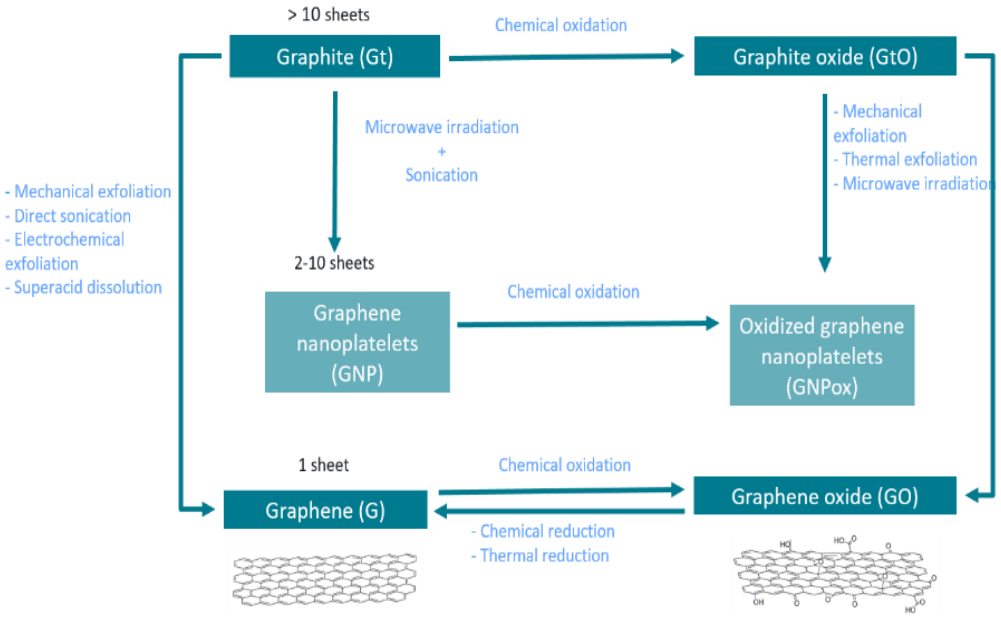


**Scheme 1:** Types of GBMs and production methods[1; 2; 3; 4]

There are also bottom-up methods like chemical vapor deposition (CVD) but are less suitable for large scale production[53]. To date, the most commonly researched routes to graphene are via GO, due to scalability. Even though these methods start from the same raw material, structure and surface characteristics may differ significantly depending on how the GO is exfoliated and reduced[2]. The method most widely used is the Hummers method which involves an oxidation–reduction process: GO is obtained from Gt oxidation and exfoliation, and then reduction converts the GO to graphene. Reduction of GO will remove most, but not all, of the oxygen-containing groups. Hence, the reduction process gives reasonably hydrophobic graphene sheets, which tend to aggregate irreversibly, greatly hindering its production, storage and processing[50]. Both G and GO can be modified in order to obtain other GBMs, altering its properties by chemical modification through either covalent bondings or non-covalent interactions[50]. This has attracted considerable attention in various applications and graphene can be modified in a number of ways, by varying the type of molecules adsorbed on its surface[54]. Numerous review articles have addressed the advancement of research in all types of GBMs, in the area of synthesis, properties and applications, such as field emission, sensors, electronics, energy[26; 32; 34; 35; 36; 37; 38;40;]and biotechnology[1; 2; 51; 55; 56; 57; 58; 59]. The biomedical application of GBMs is a relative new area with great potential. Graphene's enormous surface area, 2D structure and good conductivity make it appropriate for biological applications[50]. The applications studied include delivery of drugs and genes[60], biological

sensing and imaging[61], cancer therapy[62], antibacterial materials[63] and biocompatible scaffolds for cell culture[49; 64; 65]. The present work focuses on the antimicrobial properties of GBMs and composites containing GBMs. The purpose is to identify, summarize, and present information on the effects of GBMs on bacteria and potential mechanisms of toxicity based on the literature in the field.

# 5. Antimicrobial activity of GBMs

In terms of antimicrobial agents, it is important to make a distinction between those which inhibit bacterial attachment and those which effectively destroy bacteria on contact. Antibiofouling is the property possessed by some materials which prevent or limit the settlement of biological material on their surfaces. While agents that limit microbial growth through biocidal action should more correctly be referred as bactericidal[66; 67]. There are also agents that prevent the growth of bacteria i.e. keeps them in the stationary phase of growth, referred as bacteriostatic agents[68].

The effects of GBMs on bacteria, mammalian cells, animals, and plants have been studied, in particular biocompatibility has been intensively studied and subject of several reviews [51; 56; 69; 70; 71; 72; 73]. GBMs may elicit adverse responses from prokaryotic or bacterial cells as well as eukaryotic mammalian cells and in recent years the interest about interactions with target cells and potential toxicity has increased[74]. In 2010, Huang and co-workers explored for the first time the antibacterial properties of GO[75] and since then increasing number of studies have described GBMs as having bactericidal activity, therefore being a strong candidate for antimicrobial applications[51; 73]. It has been reported that the effect of GBMs on bacteria structure, metabolism and viability depends on the materials' concentration, physical and chemical properties, exposure time and the type of bacteria tested. In general, bacterial viability decreases with increase of contact time and the concentration of GBMs[9; 76; 77; 78; 79; 80; 81; 82; 83]. This section will review the potential toxicity of GBMs for bacteria and the different studies are summarized in Table 1 for GBMs aqueous dispersions and Table 2 for GBMs films. As mentioned earlier, functional groups can be introduced on GBMs, decorating its surface and altering its properties including antimicrobial properties, giving rise to a new class of materials, the functionalized GBMs. Therefore, on the scope of this work, GBMs are subdivided in two sections: non-functionalized and functionalized GBMs.

## 5.1. Non-functionalized GBMs

### 5.1.1. Aqueous dispersions

Investigating graphene as an antimicrobial material, Liu *et al.* compared the antibacterial activity of four types of GBMs, namely graphite (Gt), graphite oxide (GtO), graphene oxide (GO), and reduced graphene oxide (rGO), toward Gram-negative bacteria *Escherichia coli* (*E. coli)*[9]. The dispersions were prepared in isotonic saline solution and all of these GBMs showed some antibacterial activity using a colony counting method. Under similar concentration (40 µg/mL) and incubation conditions, the antimicrobial potency of these materials decreased in the order GO>rGO>Gt>GtO. GO and rGO antibacterial activity was shown to be time- and concentration-dependent with *E.coli* viability decreasing with extending incubation time and increasing GBM concentration. In this study SEM images also noted graphene nanosheets to

cause cell membrane rupture, while only traces of reactive oxygen species (ROS) was detected. Nevertheless, oxidative stress was also identified as a potential mechanism for the observed cell death: these materials could oxidize glutathione, with conductive rGO and Gt having higher oxidation capacities than insulating GO and GtO. Based on this, a three-step antimicrobial mechanism was suggested, including initial cell deposition on GBMs, causing membrane stress by direct contact with sharp nanosheets, and in turn initiating ROS-independent oxidation stress. Similar results were presented by Hu and co-workers, *E. coli* metabolic activity decreased to 70% and 13% at concentrations of 20 and 85 µg/mL of GO, respectively. When treated with 85 µg/mL GO for 2 h, *E.coli* suffered a viability loss up to 98.5%, higher than with rGO (≈90%)[75]. In contrast, rGO cytotoxicity towards a mammalian cell line (A549) was significantly higher. The authors confirmed these results using TEM analysis, which revealed the bacterial cell membrane being severely destroyed and the cytoplasm flowing out for both GO and rGO. Gurunathan and co-workers also reported the antibacterial activity of GO and rGO dispersions in saline solutions against *E.coli* using cell viability, ROS production and DNA fragmentation assays[77]. The loss of *E. coli* viability increased with GBM concentration achieving 87% and 81% at the concentration of 150 µg/ml, for GO and rGO respectively. In agreement with previous works, GO dispersions had higher antibacterial results. They also tested Gt, GtO, GO and rGO antibacterial activity towards *Pseudomonas aeruginosa* and found similar results[79]. No colonies were observed with concentrations of 175 µg/mL for both GO and rGO and they detected the generation of ROS, leading to cell death, which was further confirmed through resulting nuclear fragmentation. Strong antibacterial activity of GO, synthesized by the Hummers method, was also reported on Gram- *Klebsiella* and Gram+ *Staphylococus* bacterial species, in which the inhibition zone was a concentration-dependent parameter[82]. GO also had harmful effects on the bacteria *Pseudomonas syringae* and *Xanthomonas campestris pv. undulosa,* and the fungi *Fusarium graminearum* and *Fusarium oxysporum* (killing nearly 90% of the bacteria and repressing 80% macroconidia germination along with partial cell swelling and lysis at 500 µg/mL)[84]. In another study, the antibacterial activity of rGO and GO suspended in different dispersants was evaluated against *Xanthomonas oryzae p*v oryzae[76]. The nanosheets presented different thickness, as expected, GO were flat sheets with an average thickness of 0.76 nm, while rGO presented a sheet thickness of 1.59 nm. Besides bacteriostatic properties, antibacterial activity was also detected with GO and rGO dispersions in a buffer- and dose-dependent manner. The antibacterial effect decreased in the order DI (deionized water)>NaCl>PBS, due to increased aggregation in solutions with rich salts. The stronger effect was observed upon *X. oryzae* exposure to GO (250 µg/mL in DI) compared with rGO and bismerthiazol, a common bactericide, with a killing rate of 94.48%, 36.31%, and 13.3%, respectively. The high efficiency of GO for inactivating the bacteria was presumably due to its extremely sharp edges and the generation of reactive oxygen species. Similar results were demonstrated by other studies[78; 85; 86; 87]. Wang and co-workers reported that, with the same concentration (250 µg/mL), GO antibacterial effects were substantially higher in water than in 0.9%NaCl or PBS solutions while rGO did not exhibit significant antibacterial activity toward *R. solanacearum*[85]. In a recent work, 250 µg/mL of pristine graphene (pG), GO, and rGO completely inhibited the growth of *Listeria monocytogenes* (Gram+) and *Salmonella enterica* (Gram-), despite their difference in bacterial cell wall structure[83]. At a lower concentration (25 µg/mL), similar effects were only observed with GO. Another study used the microdilution method to evaluate the minimum inhibitory

concentration (MIC) of rGO for four pathogenic bacteria[88]. For 24h incubation, MICs values were 1 µg/mL against *E.coli* and *Salmonella typhimurium*, 8 µg/mL against *Enterococcus faecalis*, and 4 µg/mL against *Bacillus subtilis*, suggesting that rGO is more toxic to Gram-bacteria. This is in contrast to other studies which suggest that the presence of the secondary cell membrane of Gram- bacteria provides a better resistance to membrane induced damage[89]. The authors also provided evidence that enhanced lipid peroxidation occurred. Using the same method, in other study MIC values of GO were 0.5, 0.5 and 1 µg/mL for *E. coli*, *S. aureus* and *P. aeruginosa*, respectively[90]. Sawangphruk and colleagues noted that rGO displayed antifungal activity while totally inhibiting the fungi *Fusarium oxysporum*, *Aspergillus niger* and *Aspergillus oryzae* at the concentrations of 250, 500 and 500 µg/mL, respectively[91]. Recently, Perreault and co-workers investigated size-dependency of GO antimicrobial activity using the *E. coli* as a bacteria model[92]. They produced GO of average sheet area ranging 0.01 - 0.65 $\mu m^2$. In suspension the antimicrobial effect of GO increased with increasing sheet area and GO interacted with bacteria in a cell entrapment mechanism. Complete cell inactivation was observed for the 0.65 $\mu m^2$ sheets after a 3 h exposure. However, cell inactivation by GO entrapment was reversible and all initially viable cells could be recovered when separated from all GO sheets sizes by sonication, leading to the conclusion that GO acts by inhibiting, but not inactivating, cells. Similar results were obtained by Tu *et al.*[93].

Contrarily, several studies report GBMs as not having antimicrobial properties and moreover, increasing bacterial growth[94]. Indeed, the study of Ruiz and co-workers suggested that GO had no detrimental effect to *E.coli* [94]. When GO was added to a bacterial culture at 25 µg/mL in Luria-Bertani (LB) nutrient broth, the results showed that bacteria grew faster and to a higher optical density than cultures without GO. A dark precipitate was formed by a thick bacterial biofilm indicating that when a colloidal suspension of GO in water is added to a solution media containing salts, it aggregates. This precipitation is possibly responsible for the bacterial growth, acting as a scaffold for bacterial attachment, proliferation, and biofilm formation. Similarly other studies report GO [80; 95; 96; 97; 98] and rGO[95] as not having significant antibacterial effect. In Liu *et al.* study, the antibacterial test was performed in saline solutions and, at a concentration of 100 µg/mL, only 17% of *E.coli* were inactivated[80]. The authors explained this contrary results by the fact that GO sheets used had a different oxygen-containing group content compared to Hu *et al.*[75], and that may affect the interaction between GO and bacteria cells. In Xu *et al.* work, *E.coli* were grown in LB medium supplemented with rGO, which showed no growth inhibition at a concentration of 100 µg/mL[95]. Many of these studies have in common the use of LB medium for the antimicrobial activity test[96; 98; 99]. Hui and co-workers addressed these controversies related to GO antibacterial activity and found that its bactericide activity decreased with increase in Luria-Bertani (LB) broth supplementation, in saline with 10% LB GO was completely inactive[87]. This can be explained by the noncovalent adsorption of certain LB components on GO basal planes. These contrasting observations on the antimicrobial properties may also be due to the lack of standardization of GBMs preparations, producing particles with different sizes and numbers of sheets, and, moreover, differences in the methodologies employed to assess antibacterial activity.

**Table 1 -** Effects of GBMs aqueous dispersions on bacteria.

| Ref | GBM | Production method | Properties | Investigated Bacteria | Cell viability | Membrane damage | Oxidative stress | Other |
|---|---|---|---|---|---|---|---|---|
| 9 | GtO | MHM | l ≈ 6.28 µm | *E.coli* | GtO ≈ 85%, Gt ≈ 74%, rGO ≈ 54%, GO ≈ 31% (40 µg mL$^{-1}$, 2h)<br>For GO and rGO, decreases with incubation time, concentration increase and size decrease | n/s | Trace amounts of ROS for all GBMs (40 µg mL$^{-1}$, 5h)<br>Loss of gluthathione (GSH): 21, 30 , 94, 22% (40 µg mL$^{-1}$, 2h, respectively for GtO, Gt, rGO, GO) | - |
| | Gt | Commercial product | l ≈ 6.87 µm | | | n/s | | |
| | rGO | MHM + Hr | l ≈ 2.75 µm | | | Yes | | |
| | GO | MHM | t < 1 nm<br>l ≈ 0.31 µm | | | Yes | | |
| 75 | GO | MHM | t ≈ 1.1 nm | *E. coli* | Metabolic activity ≈ 70% (20 µg mL$^{-1}$, 2h), ≈ 13% (85 µg mL$^{-1}$, 2h)<br>Colony counting ≈1.5% (85 µg mL$^{-1}$, 2h) | Yes | n/s | - |
| | rGO | MHM + Hr | t ≈ 1.0 nm | | Metabolic activity ≈ 24% (85 µg mL$^{-1}$, 2h)<br>Colony counting <10% (85 µg mL$^{-1}$, 2h) | | | |
| 94 | GO | MHM + 7 days dialysis | n/s | *E. coli* | Cell proliferation: 130% (25 µg mL$^{-1}$, 16h) | n/s | n/s | - |
| 76 | GO | MHM | l = 300-600 nm<br>t ≈ 0.76 nm (flat) | *Xanthomonas oryzae pv. oryzae* | Decreases with concentration and incubation time and depends on buffer type<br>(2h, 30°C) 50 µg/mL: DI ≈ 60%; 0.9% NaCl ≈ 65%; 0.1M PBS ≈ 95%<br>(2h, 30°C) 250 µg/mL: DI≈ 5%; 0.9% NaCl ≈ 13%; 0.1M PBS ≈ 95% | Yes | (250 µg mL$^{-1}$, 2h)<br>Loss of GSH: 60%<br>↑5 fold ROS (increases with dose) | |
| | rGO | MHM + Hr | t = 300-600 nm<br>t ≈ 1.59 nm (aggregated) | | 50 µg mL$^{-1}$: DI≈ 81%; 0.9% NaCl ≈ 85%; 0.1M PBS ≈ 97%<br>250 µg mL$^{-1}$: DI≈ 64%; 0.9% NaCl ≈ 78%; 0.1M PBS ≈ 97% | No | (250 µg mL$^{-1}$, 2h)<br>Loss of GSH: 95%<br>↑2 fold ROS (increases with dose) | |
| 77 | GO | MHM + 2h sonication | l = 479 nm<br>t = mono or few layer | *E. coli* | Decreases with concentration and incubation time. (2h,37ºC) 50, 75, 100, 125 and 150 µg ml$^{-1}$: 82%, 64%, 48%, 26%, 13%<br>For 100 µg ml$^{-1}$: 0h – 100%, 1h – 76%, 2h – 51%, 3h – 32%, 4h – 12% | - | ROS (100 µg ml$^{-1}$, 4h) ↑2 fold (increases with time) | (100 µg ml$^{-1}$, 24h) DNA fragmentation |
| | rGO | MHM + dithiothreitol (DTT) reduction | l = 2.9 µm<br>t = mono or few layer | | Decreases with concentration and incubation time 50, 75, 100, 125 and 150 µg ml$^{-1}$ (2h,37ºC): 86%, 73%, 46%, 33%, 19%<br>For 100 µg ml$^{-1}$: 0h – 100%, 1h – 85%, 2h – 59%, 3h – 35%, 4h – 14% | - | ROS (100 µg ml$^{-1}$, 4h) ↑1fold (increases with time) | - |
| 88 | rGO | MHM (GO) + 1h ultrasonication + Hr | t = few layer | *E. Coli* | MIC(24h, 35 °C) = 1 µg mL$^{-1}$ | Yes | Lipid peroxidation (37ºC, 1h): ↑109% (5 µg mL$^{-1}$) ↑117% (10 µg mL$^{-1}$) | - |
| | | | | *S. typhimurium* | MIC(24h, 35 °C) = 1 µg mL$^{-1}$ | | | |
| | | | | *Bacillus subtilis* | MIC(24h, 35 °C) = 4 µg mL$^{-1}$ | | | |
| | | | | *E. faecalis* | MIC(24h, 35 °C) = 8 µg mL$^{-1}$ | | | |
| 85 | GO | MHM | l ≈ 0.5 µm<br>t = few layer | *Ralstonia solanacearum* | Vary with the type of buffers. (2h, 30ºC) 50-250 µg mL$^{-1}$:<br>Water≈ 40-12%; 0.9% NaCl= 40-20%; PBS ≈ 95% | ↑1.4 times release of cytoplasmic constituents | - | - |
| | rGO | MHM + Hr | | | (2h, 30ºC) 50-250 µg mL$^{-1}$ : Water=97-90%; 0.9% NaCl= 99-90%; PBS ≈ 97% | n/s | - | - |
| 78 | GO | MHM + dialysis + sonication for 0, 10, 30, 50, 120, 240 min (GO-0, GO-10, GO-30, GO-50, GO-120, GO-240) | t=1nm<br>Average size:<br>GO-0 = 0.753 µm<br>GO-240 = 0.010 µm | *E. coli* | Decreases with particle size<br>40 µg mL$^{-1}$ (2h, 250 rpm, 37 ºC, $H_2O$): GO-0 = 2.3%; GO-240 = 54.5%<br>Decreases with incubation time and concentration<br>GO-0 (2h, 250 rpm, 37 ºC, $H_2O$): 10 µg mL$^{-1}$ = 19.7%; 80µg mL$^{-1}$ = 0.6%<br>GO-240 (2h, 250 rpm, 37 ºC, $H_2O$): 10 µg mL$^{-1}$ = 83.3%; 80µg mL$^{-1}$ = 47.5% | Yes | 40 µg mL$^{-1}$, 2 h: GSH oxidation > 20%<br>Not dependent on lateral size | |
| 79 | Gt | sonication of Gt powders | n/s | *Pseudomonas aeruginosa* | Gt and GtO: few growth inhibition<br>GO and rGO (75 µg/mL, 15h): 92% growth inhibition<br>Decreases with concentration: (2h, 37ºC, 200rpm) 150 µg mL-1: GO ≈ 10%; rGO ≈ 15%; 175 µg mL-1: Go and rGO = 0%<br>Decreases with time: 75 µg mL-1: 1h: GO ≈ 77%; rGO ≈ 86%; 4h: GO ≈ 13%; rGO ≈ 14% | - | ROS<br>(100 µg/mL, 2h)<br>GO ↑3.8 fold<br>rGO ↑2.7 fold | (100 µg mL$^{-1}$, 24h) DNA fragmentation, only with GO |
| | GtO | MHM | n/s | | | | | |
| | GO | MHM + 2h sonication | l ≈ 0.525 µm | | | | | |
| | rGO | GO reduction with | l ≈ 3.40 µm | | | | | |

| | | | | | | | | |
|---|---|---|---|---|---|---|---|---|
| | | betamercaptoethanol (BME) | | | | | | |
| 100 | GO | MHM | n/s | E.coli | 5min in DI water= few bacteria cells were inactivated<br>30 min and 60 min= less but still plenty of colonies | - | - | - |
| 101 | GO | GO: GNPs mixed with KMnO4 + H2SO4–H3PO4 addition,50ºC, 12h + poured into 400 mL of ice with 30% H2O2 + sifted through 425 µm and 250 µm US Standard Testing Sieves + centrifuged at 4000 rpm for 4 h. | n/s | E.coli<br>Cupriavidus metallidurans<br>B. subtilis<br>Rhodococcus opacus | Toxicity, 1000 µg/mL<br>1h: E.coli = 62.0%; C.metallidurans = 62.3%; B. subtilis = 75.3%; R.opacus = 78.6%<br>3h: E.coli = 100%; C.metallidurans = 85%; B. subtilis = 92%; R.opacus = 89%<br>Metabolic activity: E.coli ≈30% B.subtillis ≈ 12%<br>Biofilm formation, 48h, 1000 µg/mL: 43-68% inhibited at GO suspensions | No | - | - |
| 102 | GO | GO: HM | n/s | E.coli | Radius of inhibition zone = 0 cm<br>(20-100µg/mL, 5h) ≈ no antibacterial activity | - | - | - |
| 103 | few-layered graphite (FGt) | GtO: Brodie method<br>FGt: $NaBH_4$ reduction of GtO | FGt ≈ 4 layers | *E. coli*<br>*S. aureus* | MIC (24h, 37ºC) > 10 000 µg/mL | - | - | - |
| 90 | GO | MHM | n/s | *E. coli*<br>*S. aureus*<br>*P. aeruginosa* | MIC (µg/mL): *E. coli* = 0.5; *S. aureus* = 0.5; *P. aeruginosa* = 1 | - | - | - |
| 104 | rGO | GO (MHM+ultrasonication) + lemon juice | n/s | *E.coli*<br>*S.aureus*<br>*Candida albicans* | MIC (µg/mL): *E.coli* = 31; *S.aureus* = 22.7; *C.albicans* = 47 | - | - | - |
| 91 | rGO | MHM + 30min sonication + Hr | l < 5 µm<br>t = few layers | *Aspergillus niger*<br>*Aspergillus oryzae*<br>*Fusarium oxysporum* | Total inhibition: *F. oxysporum* = 250 µg/mL; *A. niger* = 500 µg/mL; *A. oryzae* = 500 µg/mL<br>half maximal inhibitory concentration (IC50): *F. oxysporum* = 50 µg/mL; *A. niger* = 100 µg/mL; *A. oryzae* = 100 µg/mL | - | - | - |
| 82 | GO | Graphite flake: commercial product (mesh size 300)<br>GO: HM | GO average size = 8 nm | *Klebseilla*<br>*Staphylococus* | Inhibition zone (24h): 0.01gms of GO < 0.05gms of GO<br>Increases within the concentration of GO in both the bacteria.<br>Inhibitory activity of GO on *Klebseilla* was higher. | - | - | - |
| 92 | GO | MHM + dyalisis + 0, 1, 10, and 120 min sonication | average sheet area = 0.65, 0.29, 0.10, and 0.01 µm² | E.coli | 200 µg/mL, 3h,RT<br>↑ sheet area from 0.01 to 0.65 µm² = ↓viable CFU from 55 to 0.5%<br>complete inactivation = 0.65 µm², 3 h<br>cells could be recovered when separated from GO by sonication | - | Glutathione oxidation ↑ from 49 to 71% with ↓sheet area from 0.65 µm² to 0.01 | - |
| 87 | GO | MHM + bath-sonication | t = 1nm<br>in 5% LB broth t = 1.58 nm | *E.coli*<br>*B.subtilis* | In saline, 3h: 80 µg/mL = 72.7%; 200 µg/mL= 0.14%<br>In saline with 5% LB: 80 µg/mL = 102.2%; 200 µg/mL= 80.4%<br>In saline with 10% LB: 80 µg/mL = 101.9%; 200 µg/mL= 97.95% | Yes | - | - |
| 84 | GO | MHM + 3h bath-sonication | t= 0.794 nm | Bacteria:<br>*P. syringae*<br>*X. campestris pv. Undulosa*<br>Fungi:<br>*F. graminearum*<br>*F. oxysporum* | 0, 10, 50, 100, 250, 500 µg/mL (30ºC for 2 h)<br>*P. syringae* = 95.00%, 85.91%, 48.22%, 26.34%, 15.13% and 11.20%<br>*X. campestris pv.Undulosa* = 93.04%, 81.94%, 63.12%, 36.34%, 19.13% and 13.20%<br>Spore germination: *F. graminearum* = 97.65%, 78.34%, 63.28%, 58.09%, 38.98% and 14.51%<br>*F. oxysporum* = 96.39%, 82.69%, 74.89%, 7.27%, 27.18% and 18.84% | Yes | - | - |
| 83 | pristine graphene (pG) | phase exfoliation of natural graphite + 1h sonication | pG: irregular, angular, single to a few layers size=1.86µm<br>GO: film-like, rounded, single layers size=1.27µm<br>rGO: irregular, frayed, a few layers size=2.53µm | *Listeria monocytogenes*<br>*Salmonella enterica.* | 250 µg/mL of pG, GO and rGO = 100% growth inhibition<br>25 µg/mL, growth inhibition:<br>GO = 100% for both bacteria<br>pG: *S. enterica* = 96.5%; *L.monocytogenes* =54.5%<br>rGO: *S. enterica*=46%; *L.monocytogenes* =91% | - | - | Change of zeta potential of GBMs due to bacteria |
| | GO | MHM + 1h sonication | | | | | | |
| | rGO | GO + reducing mixture (of ammonium iodide, hydrated sodium hypophosphite, and sodium | | | | | | |

| | | | | | | | |
|---|---|---|---|---|---|---|---|
| | sulfite dissolved in DI water) + 1h sonication | | | | | | |

t=thickness; l=length, n/s= not studied, MIC= minimum inhibitory concentration, HM = Hummers method, MHM = modified Hummers method, Hr = hydrazine reduction.

### 5.1.2. Films

The unique structure of graphene provides opportunities for creating surfaces with properties which may inhibit bacterial attachment and growth as well as potentially inducing bacterial cell death[63]. Many of the studies mentioned above also investigated the interaction of bacteria with GBMs in substrates with comparable results to those involving suspensions produced from these particles[9; 92; 94]. These and other relevant studies on the effects of GBMs films on bacteria can be found in Table 2. GO and rGO films can be synthesized in large quantities through several approaches which involve drop casting, dip coating, spraying, spin coating, Langmuir–Blodgett (LB) film, and vacuum filtrations deposition[4]. The varied preparation methods of GBMs can affect the interaction with bacteria and can be the reason why some results are inconsistent and cannot be compared[69].

Li and co-workers produced graphene films on conductor Cu, semiconductor Ge and insulator $SiO_2$ by chemical vapor deposition (CVD), and found that the G-coated Cu and G-coated Ge could inhibit the growth of *E.coli* and S.*aureus*, especially the former[105]. Death of both the Gram- *E. coli* and the Gram+ *S. aureus* on these surfaces can be ascribed to severe membrane disruption and cytoplasm leakage. However, the proliferation of both bacteria couldn't be significantly restricted by the G-coated $SiO_2$. Similarly, Parra and co-worker showed that graphene-coated $SiO_2$ surface inhibited *Halomonas* bacteria adhesion but, however, didn't show bactericide effects[106]. Hu *et al.* prepared GO and rGO surfaces through vacuum filtration into a free-standing paper and determined the antibacterial activity by using airborne bacteria tests[75]. The nanomaterials could effectively inhibit the growth of bacteria. The results showed no *E.coli* cell growth on the GO paper and only a limited number of colonies on the rGO, implying the superior antibacterial effect of such graphene-based papers. Similar results were obtained by Akhavan and Ghanderi, which investigated the bacterial toxicity of single and few layer GO and rGO, obtained by electrophoretic deposition of a $Mg^{2+}$-GO suspension on stainless steel substrates with nanosheets being deposited in high-density and random orientations[107]. Loss in cell viability for *E.coli* and *S.aureus* bacteria proved both GO and rGO were effective as antibacterial materials, with the ability to inhibit attachment as well as kill the bacteria. However, in contrast with Hu *et al*., rGO exhibited the strongest antibacterial activity, assigned to the better charge transfer between the bacteria and the more sharpened edges. Akhavan and Ghaderi also examined interactions of GO films and *E. coli* living in a mixed-acid fermentation environment and anaerobic conditions[108]. In contrast with previous studies, GO acted as biocompatible for adsorption and proliferation of bacteria cells. However, they demonstrated that *E. coli* was able to reduce GO to bacterially reduced graphene (brGO) which showed some inhibition of the bacteria proliferation. The slight antibacterial property of the brGO sheets and the detaching of the already proliferated bacteria from these surface contributed to the bacteria growth in a self-limiting manner. Krishnamoorthy and co-workers produced GO-coated cotton fabrics via dip coating and tested their antibacterial activity with Gram+ *Streptococcus iniae* and Gram- *E. coli* [81]. Cotton fabrics specimens were added to bacterial suspensions in saline solution and time-dependent reduction of bacterial growth was

detected. As mentioned in the previous section, Perreault and co-workers investigated size-dependency of GO antimicrobial activity also in surface coatings[92]. The GO surface obtained was similar to the paper obtained by Hu *et al.*[75]. The antimicrobial activity of GO surface coatings increased 4-fold when GO sheet area decreased from 0.65 to 0.01 $\mu m^2$. The higher antimicrobial effect of smaller GO sheets was characterized by disruption of cell integrity, attributed to oxidative mechanisms associated with the higher defect density of smaller sheets.

Even though most studies report graphene modified surfaces as presenting antimicrobial activity, there are others reporting no antimicrobial effects[109] and others even suggesting the promotion of bacteria attachment[94]. In the study of Ruiz's group, GO paper surfaces were prepared using a modified Hummers method and filtered through a PVDF membrane[94]. They reported a dramatic increase in bacteria growth on filters coated with 25 and 75 µg of GO, 2 and 3 times faster than on filters without GO. This was due to enhanced attachment, proliferation, and biofilm formation, instead of bacterial growth inhibition. Interestingly, there was a preferential attachment and growth in areas containing GO, especially those areas containing the highest GO levels. A possible explanation is that with the vacuum filtration preparation procedure, the nanosheets laid flat on the membrane substrate with few edges exposed and, in addition, the oxidised basal planes exposed may confer an increased wettability on the particles which in turn allows a stronger interaction with the bacterial lipopolysaccharides through hydrogen bonding[63]. In this work GO was also not cytotoxic to mammalian cells.

**Table 2** - Effects of GBMs films on bacteria.

| Ref | GBM | Production method | Properties | Investigated Bacteria | Cell viability | Membrane damage | Other |
|---|---|---|---|---|---|---|---|
| 75 | GO paper<br>rGO paper | GO(MHM)/ rGO(MHM+Hr) + vacuum filtration method | GO paper t=1.5µm<br>rGO paper t=4.6µm | *E.Coli* | No cell growth on GO paper and limited number of colonies on rGO paper. | Yes | - |
| 94 | GO surface | GO(MHM + 7 days dialysis) + filtration on PVDF membrane | n/s | *E.Coli* | Enhanced microbial growth: 2 and 3 times faster when with 25 and 75 µg of GO | - | - |
| 107 | GO nanowalls (GONW) | MHM + deposition on stainless steel substrates by using EPD | t = single- and/or multilayer sheets | *E. coli*<br>*S. aureus* | (1h, 37ºC) *E. coli* = 41%; *S. aureus* = 26% | Efflux of RNA:<br>*E. coli* = 30 ng $ml^{-1}$<br>*S. aureus* = 38 ng $ml^{-1}$ | - |
| | reduced GONW (RGNW) | MHM + deposition on stainless steel substrates by using EPD + Hr | | | (1h, 37ºC) *E. coli* = 16%; *S. aureus* = 5% | *E. coli* = 43 ng $ml^{-1}$<br>*S. aureus* = 56 ng $ml^{-1}$ | - |
| 108 | GO thin films | MHM + exfoliation by heat + drop-casting onto a cleaned $SiO_2$/Si(100) substrate | t ≈ 1 nm (single-layer) | *E. coli* | Bacterial saline solution spread on films, 2h, dark, RT:<br>GO film = 100%; brGO film = 76%<br>Metabolic activity in brGO film reduced to 86% | - | - |
| | bacterially reduced GO (brGO) | GO film immersed in bacterial suspension, incubator at 37ºC in dark | | | | | |
| 81 | GO-coated cotton fabrics | GO: MHM + sonication<br>+<br>Dip coating via stirring | n/s | *Streptococcus iniae*<br>*E. coli* | Time-dependent reduction of bacterial growth:<br>*S. iniae:* 6h=32%; 12h=14%; 24h=0%<br>*E. coli:* 6h=54%; 12h=38%; 24h=26% | - | - |
| 110 | GO film on indium tin oxide (ITO) surfaces | Not mentioned | n/s | *E.coli* | Growth inhibition.<br>Live-dead staining: = 16% | - | - |
| 101 | GO film | Spin coating of GO solution onto ITO surfaces | n/s | *E.coli*<br>*B. subtilis* | Biofilm inactivity: *E.coli* ≈19.6% *B.subtillis* ≈ 20.8% | - | - |
| 105 | G-coated | G: commercial product | G: t =175 µm | *E.coli* | G-Cu = 0% | G-Cu and G-Ge = | - |

| | | | | | | | |
|---|---|---|---|---|---|---|---|
| | Cu<br>G-coated Ge<br>G-coated $SiO_2$ | G on Cu: chemical vapor deposition (CVD)<br>G on Ge: atmospheric pressure CVD (APCVD)<br>G on $SiO_2$: transferred from the graphene grown on Ge | | *S.aureus* | G-Ge = some bacterial growth<br>G-$SiO_2$ = bacteria growth<br>*S.aureus* cells more susceptive.<br>LIVE/DEAD:<br>G-$SiO_2$ = large amounts of viable cells<br>G-Cu and Ge@<br>Ge = low viable cells | severe membrane disruption and cytoplasm leakage<br>G-$SiO_2$ = no evident membrane destruction | |
| 109 | rGO paper | MHM + Hr + sonication + filtration | n/s | *Bacillus cereus* | Submerged in bacterial suspension in DI water for 1 min = bacterial attachment<br>37ºC, 16h = bacterial growth | - | - |
| 92 | GO surface coating | MHM + dyalisis + 0, 1, 10, and 120 min sonication + Filtering a 2 mL GO suspension (200 µg/mL) on a membrane (0.025 µm) and air-dried | average sheet area = 0.65, 0.29, 0.10, and 0.01 $\mu m^2$ | *E.coli* | Cell viability (3h): 0.65 $\mu m^2$ =73%; 0.29 $\mu m^2$ =61%; 0.10 $\mu m^2$ =50%; 0.01 $\mu m^2$ =30% | Yes | - |
| 86 | GO paper | Spraying GO colloid on a white cellulose chlorine-free Sveto-Copy paper + air drying | n/s | Nonluminiscent and luminescent *E.coli* | Very slow decline in light production = nontoxic. | - | - |
| 106 | graphene-coated $SiO_2$ | Chemical vapour deposition (CVD) graphene grown on Cu + transferred onto $SiO_2$ samples by PMMA assisted method | single layer with wrinkles<br>Area= 1 $cm^2$ | *Halomonas spp.* CAM2 | 72h, 20ºC: few cells | No | Lower expression of adhesion-related genes |

t=thickness; l=length, n/s= not studied, MIC= minimum inhibitory concentration, HM = Hummers method, MHM = modified Hummers method, Hr = hydrazine reduction.

### 5.1.3. Mechanisms for antibacterial effect

The current cytotoxicity studies on GBMs suggest some similarity between graphene and other synthetic carbon nanomaterials. The antimicrobial activity of carbon nanotubes (CNTs) has been found to be the synergy of both "physical" and "chemical" effects[111; 112]. The material characteristics that influence how GBMs physically interact with bacterial cells, such as solubility, dispersion, and size, should strongly influence their antibacterial effects[9].

In general, the dispersibility of GBMs in solutions depends on functional groups on graphene sheets. The carboxyl, hydroxyl, and epoxy groups introduced on graphene sheets form much more stable dispersions. GO can form stable dispersions with small nanosheets, thus offering more opportunities to interact with cells. Comparably, Gt and rGO dispersions are unstable, and contain large particles, and thus, they have fewer chances to mix with cells[9; 75]. In terms of antimicrobial surfaces, the surface chemistry and physical structure of the bacteria as well as the substrate to which the bacteria may attach will determine whether they promote or inhibit bacterial attachment, and subsequent biofilm formation[63]. Below are presented the mechanisms so far proposed for the antimicrobial activity of GBMs. These include: membrane damage, cell coverage, oxidative stress and DNA damage. However, there is still no consensus in regard to the antibacterial mechanisms and further investigations are needed to unravel the exact contribution of oxidative and physical pathways.

A physico-mechanical antimicrobial effect is normally characterized by surfaces with significant roughness or peaks with high aspect ratios which can cause the bacterial cell wall to rupture under its own weight upon contact[63]. In the case of graphene, the edges also fulfil this latter criterion however the basal planes can be considered atomically smooth. Thus, the interaction of bacteria with graphene will be highly dependent on the orientation of the particles exposed on the surface[63]. This is also true in suspension, the orientation of the particles may interact with bacteria in a manner of edgewise contact inducing cytotoxicity.

Indeed, GO and rGO with the sharp edges exposed to contact with the bacterial membrane seem to induce rupture and pore formation[113]. In contrast, the studies which have shown no antibacterial activity tend to involve surfaces with the basal planes at the interface[63; 94]. Thus, there are two possible actions for membrane stress: through GBMs sharp edges, which may disrupt the bacterial cellular membranes and cause leakage of intracellular substances such as DNA; and the basal planes, which may contribute, for example, by destructively extracting membrane lipids[93]. The importance of the basal planes are demonstrated in the Hui *et al.* study[87]. SEM images (Figure 6) performed by Liu *et al.* suggested that cell direct contact with graphene nanosheets disrupted the cell membrane[9]. Loss of cell membrane integrity upon direct contact with the particulate edges when treated with GBMs, namely GO and rGO, was also demonstrated in other works[75; 76; 84; 85; 88; 107]. Severe membrane disruption and cytoplasm leakage of bacteria on graphene films was also reported by Li and co-workers[105]. Cytotoxic effects seem to be greater for Gram+ than for Gram-[81; 89; 105; 107; 114]. This can be explained by the presence of an outer membrane outside a thin peptidoglycan layer in Gram- bacteria which is composed mainly of lipopolysaccharides (LPS) and phospholipids, and protects the bacterial cells from attack by foreign compounds (Figure 7). So despite having a thicker and more rigid peptidoglycan layer, Gram+ bacteria can be more susceptible due to the absence of an outer membrane. In dispersions, some report GO[114] and rGO[88] as more toxic to Gram- bacteria than Gram+. While in films the opposite has been reported[107]. GO-based surface coatings reduce cell contact with sheet edges and enhance interactions with basal planes due to flat sheet stacking[92]. Therefore, the interactions between GO-coated surfaces and bacterial cells are different from those in dispersions, where structure is looser and more undefined.

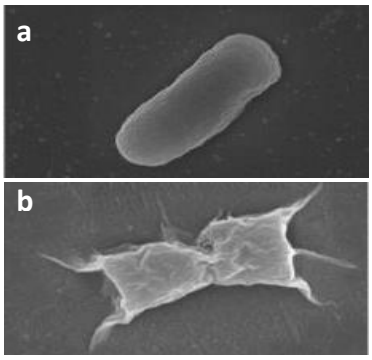


**Figure 6.** SEM images of E. coli after incubation with saline solution without GO (a), and with GO dispersion (40 µg/mL) for 2 h (b). Adapted from Liu et al.[9]

Increasing number of studies have been performed to better understand the mechanisms underlying the interaction between GBMs and cell membranes[93; 113; 115; 116]. The interaction of GBMs with lipid bilayers may lead to direct physical toxicity or adsorption of biological molecules leading to indirect toxicity[49]. Indeed, interaction between GO sheets and lipid bilayers was found to induce a local perturbation of the lipid bilayer. In these simulations, the highest perturbation was observed for GO nanosheets with higher oxidization degree destroying the integrity of the membrane, and the perturbation degree of the lipid membrane increased with increasing the nanosheets edge length[117]. Other simulations have shown that, in order to penetrate the lipid bilayer, contact must be made through the edges of graphene sheets. The sharp, atomically thin edges of graphene sheets induce a spontaneous piercing of the membrane, which decreases the energy barrier for their penetration into the membrane[115]. Tu *et al.* reported that graphene can also destructively extract phospholipids from both outer and

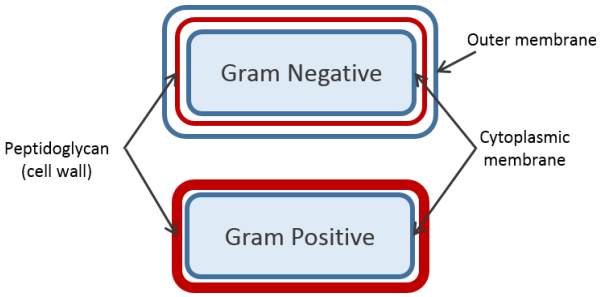


**Figure 7.** Differences between the structures of gram-positive and gram-negative bacteria.

inner membranes of *E.coli* and that the resulting antibacterial activity increased with increasing graphene lateral size and concentration[93].

By comparing GO with GtO, Liu *et al.* showed that, although they have almost the same functional groups, GO dispersion could kill much more bacteria than GtO[9]. And, although rGO shows much stronger oxidation capacity toward GSH, smaller size GO had much higher antibacterial activity than rGO. SEM also indicated that small GO nanosheets can wrap bacterial cells, while large rGO aggregates would trap cells. So the particle size influences directly the cell coverage mechanism. Similar results were obtained in other studies[76]. To address this effect more thoroughly they studied the antibacterial activity of GO sheets differing in lateral size by more than 100 times, and demonstrated that larger GO sheets displayed stronger bactericide activity against *E. coli* than smaller ones[78]. The different sized sheets were prepared through varying the sonication time used to prepare the GO suspensions. Once GO sheets were all well dispersed and their oxidation capacity toward glutathione similar, the lateral size-dependent antibacterial activity was not due to differences in aggregation state nor oxidation capacity. Again, AFM analysis showed that large GO sheets covered bacteria more efficiently, preventing proliferation once fully covered. In contrast, small GO sheets are less efficient in effectively isolating and wrapping bacteria from its surrounding. Using sonication, the bacteria confined by the both small and large GO sheets were released and the viability test confirmed there were no living cells. Similar results were reported by Perreault *et al.*[92]. However it is important to highlight that this entrapment mechanism is only important when testing antimicrobial activity of GBMs in suspension, for surfaces it does not apply[92].

Oxidative stress mediated by GBMs may come from several paths, one is reactive oxygen species (ROS)-mediated oxidative stress, in which oxidative stress is induced by ROS generated by GBMs, and the other possible path is ROS-independent oxidative stress, in which GBMs may disrupt a specific microbial process by disturbing or oxidizing a vital cellular structure or component without ROS production[9]. Direct or indirect generation of ROS leading to oxidative stress in target cells is currently the main mechanism proposed for the toxicity of engineered nanomaterials[118; 119] and it has also been identified as a potential mechanism for GBM's toxicity[116]. Cellular homeostasis is a balance between the level of ROS generation and its elimination or reduction by antioxidant enzymes. The levels of ROS are controlled by enzymes, namely superoxide dismutase (SOD), catalase and glutathione (GSH) peroxidase. When ROS cannot be reduced by cellular antioxidant activity, this may lead to alteration of macromolecules such as polyunsaturated fatty acids in membrane lipids, protein denaturation, and ultimately DNA destruction[49]. Some studies indicate that ROS are generated in a concentration- and time-dependent manner after exposure to GBMs, suggesting an oxidative stress mechanism[69; 76; 77]. On the other hand, ROS-independent oxidative stress can be examined by the *in vitro* oxidation of GSH[78]. In Perrault *et al.* study, GSH oxidation was found to be influenced by the size of GO sheets[92]. As the sheet area decreased from 0.65 $\mu m^2$ to 0.01 $\mu m^2$, GSH oxidation increased from 49 to 71%. The increased oxidative potential of GO as sheet area is decreased likely contributes to the higher antimicrobial activity of small GO sheets, especially in surfaces. ROS production seemed to be higher for GO than for rGO[76; 77; 79] probably due to different physicochemical properties, such as size, conductivity, and functional group in the surface[76]. This was suggested in other study by evaluating GSH oxidation, in which Liu *et al.* reported that the oxidative capacity of GO sheets is not a function of the number of

their edge sites related to their lateral size[78]. ROS production can consequently lead to DNA fragmentation[77; 79] and lipid peroxidation[88], causing cell death. Lipid peroxidation is considered to be the main oxidative pathway leading to oxidative stress in bacterial cells exposed to GO[88], a chain reaction that is initiated by the oxidation of lipid molecules by reactive oxygen species, forming lipid peroxide radicals that will propagate the oxidative damage through the membrane[92]. DNA fragmentation has been reported in some studies, for E.coli[77] and *P. aeruginosa*[79]. Compared to GO, rGO dispersion didn't show significant DNA damage after 24h[79], possibly because it takes longer exposure time or maybe this is not an important mechanism for cell death in the case of rGO. Due to its excellent photothermal properties some report that GBMs can also kill by a photothermal mechanism[120; 121].

## 5.2. Functionalized GBMs

GBMs have also been examined in relation to building new graphene derivatives with different molecules with great potential for application, such as constructing electrochemical devices, energy storage devices as well as catalysts [71], and more importantly, in biomedical applications[55]. Polymer chains, drugs, and targeting molecules can be covalently attached to the graphene surface and edge site, or polymers may be adsorbed onto the graphene surface to alter its properties[122; 123]. Graphene–nanoparticles (NPs) conjugates are explored to achieve the synergistic effects of individual components. Various metals, metal oxides and semiconducting NPs are directly decorated on GBMs sheets with no molecular linkers needed[4]. Also, many types of second phase NPs can be deposited on graphene sheets to confer new functionalities[123; 124]. The functionalization of GBMs affects their interactions with cells and associated toxic effects. Thus, GBMs can be used as carriers for other antimicrobial agents, for example quaternary phosphonium compounds[103], metal and metal oxides NPs[72; 123; 124]. The main approaches for modification of graphene can be performed through physical or chemical processes and grouped in: (a) covalent attachment of chemical moieties through reactions with the π-conjugated skeleton and defects of graphene, and (b) adsorption of various functional molecules and conjugated polymers via noncovalent interactions[63; 122; 124; 125]. The last is due to the introduction of reactive sites or more simply charged groups (functional groups) on the chemically modified graphene which may lead to electrostatic adsorption of oppositely charged (cationic) polyelectrolytes and hence, grafting of polymer chains onto graphene surfaces can occur[2].

These functionalized GBMs have also been applied in antimicrobial studies both in aqueous dispersions and films, discussed in the next sections and summarized on Table A 1 (see APPENDIX).

### 5.2.1. Aqueous dispersions

Xie and co-workers synthesized quaternary phosphonium salts tetradecyl triphenyl phosphonium bromide (TTP) functionalized few-layered graphite (TTP–FGt) by introducing different content of TTP into FGt[103]. TTP–FG with 33.7 wt% of TTP, displayed excellent thermal stability and long-acting antibacterial activity with MICs against *E.coli* and *S.aureus* of 580 μg/mL and 280 μg/mL, respectively, after 72 h soaking, while FGt showed poor antibacterial activity. Cai *et al.* prepared brilliant blue-functionalized reduced graphene oxide (BB-rGO) as

well as water-soluble brilliant blue/reduced graphene oxide/tetradecyl triphenyl phosphonium bromide composite (BB-rGO-TTP) suspended in Mueller-Hinton broth medium[126]. They possessed antibacterial activity attributed to membrane damage and, in the later, also to TTP release and reaction with cytoplasmic constituents. However, the authors didn't study the effects of rGO alone. Methanol derived graphene (MDG) was synthesized by Pandey's group, and they also loaded it with antibiotic gentamicin sulfate[127]. *E.coli* viability loss was 43.5% when treated with 40 µg/mL of MDG for 2h, and 82.2% when loaded with the antibiotic. In another study, based on the zone of inhibition created, a chloro phenyl grafted graphene (CBG) was found to be more than twice as effective as unmodified G and GO, to *E.coli* and *S.aureus* [128]. It combined the antibacterial effects of G with the chlorine atom of the grafted group which caused damage of the DNA of bacteria. In another work with graphene, Kavitha *et al.* decorated graphene with zinc oxide (ZnO) NPs which exhibited excellent photocatalytic activity, with potential for an electrochemical glucose biosensor[129]. The complete inhibition of *E. coli* at a concentration of 3 mg/ml ZnO-G in medium was attributed to graphene effects, however ZnO NPs control was not used. Cai and co-workers produced sodium 1-naphthalenesulfonate-functionalized rGO (NA-rGO) and NA-rGO decorated with silver nanoparticles (Ag-NA-rGO) dispersed in sterile 0.8 wt.% saline water for antibacterial tests[130]. With a concentration of NA-rGO approximately 1000 µg/mL, the sterilizing rate against *E. coli* and *S. aureus* was 7.5% and 11.2%, respectively. The antibacterial activity of Ag-NA-rGO increased compared to NA-rGO and to polyvinyl pyrrolidone (PVP)-stabilized AgNPs, suggesting a synergistic antibacterial effect: the "blade-like edges" of rGO that damage the cell membrane, and make the $Ag^+$ react effectively with cytoplasmic constituents. In fact, Ag NPs have attracted particular interest and have been used in several studies to decorate or functionalize GBMs. Ag-GO has demonstrated enhanced antibacterial activity compared to pure GO and pure Ag NPs[80; 100]. Hence, demonstrating again a synergetic effect on antibacterial activity when combining GO with Ag NPs. Identical results have been obtained for rGO-Ag[89; 95; 131; 132; 133] and Ag-G[134]. However in some of the works with AgNPs, GO[97; 135] and rGO[133; 136] used as control didn't show significant antibacterial effect, while the conjugates showed strong antimicrobial activity[97; 102]. Das *et al.* showed that, when GO was placed in the center of a nutrient media plate previously inoculated with *E. coli and P. aeruginosa* bacteria, a growth inhibition zone was not formed. Alternatively, when Ag-decorated GO was used, a clear inhibition zone was formed[97]. They produced again AgNPs-GO but using citrate as a stabilizing agent to prevent agglomeration of the AgNPs and found AgNPs-GO suspension to have considerable effect on membrane leakage of reducing sugars and proteins compared to AgNPs and GO alone and to be more effective against *S. aureus* than *B. subtilis*[137]. In a different strategy, Zhang *et al.* used gelatin as a "green" reducing agent for $Ag^{2+}$ ions to form AgNPs of size about 100 nm[99]. The positively charged amino groups of the gelatin stabilised AgNPs were then mixed with a GO suspension and electrostatically attracted to the negatively charge groups on the GO surface. Ag-GO showed concentration-dependence for the growth inhibition of *E. coli* with as little as 10 ppm required to reduce growth by 99.9% (the corresponding GO reduced growth by 38%). Kumar and co-workers reported that smaller sized AgNPs (24 and 38 nm) decorating the GBMs were able to inhibit *E.coli* more effectively, due to their high specific surface area and ready cell penetration, while functional GO (FGO) didn't reduce bacterial growth[138]. In another study, Ag-GO exhibited stronger antibacterial properties against Gram-bacteria (*Salmonella typhi* and *E. coli*), effectively inhibiting growth at 6.25 µg/ml, while failing

to inhibit Gram+ bacteria (*S. aureus* and *S. epidermidis*)[139]. In this work Ag-GO presented better antimicrobial effect than AgNPs and GO alone. Similar results were obtained with poly (diallyldimethylammonium chloride) (PDDA)-protected Ag–rGO achieving 100% disinfection rate of *E.coli* at 50 μg/mL[140]. Ag-polydopamine (PDA)-GO has also shown to fully inhibit growth of *E.coli* and *B.subtilis* in LB-agar plates containing 1% (v/v) Ag-PDA-GO, however no conclusions can be taken since no controls were used for the assessment of the antibacterial activity[124]. Shen and co-workers studied the antimicrobial activity of Ag-rGO towards Gram+ *S.aureus*, Gram- *E.coli* and fungi *Canidia albican*[141], with a concentration of 50 μg/mL achieving approximately 100% disinfection rate for all. Consistently, in another study MIC value of $Ag_xO_y$-rGO for *E.coli* and *S.aureus* was 62,5 μg/mL[132]. In another study, MIC values of Ag-rGO against *E.coli* were 5 and 10 μg/mL for 5 and 3h respectively, while rGO alone didn't show detectable inhibition in LB medium[136]. Ag-rGO antibacterial effects to *P. aeruginosa* have also been demonstrated with a minimal bactericidal concentration (MBC) of 15 μg/ml[133]. Nguyen at al. reported identical results for *Bacillus cereus*, *Listonella anguillarum*, *E. coli*, and *S. aureus* with lower MIC values (0.04, 0.08, 0.16, and 0.16 μg/ml) for the sample with highest Ag content[142]. Different toxicity values can be due to different antimicrobial tests, for example different incubation times, ranging from 5 to 24h. Conjugating GO with two different nanoparticles, Tain *et al.* decorated GO surface with both iron oxide nanoparticles (IONPs) and AgNPs, combining antibacterial properties of Ag, photothermal killing of GO, and the magnetic properties of IONPs for magnetic separation and recycling of materials[120]. Similarly, water-dispersible 2D assemblies of Au–Ag NPs were obtained through a selective Ag deposition on preassembled gold nanoparticles on bovine serum albumin (BSA)-coated graphene oxide (BSA-GO)[123]. This GO@Au@Ag conjugate exhibited enhanced antibacterial activity against *E.coli* compared to BSA-GO and AuNP-decorated BSA-GO attributed to the increased local concentration of AgNPs, with GO only serving as a platform for AgNPs[123]. Similarly, in order to improve the stability of AgNPs, a polyethyleneimine-modified rGO (PEI-rGO) was used as the substrate of AgNPs[143]. Improved antibacterial activity compared to polyvinyl pyrrolidone (PVP)-stabilized AgNPs (PVP-AgNP) and PEI-rGO was observed, and the AgNPs on PEI-rGO were more stable than the AgNPs on PVP, resulting in long-term antibacterial effects. Excellent water-solubility of nanocomposite and lower cytotoxicity (towards CNE1 cells), suggests a potential application as a sprayable graphene-based antibacterial solution. Li's group combined the advantages of rGO, β-cyclodextrin (CD) and Ag on antibacterial activity, and obtained a hydrophilic rGO–CD–Ag supramolecular hybrid with stronger antibacterial activity (rGO–CD–Ag > Ag–CD > rGO–Ag > Ag > rGO–CD)[144]. In a different strategy, Ocsoy *et al.* developed DNA-directed Ag NPs grown on GO and found it effectively decreased *Xanthomonas Perforans* cell viability in culture and on plants[145]. At a very low concentration of 16 ppm, Ag@dsDNA@GO showed excellent antibacterial capability. Despite GO alone didn't show significant cell death, it interacted with cell membrane and contributed to the increase in antibacterial activity compared to AgNPs.

There are many studies reporting a photocatalytic killing mechanism of functionalized GBMs. Liu *et al.* functionalised GO surface with $Ag_3PO_4$ NPs and found that *E. coli* was completely killed in the presence of bare $Ag_3PO_4$ and the GO–$Ag_3PO_4$[146]. The mechanism of action was suggested to be the oxidative stress upon exposure to visible light. Identical photocatalytic effect was reported for GO–$TiO_2$ nanorod composites (GO–$TiO_2$ NRCs), with GO sheets entirely covered by $TiO_2$ NRs[147]. While GO sheets presented low toxicity to *E. coli*, GO–$TiO_2$ NRCs presented high antibacterial activity under solar irradiation, totally inactivating *E.*

*coli* after 2 h. Similar results were obtained by Cao *et al*., who reported the optimization of the GO content in GO-$TiO_2$[148]. $TiO_2$/4.2 wt% GO sample exhibited the best photocatalytic antibacterial activity under ambient visible light. Antibacterial photothermal treatment has also been demonstrated for rGO functionalized with magnetic NPs (MRGO) and MRGO functionalized with glutaraldehyde (GA) (MRGOGA)[121] due to GA high bacteria capturing capability and rGO light to heat conversion ability.

The combination with inherently antibacterial polymers such as those containing quaternary ammonium groups (like chitosan) has proven highly useful. Ko *et al.* performed a noncovalent functionalization of chitosan on rGO, which showed enhanced antibacterial activity for *E. coli* compared with GO, suggesting that noncovalent chemistry can minimize any detrimental effects on the bioactivity[149]. In a different work, Sreeprasad and co-workers produced GO/rGO with different anchored materials: native lactoferrin (NLf), NLf protected Au clusters (Au@NLf) and chitosan (CS), and tested their antibacterial activity against *E. coli* [125]. All materials showed antibacterial activity but rGO/GO-NLf-CS and rGO/GO-Au@NLf-CS showed several folds higher antibacterial activity than the parent GO/rGO due to the synergetic effect of the combination of lactoferrin and chitosan (GO≈rGO < GO/rGO-Lf < GO/rGO-Lf-CS≈ rGO/GO-Au@NLf-CS). In a different work, Li and co-workers synthesized a polyethylene glycol (PEG) and polyhexamethylene guanidine hydrochloride (PHGC) dual-polymer-functionalized graphene oxide (GO) (GO-PEG-PHGC) and the evaluation of the antibacterial effect towards *E.coli* and *S.aureus* showed enhanced activity compared to GO, GO-PEG or GO-PHGC alone (GO-PEG-PHGC > GO-PHGC > GO > GO-PEG)[150]. In another study, carboxylated graphene oxide complexes (GO-COOH) with lanthanum(III) (GO–La) showed good inhibitory effect under the concentration of 1.0 mg/mL for *E.coli* and *S.aureus*[151]. Besides antibacterial, GO-La presented anticoagulation properties. Poly-L-lysine (PLL) is a cationic polyelectrolyte and has also been used to construct a graphene oxide-polymer material[152]. Some *et al.* reported antibacterial activity of the conjugate towards *E.coli*, as well as the promotion of the growth of human cells (adipose-derived stem cells). This study showed that there was no antibacterial activity of unmodified GO, which can be explained by the fact that, as with previous studies, the surfaces formed by sample precipitation were essentially arranged in a flat conformation and hence, edges were not exposed or because tests were performed in LB broth and it has been indicated that colloidal GO has a direct effect on bacterial proliferation when added to liquid media[94]. However, GO-PLL showed potent antibacterial activity. The relatively highly cationically charged surface was speculated to be the mechanism inhibiting attachment. The group also modified the composite to boost the amount of cationic charges through covalent attachment of a diazonium salt which resulted in a decrease in cell adherence and death. Similarly, poly-l-lysine/rGO/copper nanoparticles hybrid (PLL–rGO–CuNPs) presented higher killing rate than PLL-rGO for both *E.coli* and *S.aureus*, with MIC values decreasing in the order: rGO>PLL-rGO>PVP–CuNPs>PLL–rGO–CuNPs[153]. The antibacterial activity can be explained by combining the effect of PLL–rGO to adsorb and damage the cytoplasmic membrane of the bacterial cell, with the $Cu^{2+}$ reaction with cytoplasmic constituents. Polyvinyl-N-carbazole (PVK) has inherent antibacterial characteristics and has also been used to form GO conjugates[101; 110; 154]. Carpio *et al.* investigated the effects of PVK-GO on both planktonic microbes and biofilms, but also against NIH 3T3 fibroblasts[101]. The antibacterial effects were evaluated against two Gram- (*E. coli* and *C.metallidurans*) and two Gram+ (*B. subtilis* and *R. opacus*) bacteria. The results showed the PVK-GO nanocomposite to have 30% higher antimicrobial potency than

GO, due to the increased dispersion of GO. In suspension, the nanocomposite effectively encapsulated bacteria, causing reduced microbial metabolic activity and cell death. In parallel, PVK-GO did not show any significant cytotoxicity to fibroblast cells. In another study the E.coli growth inhibition was in the order GO-PVK > GO > PVK[110].

### 5.2.2. Films

Again, many of the studies mentioned above also investigated the same particles in substrates[94; 101; 125; 152]. Ag-decorated GO films, but not bare GO films, showed strong antibacterial activity against *E. coli* [80; 94; 95]. Ruiz *et al.* didn't detect growth inhibition with GO film but Ag-decorated GO showed large growth inhibition zones[94]. The diameter of inhibition zone for AgNP-GO paper was almost 100% larger than that observed with GO, for both *E. coli* and *S. aureus*[114]. Tai and co-workers decorated rGO by in situ polymerization of acrylic acid monomers, to generate poly(acrylic acid) (PAA)-grafted rGO[155]. The PAA-grafting not only realized the dispersion in aqueous solution of rGO but created a distribution of negative charges on the surfaces of rGO, thus favouring subsequent high quality Ag/rGO-g-PAA nanohybrid formation. The formation of a clear zone inhibition showed that Ag/rGO-g-PAA was effective in inhibiting bacterial growth, attributed to Ag ions diffused after Ag/rGO-g-PAA absorbing water and swelling. In another work, a free-standing paper composed of a polyoxyethylene sorbitan laurate (TWEEN)/ rGO hybrid tested against Gram+ *Bacillus cereus* showed no bacterial attachment nor growth, contrarily to rGO paper[109]. Kumar' group fabricated a porous carbon foam (CF) electrode modified with rGO-Ag to purify water[89]. It could perform as an antibacterial device by killing pathogenic microbes with the aid of a 1.5 V battery, with very little power consumption. The mechanism for the antibacterial activity can be either or the combination of production of ROS by rGO–Ag–CF, contact killing through device–microbe interaction and an electric field effect. Kholmanov and colleagues fabricated a complex transparent conductive film (TCF) composed of Au NPs, 1D Ag nanowires (NWs), and 2D rGO platelets, by consecutive spin coatings, that completely inactivated *E.coli*[156]. The toxicity of the hybrid films can be ascribed mainly to the rGO since it is the top layer and in direct contact with the bacteria. Polymers with inherent antibacterial characteristics have been used to form GBMs composite films, like polyvinyl-N-carbazole (PVK). Santos *et al*. fabricated PVK-G in solution and thin films[154]. The antimicrobial properties of PVK-G films, as well as solution conjugates, were investigated for *E.coli* and *B.subtilis*. Bacterial viability, metabolic activity and live/dead assays all showed fewer viable and active bacteria than after exposure to either PVK or G alone. The nanocomposite also supressed biofilm suppression. The improved antibacterial activity can be explained due to a better dispersion of graphene in the presence of PVK. The conjugates also presented some toxicity to NIH 3T3 cells, showing a slight decrease (≈ 80 % cell viability). Similarly, Carpio *et al.* investigated PVK-GO films and reported 57% higher biofilm inhibition and inactivity than GO alone for both Gram- *E. coli* and Gram+ *B.subtillis*[101]. *E.coli* biofilm inhibition by PVK-GO films was also reported to be higher than in GO film in another study[110]. Akhavan and Ghaderi produced a GO surface by depositing GO on anatase $TiO_2$ thin films and studied the UV-visible light-induced photocatalytic reduction of the GO platelets of the GO–$TiO_2$ thin films immersed in ethanol for different irradiation times[157]. After photocatalytic reduction for 4 h, the antibacterial activity towards *E.coli* of the rGO-$TiO_2$ thin film was improved by a factor of about 7.5 relative to the activity of the bare

$TiO_2$ thin film. Here, the antibacterial effect of GO alone was not studied and the enhanced antibacterial effect was attributed to the better reduction of the GO (better conductivity of the platelets and so more accumulation of the photo-excited electrons on them) which results in the better photocatalytic performance of the $TiO_2$ thin film. In a different method, Wang *et al.* used GO in a controlled drug release system. They fabricated GO–benzylpenicillin (BP) anion intercalated Mg–Al layered double hydroxide (GO–BP-LDH) hybrid films with enhanced synergistic antibacterial effect compared with single GO film, which can be attributed to the combination of the antibacterial activity of GO and BP anions released from the system[158].

### 5.2.3. Mechanisms for antibacterial effect

In general, cytotoxic effects also seem to be greater for Gram- than for Gram+[96; 114; 139; 142; 153]. However some report the opposite[103; 130]. Ag-GO nanocomposite functioned as a bactericide against the *E. coli* through disrupting bacterial cell wall integrity, whereas it exhibited bacteriostatic effect on the *S. aureus* by dramatically inhibiting cell division. GO[48100; 123; 145] and rGO[95] sheets and Ag nanoparticles when combined show a synergetic effect on antibacterial activity. A possible mechanism for the antibacterial activity of Ag-GO involves the adsorption and gathering of bacteria onto the surface of water-soluble GO sheets, which may enhance the interaction between bacteria and Ag nanoparticles on GO sheets, and then Ag nanoparticles damage the bacterial cell wall by contact[80; 97; 139; 146]. Additionally, the use of GBMs prevent the aggregation of AgNPs and increase their local concentration in the vicinity of bacteria[123]. Ma *et al.* also reported that the significant decrease of the negative charges of Ag-GO compared to GO nanosheets facilitated strong contact between the cell membrane of the *E.coli* bacteria and Ag-GO [100]. Thus, GO, besides serving as a functional material, can act as a coating material for living cell due to its sheet-like structure that lacks in AgNPs alone. Ag-GO can then break the permeability of bacterial outer membrane, stimulate the leakage of membrane constituents, resulting in cell putrefaction and death[114; 137]. Similarly, rGO can prevent AgNPs aggregation and the bacterial cells can be adsorbed onto the rGO surfaces[95; 136; 140]. rGO was also the responsible for the antibacterial activity of some other type of conjugates[153; 156]. In the cases where GBMs alone don't show significant antibacterial activity, the decorating particles are the main responsible for the effects observed[138; 147; 155]. Moreover, in many studies the killing mechanism was attributed to a photocatalytic treatment[120; 121; 146; 147]. Synergetic effects are mentioned in studies with other decorating molecules[128]. Oxidative stress and membrane damaged are also hypothesis for the antimicrobial mechanisms of functionalized GBMs[89; 101; 120; 129; 145; 153; 156], however very few studies actually further investigated the antimicrobial effects causes[89; 101; 120].

## 6. Composites containing GBMs

The discovery of graphene's extraordinary physical properties and ability to be dispersed in various polymer matrices has created a new class of polymer composites with GBMs as fillers. GBMs incorporation can significantly improve physical properties of host polymers even at extremely small amounts[2]. The production methods, characterization techniques, properties and applications of these graphene-based polymer composites have been extensively reviewed in the literature[1; 2; 3; 4; 159]. The properties of these composites depend strongly on

how well the GBMs are dispersed. This can be hindered by the restacking of the flat sheets, especially after chemical reduction. Restacking can be prevented by the use of surfactants/dispersants that can stabilize the reduced particle suspensions, by blending with polymers prior to the chemical reduction, or even by performing chemical reduction in situ in the presence of the polymer, which may result in polymer degradation[2]. To achieve phase compatibility, functionalization of the filler surface or polarization of the polymer matrix by the addition of compatibilizers can also be done[159]. Graphene composites can be produced via solvent blending consisting on blending with organic solvents followed by solvent removal, melt blending which involves mixing polymer melt and filler (in a dried powder form) under high shear conditions, in situ polymerization which involves mixing of GBM-filler in a solution of the monomers followed by polymerization, and through covalent bonds between polymer matrix and GBM-filler[3]. The use of melt blending has been hampered due to the thermal instability of most chemically modified graphene and comparing with solvent blending, the last produces better dispersion[2]. However, it's the method that allows a more economical production in large scale using melt extrusion, and solvent blending has the disadvantage of using organic solvents. Electrospinning and electro-deposition are two other approaches used to prepare composite nanofibers and nanocomposite films, respectively[1]. Thereby, some challenges need to be overcome to produce GBM-based polymer composites, namely the homogeneous dispersion of GBMs with minimal restacking, and the effective blending of GBMs with polymer matrix[4].

The incorporation of GBMs into polymeric chains has been used to improve their mechanical, thermal or electrical properties. GBMs addition has been reported for several polymers including natural polymers, like chitosan[160], cellulose[161] and poly (lactic acid) (PLA)[162], and synthetic polymers, including polystyrene (PS)[163], poly(vinyl alcohol) (PVA)[164], poly(ethylene) (PE)[165], poly(N-isopropylacrylamide) (PNIPAM)[166], polypropylene[167] poly(propylene carbonate) (PPC)[168] and polyurethane (PU)[169] among many others[1; 2]. Having in regard the purpose of this work, next the focus will be on polyurethane (PU) composites.

## 6.1. PU/GBMs Composites

In terms of polyurethane (PU) composites, GBMs have been used to improve mechanical[169; 170; 171], electrical[169; 172; 173] and thermal properties[169; 174]. Jingling *et al.* developed a PU/GO composite for anterior cruciate ligament tissue engineering, through solvent blending and with 0.3%wt GO[170]. The GO particles were uniformly distributed inside the PU matrix, but with some extent of agglomeration. GO increased the strength of the composite, attributed to the GO induced heterogeneous crystal increasing and the interaction between the GO and PU due to the hydroxyl group on GO surface. Besides, it presented good biocompatibility. Recently in another study, 0.8wt% weight ratio of G to waterborne polyurethane (WPU) was considered the optimum value for obtaining well-dispersed G/WPU composite, which was then used as a coating for cotton fabrics[174]. The fibers of the fabric showed a compact and homogeneous distribution of GNPs, rough surface, and increasing numbers of irregular graphene wrinkles and protuberances. Kim *et al.* prepared Graphene/Polyurethane composites and compared GBMs obtained via 2 different processes: chemical modification (isocyanate treated GO, iGO) and thermal exfoliation (thermally reduced GO, trGO); and 3 different methods of dispersion: solvent blending, in situ polymerization, and melt compounding[175]. They concluded that

solvent-based blending techniques are more effective in distributing GBMs in the polymer matrix and found that the resistance of the composite started to decrease at 0.3 vol% trGO (about 0.6 wt%). This reflects in the number of works using solution mixing methods[170; 171; 172; 176]. However, other methods, especially *in situ*-polymerisation are receiving much adherence[177; 178]. Raghu's group suggested that 3 parts of graphene per 100 parts of WPU can be the optimum composition in the production of WPU/G composites[172]. Bian and co-workers produced microwave-exfoliated GO-thermoplastic polyurethane (MEGO-TPU) composites via melt blending followed by injection molding and reported that thermal, conductive and mechanical properties were enhanced by GO incorporation[169]. They found MEGO effectively dispersed when at low contents, however higher MEGO content (> 4.0 wt%) resulted in aggregation and thus couldn't provide the optimum reinforcement. To attain better dispersions and avoid GBMs aggregation, there are various strategies including high-shear force/sonication, use of surfactants, and functionalization with stabilizers[173; 176; 177]. For example, no significant re-stacking of rGO in PUR composites containing PVP was found even for 2 wt% of rGO loading[176].

# 7. Antimicrobial activity of composites containing GBMs

The incorporation of GBMs in polymer matrixes has been shown to reduce bacterial cell viability, conferring the material antibacterial properties, explained by GBMs direct damage on bacterial cell membrane[98]. The effectiveness of the antibacterial action depends on the type and amount of incorporated GBM, as well as on the material fabrication technique. A summary of the effects of composites containing GBMs on bacteria can be consulted in Table 3. Jin and co-workers explored the use of GO as a reinforcement in polyethylene (PE) matrix for application in biomedical catheter materials[179]. PE-modified graphene oxide nanocomposite with 2-(methacryloyloxy)ethyl phosphorylcholine (PE-GO-MPC) was synthesized via melting intercalation and showed bacteriostatic activity to *E.coli* and *S.aureus,* as well as improved anticoagulant property compared to PE. The antibacterial activity was explained by the inactivation of the adhered bacteria due to GO, and by the large number of $–COO^-$ which adsorbed the cytoplasm of bacterial cells and engendered flocculation, thus preventing the cells from the normal activities and killing bacteria. Furthermore, the tensile strength and elongation of PE-GO-MPC nanocomposites were enhanced by 15.5 and 97.3%, respectively. The antibacterial activity of graphene-based chitosan (CS) films was screened against *P.aeruginosa*, where bacterial growth was completely inhibited by CS-rGO independently on the concentration and size of rGO[98]. Interestingly, the CS-GO, for both the small area GO and large area GO, failed to manifest complete antibacterial property compared with the CS-rGO, which can be explained by the more sharpened edges of rGO[107]. Since CS, rGO and GO alone didn't show significant growth inhibition, a symbiotic effect between chitosan and GBMs was confirmed. Moreover, large area GO proved to be a better filler for chitosan film than small area GO in terms of thermal and mechanical tensile properties. Similarly, Mazaheri and colleagues produced GO–CS film with various GO contents from 0 to 6 wt%, increasing the strength and elastic modulus by ∼80% and 45%, respectively[180]. All these films, including GO films, showed significant antibacterial activity (>77% inactivation after only 3h) against *S.aureus*. The antibacterial activity increased by increasing the GO content, as well as the surface roughness parameter which increased by a factor of >15 with 6 wt% GO. Lu *et al.*

reported for the first time the use of graphene in wound healing to confer antibacterial properties to chitosan–PVA nanofibers[181]. Antimicrobial effects of CS-PVA nanofibers membranes containing graphene were reported for *E. coli* and *Agrobacterium* (prokaryotic cells), but not for yeast cells (eukaryotic cells). Thus, a mechanism was proposed to explain the wound healing and antimicrobial effects: when cells meet graphene, it is easy for an electron to escape from graphene and move into the cells due to the potential of the cell membrane. For eukaryotic cell it is hard for an electron to enter the nucleus through the nuclear membrane, however a prokaryotic cell does not possess this membrane, and thus electrons can reach the genetic material. Similarly, polyvinylidene fluoride (PVDF) nanofiber membranes containing 0.2 wt.% of GO in the PVDF electrospinning solution had a disinfection rate over 95% of *E.coli* and *Bacillus*[182]. GO-based nanopaint for corrosion resistance and antibacterial applications was developed by Krishnamoorthy *et al*.[90]. Viable cells on painted surfaces were reduced by 76%, 73%, and 69% after 24h, and 94%, 88%, and 85% after 48h of incubation for *E. coli*, *P. aeruginosa*, and *S. aureus*, respectively. This study suggested that GO nanopaint inhibited the growth of all the tested bacterial strains and long-time exposure increased the death rate. Again for wound dressing application, Fan and co-worker prepared hydrogels by crosslinking of Ag/graphene composites with acrylic acid (AA) and N,N'-methylene bisacrylamide (BIS) at different mass ratios Ag/GO weight ratio (0.5, 1 and 5)[183]. The optimal Ag to GO mass ratio of 5:1 (Ag5G1) exhibited stronger antibacterial towards *E.coli* and *S.aureus* abilities than other hydrogels (Ag5GO1 > Ag1GO1 > Ag0.5GO1 > Ag0GO1). Higher AgNPs loading and size lead to better antibacterial effect, still they didn't study the addition of Ag NPs alone in the hydrogel. As hypothesized in other works, graphene prevents AgNPs aggregation and allows their integration on its surface, however the antibacterial mechanism was not further investigated. Meanwhile, Ag5GO1 hydrogel exhibited excellent biocompatibility, high swelling ratio, and good extensibility. Graphene nanosheets (GNs) together with methylated melamine grafted polyvinyl benzylchloride (mm-g-PvBCl), a polymeric biocide, were used as additives in poly(vinyl alcohol) (PVA) by Cao and co-workers[184]. Films of this composite (G/PVA-biocide) showed increased antimicrobial activity with increase in concentration of biocide, with the control G/PVA not showing any antibacterial activity. In this work the toxicity effects of graphene were not considered and was used only in view of mechanical reinforcement. The incorporation of GBMs in polymer for increased antimicrobial properties is still a very raw field that holds great promises for the future.

## 7.1. PU/GBMs Composites

There are very few studies reporting the reinforcement of polyurethane with GBMs to confer antibacterial properties[104; 185]. An *et al.* produced GO reinforced polylactic acid/polyurethane (PLA/PU/GO) composite films to which GO provided good antibacterial activity against both *S.aureus* and *E. coli*[185]. The incorporation of 5wt% GO reduced bacteria growth up to 100%. Moreover, SEM images of fracture surfaces showed that in the case of the PLA/PU film, the surface of the individual PU particle is relatively smooth, while for the PLA/PU/GO (0.5%) film, the surface of the individual PU particle is wrapped by layer-stacked GO sheets. This is explained by the liquid-phase mixing method (solvent blending) used and, since PU molecule chains contain plenty of N-H groups and GO sheets contain many oxygen-containing groups, when PU is mixed with GO sheets they will preferentially stick together due

to the strong interactions, as a result PU particles are wrapped by GO sheets. In another work, hyperbranched polyurethane/sulfur nanoparticles decorated rGO (HPU/SRGO) composite was prepared with 0.5, 1 and 2 wt% of SRGO, with enhanced mechanical properties as well as microbial inhibitory effects against *S.aureus*, *E.coli* and *Candida albicans,* inhibiting the growth rate and causing membrane disruption[104].

**Table 3** - Effects of GBMs composites on bacteria.

| Ref | Material | GBM production method | Composite production method | Properties | Investigated Bacteria | Cell viability | Membrane damage |
|---|---|---|---|---|---|---|---|
| 179 | PE/GO-MPC films | GO: Modified Brodie method + sonication<br>GO-MPC: GO and MPC dispersed in water + 30min sonication | Melting intercalation: premixed PE and GeneO-MPC were blended with Haake torque rheometer + two-roll mill at 130ºC, 5 min with the thickness of 1 mm | GO: Size=0.5µm x 1.5µm; t= 1–1.2 nm.<br>GO-MPC: t≈ 1nm | *E. coli*<br>*S. aureus* | PE/GeneO-MPC (0.2wt%) ≈ no activation of adhered bacteria | - |
| 98 | chitosan/small area rGO and chitosan/large area rGO | Small area GO: Hummer's method from graphite powder<br>Large area GO: simplified Hummer's method from graphite flakes<br>rGO: GO reduced by NaOH | Drop-casting technique to produce a thin film: rGO incorporated in chitosan solution and then casted onto a hydrophobic petri dish, left to dry and peeled off as a composite film. | small area GO: area<50 µm$^2$; lateral size=5µm<br>large area GO: area≈7000 µm$^2$; lateral size=100µm | *P.aeruginosa* | CS/rGO film =0%<br>independent on the concentration and size of rGO.<br>CS/GO failed to manifest complete antibacterial property compared<br>with the CS/rGO | - |
| 181 | Chitosan (CS)-PVA nanofiber membrane containing G | Micromechanical cleavage: highly oriented pyrolitic graphite peeled using Scotch tape | A PVA-DW solution mixed with a CS solution and stirred for 30 min at RT-A + G and DMF addition, ultrasound stirring treatment at RT-A for 30 min + Electrospinning | G: few layers<br>Nanofibers diameter ≈ 120 nm | *E. coli*<br>*Agrobacterium*<br>Yeast | *E. coli* and *Agrobacterium* = limited number of cells near the membrane<br>Yeast = no difference | - |
| 180 | Graphene oxide (GO)–chitosan layers | MHM + 1h ultrasonication | Dissolving Ch in acetic acid solution + GO suspension slowly added during a vigorous stirring + 10min ultrasonic bath + 2h stirring + solution-casting method | GO:<br>l ∼1µm<br>t <1nm<br>GO-Ch layer:<br>t∼200–500 nm | *S.aureus* | Bacterial viability (3h) ≈ 16-23% | - |
| 90 | graphene oxide (GO) nanopaint | GO: MHM | Incorporating GO sheets in an alkyd resin using ball milling. | n/s | *E.coli*<br>*S.aureus*<br>*P. aeruginosa* | Viable cells,24 h: *E. coli* = 24%; *S. aureus* = 69%; *P.aeruginosa* =73%<br>48 h: *E. coli* = 6%; *S. aureus* = 15%; *P.aeruginosa* =12% | - |
| 185 | PLA/PU/GO composite films | MHM + ultrasonification | Liquid-phase mixing and casting: PLA and PU dissolved into the GO suspension with ultrasonication and stirring + Casting the suspension onto a Si wafer, evaporating organic solvents, drying at 60ºC for 24 h, and peeling. | n/s | *E.coli*<br>*S.aureus* | PLA/PU<br>24h: *E.coli* = 6%; *S.aureus* = 2%<br>PLA/PU/GO (5wt%GO)<br>24h = 0%<br>4h: *E.coli* = 9%; *S.aureus* = 11%<br>PLA/PU/GO (3wt%GO)<br>24h: *E.coli* = 0%; *S.aureus* = 1%<br>4h: *E.coli* and *S.aureus* = 46% | Yes |
| 104 | hyperbranched PU/ sulfur nanoparticles decorated RGO HPU/SRGO | thiosulfate solution + GO (MHM + ultrasonication) solution + 30min sonication + lemon juice and 60min stirring + 10min sonication | *in-situ* polymerization:<br>Pre-polymer: PCL, BD and dispersion of SRGO in DMAc in flask with xylene + TDI addition, 3h + monoglyceride of castor oil addition, 110ºC, 2.5h | n/s | *E.coli*<br>*S.aureus*<br>*Candida albicans* | HPU/SRGO2 (2wt%SRGO)= growth and fouling inhibition | Yes |
| 183 | Ag/Graphene Polymer Hydrogel | GO: MHM + 1h sonication + glucose addition as reducing agent<br>+ ammonia in $AgNO_3$ solution<br>Ag/GO weight ratio (0.5, 1 and 5) = Ag0.5GO1, Ag1GO1 and Ag5GO1 | in situ polymerization: crosslinking of Ag/graphene composites with acrylic acid (AA) and *N* , *N* '-methylene bisacrylamide (BIS) + Dispersion poured into a petri-dish, 65 ºC for 4 h. And then peeled off. | Ag NPs average size = 11.5-39.0 nm | *E.coli*<br>*S.aureus* | Ag0GO1 and Ag0.5GO1= poor antibacterial activity<br>Ag1GO1: E.coli = 0; S.aureus = 2 colonies<br>Ag5GO1= 0 colonies<br>Inhibition zone: Ag1GO1 and Ag5GO1 > Ag0GO1 and Ag0.5GO1 | - |
| 184 | Graphene Reinforced Poly(vinyl alcohol) Films | Expandable graphene (EG) (100nm thick): commercial product + Microwave irradiation, 15s + Blending + Ultrasonic bath at 65ºC for 6h | PVA and biocide (qPvB/Cl−)dissolved and mixed together thoroughly in DMF at 80ºC + Mix with graphene + Casting method | t = 0.1mm | *E.coli*<br>*S.aureus* | *E.coli*<br>G/PVA-(1% biocide)= 8%%<br>G/PVA-(5%biocide)=4.2%<br>G/PVA-(10% biocide)=2.9%<br>*S.aureus* | - |

| | | | | | | | |
|---|---|---|---|---|---|---|---|
| | graphene/PVA-biocide | | | | | G/PVA-(1% biocide)= 7.7%<br>G/PVA-(5%biocide)=0.4%<br>G/PVA-(10% biocide)=0.3% | |
| 182 | polyvinylidene fluoride (PVDF) nanofiber membranes containing GO | HM | Preparation<br>of PVdF polymer solution in a mixture of acetone and DMAc + Electrospinning | mean pore-size: 0.28-0.35 µm<br>t= 36-62 µm | *E.coli*<br>*S.aureus* | Removal rate (2h):<br>*E.coli:* GtO powder = 90.4%; 1mg/mL GO =93.3%; 2mg/mL GO =99.6%<br>*S.aureus:* GtO powder= 99.5%; 1mg/mL GO=98.9%; 2mg/mL GO=95% | - |

t=thickness; l=length, n/s= not studied, HM = Hummers method, MHM = modified Hummers method, Hr = hydrazine reduction, RT-A = room temperature in air.

# CHAPTER III:
# Materials and Methods

## 1. Materials Production

### 1.1. Graphene Nanoplatelets (GNPs) Powders

#### 1.1.1. Graphene Nanoplatelets (GNPs)

In this work the GBMs used were graphene nanoplatelets (GNPs) because these are commercial and well characterized forms, and are adequate for initial studies like the present one, saving the time-consuming and expensive procedure of graphene production, while insuring reproducibility and availability. Graphene nanoplatelets (GNPs) grade M were purchased from XG Sciences (Lansing, USA). According to the supplier, GNPs were prepared through exfoliation of sulfuric acid-based intercalated graphite by rapid heating in a microwave environment, followed by ultrasonic processing[186]. GNPs grade M (GNP-M) have a typical surface area of 120-150 $m^2/g$, an average thickness of approximately 6 to 8 nm, corresponding to only a few sheets of graphene stacked, and are available with different average particle diameters of 5, 15 or 25 µm. GNP-M with 5 and 15 µm diameter were used in this work and are designated as GNP-M5 and GNP-M15.

#### 1.1.2. GNPs Oxidation

For the GNP oxidation two methods were initially tested: the modified Hummers method, the most widely applied, and a method described by Marcano and co-workers as more efficient[187].

The modified Hummers method (MHM) was performed using a GNP-M : $KMnO_4$ ratio of 1:6. Protocol adopted was as follows: 3 g of GNP were added to 150 ml of 95 % $H_2SO_4$ (VWR, Germany) with stirring at room temperature. The solution was cooled at approximately 0 °C using an ice bath, followed by the gradual addition of 18 g of $KMnO_4$ (JMGS, Portugal), production a large exotherm. The mixture was kept at 35 °C and stirred for 2 h, followed by a slow addition of 450 ml of distilled water, while maintaining the mixture in the ice bath and stirring. Then $H_2O_2$ (35 %) was gradually added until no gas (oxygen) was produced (to reduce the $KMnO_4$ in excess). After overnight resting the mixture was decanted to separate the GNPs from the acidic solution. The oxidised GNPs obtained were washed and centrifuged at 4000 rpm for 20 minutes with distilled water and ethanol, six and four times respectively[188]. Afterwards, the solid was washed and centrifuged with ethanol for four times. The oxidized material was left in ethanol suspension and also dried overnight at 70°C.

In the Marcano's method the GNP-M:$KMnO_4$ ratio of 1:6 was maintained. Here, to the mixture of 3g of GNP-M and 18 g of $KMnO_4$, a mixture of the concentrated acids $H_2SO_4$ and $H_3PO_4$ (Chem-Lab, Belgium) was added (120 mL $H_2SO_4$ and 30 mL $H_3PO_4$). The reaction was heated to 50 °C and stirred for 12 h. Then the mixture was cooled down to room temperature and 400 mL of ice were added. $H_2O_2$ (35 %) was gradually added until no gas was produced. The mixture was centrifuged at 4000 rpm for 30 minutes, and the supernatant was decanted away. Then the remaining material was washed in succession with 200 mL of water, 200 mL of

30% HCl, and two times with 200 mL of ethanol (centrifuging each time at 4000 rpm for 30 min). After the last washing, 200 mL of diethyl-ether were added and the resulting suspension was filtered through a polyamide membrane (GE Healthcare) with a 0,45 µm pore size. Finally, the solid was vacuum-dried overnight at room temperature[187].

### 1.1.3. GNPox Dispersions Stability

The dispersion stability of oxidized graphene nanoplatelets (GNP-M5 ox and GNP-M15 ox) obtained from MHM was evaluated in different organic solvents, commonly used for composite preparation. The solvents tested were dimethylformamide (DMF, Fisher Scientific, UK) and tetrahydrofuran (THF, JMGS, Portugal). The concentration of GNPox ethanol dispersions was determined by weighting a flask before and after drying at 70°C a fixed volume of solution. The concentration value was used to calculate the different volumes of the dispersions needed to obtain the GNPox mass necessary to produce dispersions with increasing amounts of GNPox (2 wt%, 5 wt% and 10 wt%) in DMF and THF. GNPox dispersions in ethanol were centrifuged at 4000 rpm for 15 min, supernatant decanted and descarded followed by the addition of a fixed volume (depending on the flask size) of DMF or THF. At last, GNPox dispersions in DMF or THF were subjected to ultrasound bath (Model ATM40-3LCD, OVAN) for 1h. Dispersions were left to settle for a total of 4 days and images were taken at different times: 0h, 2h, 1 day, 2 days and 4 days.

## 1.2. GNPs-containing Materials

### 1.2.1. Polyurethane (PU)

As mentioned in section 3 of Chapter II, Tecothane® is one of the most used PUs for catheter manufacturing and is a medical grade aromatic polyether-based thermoplastic polyurethane (TPU). Tecothane aromatic grade TT1095 A was commercially obtained from Lubrizol LifeSciences (Ohio,USA) in the form of colourless pellets (Figure 5). The product was handled and treated as received from the manufacturer, without any treatment and according to the supplier's processing recommendations.

### 1.2.2. PU/GNP Composites by Melt-Blending

The fabrication method used in this step of the work was melt-mixing due to its simplicity and compatibility with the polymer processing techniques extrusion and injection molding. For melt processing the adequate temperature was consulted on the PU supplier's processing guide (190 °C-230 °C). Melt compounding was performed with Micro-Compounder Xplore (DSM) MC5 (5 mL capacity, vertical, co-rotating twin-screws) and, injection molding was performed using the Xplore micro injection moulder IM5.5 which consists in a temperature controlled mould housing for a conically shaped mould with a heated, removable injection nozzle unit (Figure 8). These equipments were used in the lab of Associação Rede Competência em Polímeros (ARCP).

GNP-M powder together with the PU pellets were, directly and gradually, added into the melt compounder and under continuous high shear mixing. The mixture was introduced into the compounder at 200 °C ($T_{melting}$) with a screw speed of 50 rpm, and when all the sample

was added the screw speed was increased to 200 rpm and left to operate for 3 min. Then the compounded material was fed to the injection unit through the outlet nozzle. The melt was transferred to the micro injector operating also at 200 °C and with the mold at 50 °C ($T_{mold}$). The injection pressure was set at 12 bar and the mould's geometry gave dog bone shaped tensile bars. The operating conditions used for both the melt compounder and the injector were optimized. The range of temperatures recommended by the PU supplier (190 °C-230 °C) were consulted and some optimization on the working conditions was necessary (Table 4). Different $T_{melting}$, $T_{mold}$ and injector's temperatures were tested, as well as different mixing period times. Optimization was based in visible characteristics such as bubbles at the surface, surface defects that appeared as lines and marks or yellow colour (visible only in the case of PU without GNP).

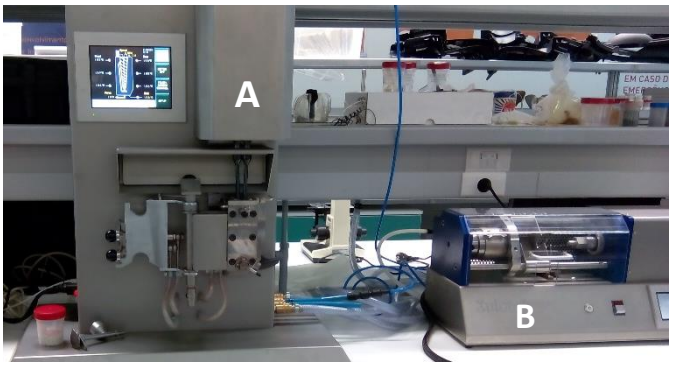


**Figure 8**.The melt compounder (A) and injection moulder (B) used to produce PU/GNP-M composites by melt blending.

**Table 4** - Different parameters tested for melt compounding optimization.

| $T_{melting}$ (°C) | $T_{mold}$ (°C) | $T_{injector}$ (°C) | Mixing Time (min) |
|---|---|---|---|
| 200<br>220 | 20<br>40<br>50 | 200<br>210 | 2<br>2,5<br>3<br>3,5<br>5<br>15 |

## 1.3. PU/GNP Coatings by Dip Coating

### 1.3.1. Glass coverslip as substrate

Coated samples were first produced using glass coverslips as substrate (Figure 9). The glass coverslips used had a diameter of 13 mm (Microscope Cover Glasses, VWR, Germany). To produce the samples, PU solution and GNP dispersions were prepared in tetrahydrofuran (THF).

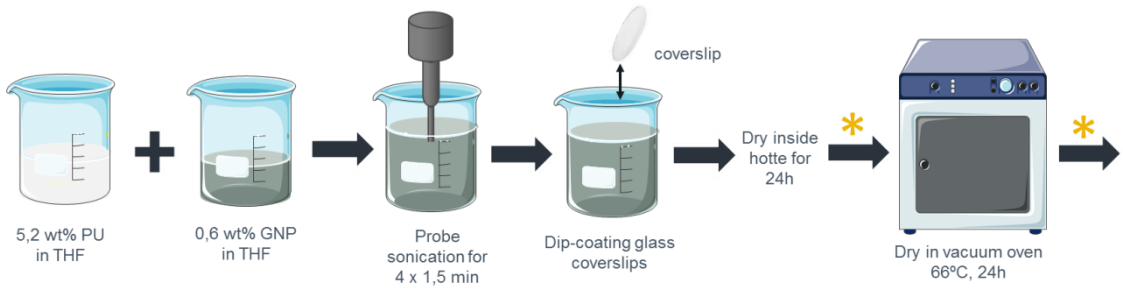


**Figure 9.** Schematic of glass coverslips dip-coating into PU/GNP solution. The * marks the time points where thermogravimetric analysis (TGA) was performed.

PU solution was prepared at a concentration of 11,1 wt% and GNP-M5, GNP-M5 ox, GNP-M15 and GNP-M15ox solutions were prepared at a concentration of 5,6 wt%. After mixing the two solutions the mixture was submitted to 1,5 h ultrasound treatment in the ultrasonic bath. Then, to lower the mixture viscosity, an additional volume of solvent (THF) was added. As suggested by the GNP supplier, probe sonication was performed to obtain well-dispersed solutions using the Hielsher UIP 1000 probe (1000W, 20kHz) in four periods of 1,5 min. Between sonication periods the mixtures were allowed to cool down to avoid overheating and solvent evaporation. In the final solution the PU and GNP concentrations are 5,2 wt% and 0,6 wt%, respectively (12 wt% of GNP in PU). Glass coverslips were dipped in the PU/GNP mixture solution and left to dry at room temperature for 24 h followed by another period of 24 h in a vacuum oven (BINDER, Germany) set at 66 °C (THF boiling point).

### 1.3.2. PU film as substrate

PU samples (without GNP) obtained from injection molding were also coated with the solutions produced in the previous section. However, results demonstrated that further optimization was necessary by varying the organic solvent used, the GNP concentration and the PU content in the final mixture. For that, since a large number of PU substrates were needed and since injection molding was a very time consuming processe, PU films were produced in a larger scale from a different method, described next. Figure 10 illustrates the procedure of PU films preparation and sequent dip-coating.

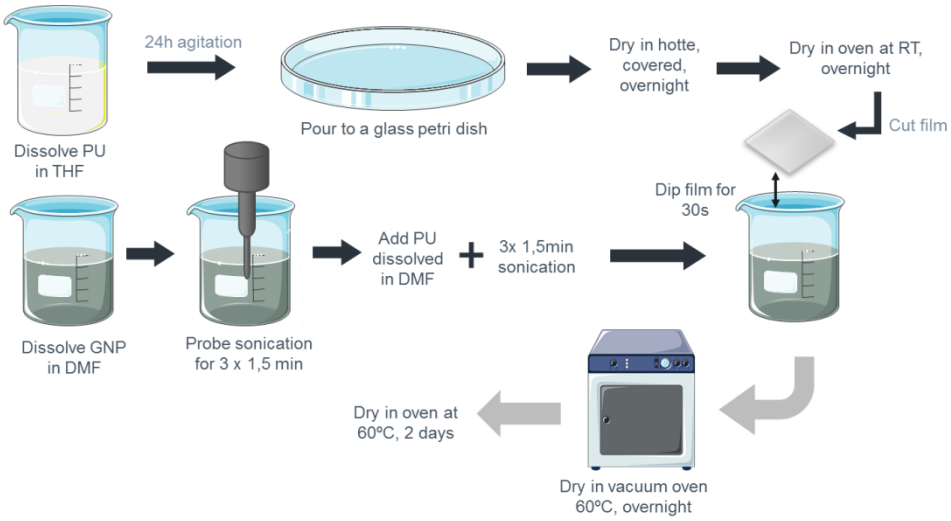


**Figure 10.** Schematic of PU films dip-coating into PU/GNP solution.

PU films were first prepared by casting following a method previously described[189]. PU pellets were dissolved in tetrahydrofuran (THF) at a concentration of 12,5 wt% and the solution magnetic stirred for 24 h. Then 80 mL of the solution were casted onto clean glass petri dishes of 14 cm in diameter. The petri dish was covered with perforated aluminium foil and left at room temperature overnight for a slow evaporation of THF. After removing the films from the petri dishes they were allowed to dry at room temperature for 12h and cut in squares of 2 x 2 $cm^2$.

A PU solution in DMF was prepared at a concentration of 50 mg/mL and mixed by magnetic stirring for 6 days (initial PU solution). Different masses of GNP were dispersed in 30

mL of DMF with mechanical stirring and probe ultrasonication in three periods of 1,5 minutes to form a uniform suspension. Then 20 mL of PU solution at different concentrations, prepared from the initial PU solution, are added to the GNP suspension with continuously stirring followed by three periods of 1,5 minutes of ultrasonication, to obtain homogenous dispersion of the nanoparticles into the matrix. The solutions were left to cool-down in between ultrasonication periods to avoid overheating. Then PU film squares were dipped in the solution for 30 seconds. To evaporate the organic solvent the samples were dried at 60 °C in vacuum for 12 h in a vertical position and further dried at 60 °C in a normal oven for 2 days.

Different concentrations of GNP dispersions and different PU:GNP weight ratios were tested (Table 5). Moreover, another organic solvent recommended by the GNP suppliers was tested, isopropyl alcohol (IPA) also called isopropanol, only for one of the tested conditions (1 mg/mL 1:1) to compare with DMF dispersion.

**Table 5** – The different GNP concentrations and PU:GNP ratios tested to produce coatings on PU films.

| GNP dispersion concentration (mg/mL) | PU:GNP weight ratio (mg/mg) |
|---|---|
| 1 | 1:1 |
| | 1:2 |
| | 1:4 |
| 0,5 | 1:1 |
| | 1:2 |
| | 1:4 |
| 0,25 | 1:1 |
| | 1:2 |
| | 1:4 |

# 2. Materials Characterization

## 2.1. X-ray photoelectron spectroscopy (XPS)

X-ray photoelectron spectroscopy (XPS) analysis was performed to confirm the oxidation of the GNPs powders and to investigate the changes in the chemical states. This technique was performed at CEMUP (Centro de Materiais da Universidade do Porto) using Kratos Axis Ultra HSA equipment. A monochromatic Al X-ray source operating at 15 kV (90 W) was used. The analyzer pass energy was 80 eV for survey spectra and 40 eV for O 1s and C 1s high-resolution spectra. The electron gun used focused on the specimen in an area close to 5 $mm^2$. The photoelectron take-off angle (the angle between the surface of the sample and the axis of the energy analyzer) was 90°. The effect of the electric charge was corrected by setting the reference of the C1s peak to 285,0 eV. The deconvolution of spectra was performed with the CasaXPS processing software for XPS spectra version 2.3.16, using Gaussian-Lorentzian peak shape and background type Shirley.

## 2.2. Scanning electron microscopy (SEM)

The morphology of GNP and GNPox powders and the surfaces of the materials produced were observed using SEM FEI Quanta 400FEG, with acceleration voltage of 10 or 15 kV at CEMUP (Centro de Materiais da Universidade do Porto). The powder samples were applied on conductive carbon strips. Composites and coatings selected for SEM analysis were fractured transversely after freezing with liquid Nitrogen and applied on carbon tape. The surface and the transversal fracture surface of the samples were then analysed using the same equipment and conditions. Pictures of different magnifications were taken of the surface and the matrix of each sample. All samples were coated with an Au/Pd thin film, by sputtering, using the SPI Module Sputter Coater equipment for 50 seconds and with a 15 mA current (to improve samples' conductivity).

## 2.3. Water Contact Angle

Contact angle measurement is a technique to characterize the surface of materials. These measurements give information on the wettability and the surface free energy. The interface water/material is extremely affected by several factors such as: curvature, roughness and chemistry of the surface, and is therefore useful to detect surface modifications as well as contaminations. The phenomenon of the contact angle is explained as a balance between the cohesive force that attracts the molecules of the liquid (in the drop) to each other and the attraction of the liquid molecules for the molecules that make up the surface (an adhesive force)[38]. The equilibrium between these forces is manifested through the contact angle (θ) of the drop with the surface and can be described by the Young equation.

The water contact angle can be measured through various manners, being the most common and simple the sessile drop method. A measured contact angle less than 90° indicates that the liquid spreads over a large area of the surface (wetting the surface) and we are in the presence of a hydrophilic surface, while a contact angle higher than 90° indicates that the liquid minimizes the contact with the surface and the surface is considered hydrophobic[190].

In this work contact angle measurements were performed using the static sessile drop method and performed with an OCA 15 goniometer (DataPhysics, Germany). Samples were placed in a closed thermostatic chamber (25°C) saturated with water to prevent droplet evaporation. Drops of 4 µL ultrapure water were placed on the samples' surface and pictures were taken when the drop contacted the surface. The results treatment was performed with SCA20 software and the angle measured using Young-Laplace fit. Determinations were made on 2 different locations for each sample and using three samples of each condition.

## 2.4. Stereomicroscopy

Dip coating samples digital images were taken using OPTIKAM B9-4083.B9 equipment, at Associação Rede Competência em Polímeros (ARCP).

### 2.5. Thermogravimetric (TG) analysis

Thermogravimetric analysis (TGA) is a useful technique to measure physical and chemical changes in materials while increasing the temperature. In this method, the mass of the sample is monitored as a function of temperature or time. The sample is continuously weighed as it is subject to a period of increasing temperature. The graphic presentation of the data (TG thermal curve) can be plotted as result of the mass loss as a function of temperature or in differential way where the change in mass with time is plotted as a function of temperature[191]. The samples are loaded in a suspended micrograviметric electronic balance and placed in a furnace, and the weight change is recorded while the sample is subjected to a programmed heating sequence.

Dip coating films were analysed by thermogravimetry to assess their thermal stability and in particular to confirm the total evaporation of the solvent (THF). The TG analysis was performed using TG 209 F1 equipment (NETZSCH, Germany). Films were detached from the glass coverslips and loaded in aluminium crucible (pans). The experiments were run at a heating rate of 10 K/min, under a nitrogen atmosphere with a temperature range of 30 °C to 200 °C. TGA was performed before and after the drying period at the vacuum oven (Figure 9).

### 2.6. Rubbing test

To determine the adhesion of the nanoplatelets exposed at the surface of the dip coating samples a simple though effective test was performed. A common white eraser was used to scrub the surface of the samples and pictures were taken before and after. If black/brown residues were retained in the eraser surface, the platelets were not considered well-adhered to the surface.

## 3. Antibacterial Properties

### 3.1. Bacteria Strains and Growth Conditions

*Staphylococus epidermidis* (ATCC 35984), clinically isolated from catheter catheter sepsis, was obtained from the American Type Culture Collection. Bacteria were grown in Trypticase Soy Agar (TSA, Merck) plates overnight at 37°C and used immediately or stored at 4°C up to one week. Then 2 colonies are collected and inoculated into 5 ml of Trypticase Soy Broth (TSB, Merck) and cultured overnight at 37°C with agitation at 150 rpm.

### 3.2. Minimum inhibitory concentrations (MICs)

Minimum inhibitory concentration (MIC) protocol was followed to determine the effect of GNP dispersions on the *S.epidermidis* bacteria growth and viability. The procedure followed was similar to the described in several reference papers using a two-fold diluting method[103; 192; 193].

Overnight cell culture of *S. epidermidis* in the exponential phase of growth[194] was adjusted by $OD_{600\ nm}$ to an initial inoculum concentration of $2\times10^5$ Colony-Forming Units (CFUs) /mL in fresh TSB medium. The test materials GNP-M5, GNP-M15 and respective oxidised forms (GNP-

M5ox and GNP-M15ox) were dispersed in $dH_2O$ using ultrasound bath. Such suspensions were then diluted with $dH_2O$ preparing 2-fold serial dilutions with concentrations ranging from 1024 to 2 µg/mL. To each well of a round bottom sterile 96-well polystyrene microtiter plate 100 µL of the initial bacterial inoculum and 100 µL of each of the different material were added (50% v/v). In the end, the bacteria concentration is $1\times10^5$ CFU/mL and the GNP concentration ranges from 512 to 1 µg/mL. Wells containing only TSB, only bacteria suspension in TSB, or materials suspensions in TSB (without bacteria) were used as controls. Incubation was performed between 18-24h at 37°C under static conditions. In order to avoid water evaporation, the remaining empty wells of the 96-well plate were filled with $dH_2O$ or PBS, and the plate was placed into a container with moisted paper. MIC values are commonly determined by visual analysis of bacterial growth on the bottom of the wells, however since GNP turns the solution black and deposit at the bottom, visual assessment was not possible.

As such, after the incubation period the metabolic activity of bacteria was determined by resazurin assay (Alamar blue assay). 20 µL of resazurin were added to each well and incubated for 3h at 37°C. Then, 100 µL of the wells were transferred to a 96-well black plate and the relative fluorescence units (RFUs) of the medium ($\lambda_{ex}$: 530 nm and $\lambda_{em}$: 590 nm) were measured using a fluorometer. The wells where reduced metabolic activity was detected (compared to the control with bacteria only), and therefore expected as being MICs, were selected for evaluation of minimal bactericidal concentrations (MBCs). This was performed by CFUs counting, where viable bacteria are counted by the agar plate culture method. For that 10-fold serial dilutions were made and three drops of 10 µL each per dilution factor were plated in TSA containing Petri dishes and incubated overnight at 37°C. Finally, CFUs were visually counted.

## 3.3. Antibacterial assessment

The measurement of antibacterial activity for composites and dip coating samples was based on the standard ISO 22196 Plastics-Measurement of antibacterial activity on plastics surfaces and similarly to the tests performed by others (Figure 11) [105; 184; 195; 196]. Composite samples were sterilized with ethylene oxide at Hospital de São João since it is the recommend sterilization method for catheters. Ethanol and ethylene oxide sterilization methods were tested to assess if ethanol had influence on the samples' surface, possibly degrading the polymer. No differences were seen (Figure A 1). The extremities of the samples were cut to obtain square samples of approximately 1 x 1 $cm^2$ and were then washed three times with PBS. Afterwards, samples were dried with argon in sterile environment and placed in a 24-well TCPS plate. For dip coating surfaces, round samples were obtained by punching the dip-coated film squares with a circular form with 14 mm diameter. These samples were sterilized with 70 v/v% ethanol for 30 minutes and then washed three times with PBS.

Overnight cell culture of *S. epidermidis* was adjusted to a target initial inoculum concentration of $6\times10^5$ CFUs/mL in fresh TSB medium, following the ISO 22196 guidelines. Polypropylene (PP) round films with diameter ≈ 0,9 cm were cut from a PP sheet, sterilized with 70 v/v% ethanol for 30 minutes and then washed three times with PBS. A drop of 15 µL of bacterial suspension was placed on top of the surfaces and then carefully covered with PP films to facilitate the contact between the bacteria cells and the sample surface. The film was gently pressed down so that the test inoculum spread over to the edges. Samples were incubate for 24 h under static conditions at 37°C. In order to solve the potential problem of

water evaporation, the remaining empty wells of the 24 well plate were filled with with $dH_2O$ or PBS, and the plate was placed inside a container with moisted paper. Three replicas of PU were used to measure viable cells immediately after inoculation to determine the recovery rate of the bacteria from the test specimens. Experiments were conducted with 5 replicates of every sample. Besides PU samples, PP films were also used as control for normal bacterial growth and three replicates of every sample was also incubated with only TSB medium, without bacteria. On the dip coating samples assessment new control was used, polyethylene terephthalate (PET) tissue culture coverslips for the cultivation of adherent cells with 13 mm diameter (SARSTEDT, USA).

After the incubation period, 1,4 mL of fresh TSB were added to each well and samples were re-suspended until detachment of the PP round film. After that, the PP film was removed and the supernatant collected. Then, planktonic and adherent bacteria are analysed separately.

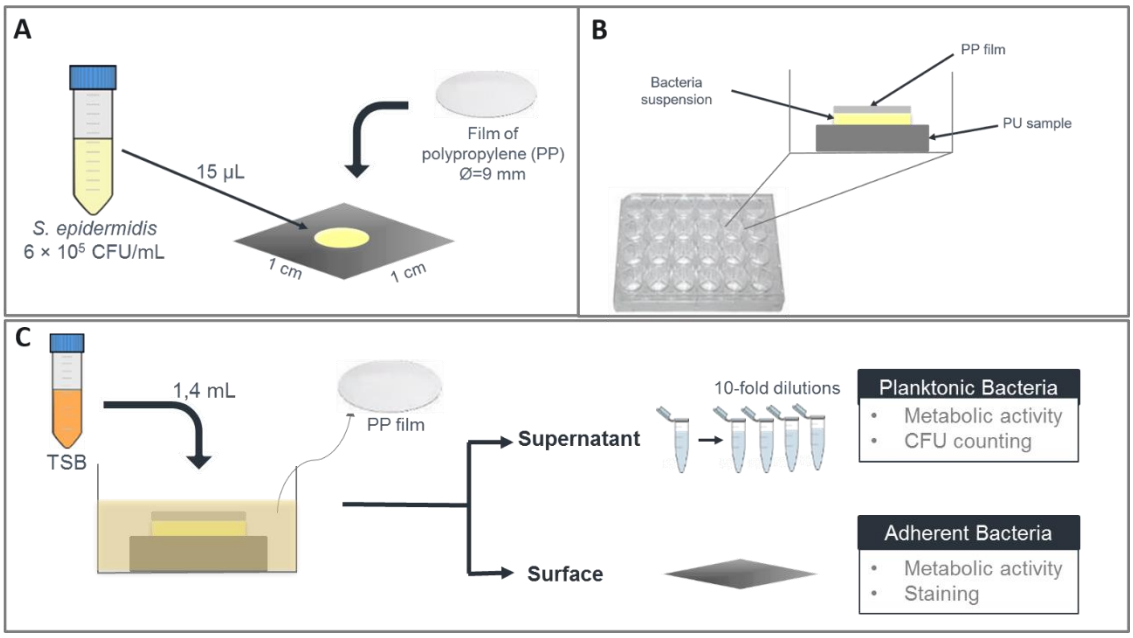


**Figure 11.** Schematic representation of the essential steps of the antibacterial assessment. (A) Inoculation of the samples and placement of cover film; (B) Bacterial suspension held in intimate contact with the sample's surface by the polypropylene (PP) film for 24 h at 37°C. ; (C) Detachment of the PP film and further analysis of the bacteria present in the supernatant and bacteria adherent to the surface.

### 3.3.1. Planktonic Bacteria

Metabolic activity was determined using the Alamar blue assay, similarly to Barros *et al.*[197]. A volume of 450 µL of the washings was transferred to a new 24 well plate and 450 µL of TSB was added to 3 wells for control. Then 50 µL of resazurin were added to each well (10% resazurin) and plate was incubated at 37°C for up to 3 h. After the incubation period, 100 µL of the supernatant were transferred to a 96-well black plate and the relative fluorescence units (RFUs) of the medium ($\lambda_{ex}$: 530 nm and $\lambda_{em}$: 590 nm) were measured using a fluorometer in order to determine the metabolic active bacteria.

Viable cell count of bacteria by the agar plate culture method was also performed. For that 10-fold serial dilutions ($10^{-2}$, $10^{-4}$, $10^{-6}$) of the washings of the samples (supernatant) were

prepared. Then three drops of 10 µL were placed in a TSA plate for each dilution, including non-diluted. Plates were incubated overnight at 37°C and CFUs counted.

### 3.3.2. Adherent or Sessile Bacteria

Samples were transferred to a new 24-well plate and 750 µL of fresh TSB containing 10% of resazurin were added to each sample and to three additional wells (control). Plate was incubated at 37°C for up to 3 h. After the incubation period, 100 µL of the supernatant was transferred to a 96-well black plate and the relative fluorescence units (RFUs) of the medium ($\lambda_{ex}$: 530 nm and $\lambda_{em}$: 590 nm) were measured using a fluorometer in order to determine the metabolic active bacteria without detaching bacteria from the surfaces.

Afterwards, the viability of adherent bacteria was assessed. Samples were washed twice with PBS followed by a staining protocol. The LIVE/DEAD® Bacterial Viability Kit (BaclightTM) was firstly used since it is an easily, reliably and quantitative method to label and distinguish live and dead bacteria. This kit contains a mixture of two stains: SYTO 9 green-fluorescent nucleic acid stain, which stains bacteria with intact and damaged membranes, and the red-fluorescent nucleic acid stain, propidium iodide (PI), which only stains bacteria with damaged membranes. Thus, with this kit bacteria with intact cell membranes stain fluorescent green, whereas bacteria with damaged membranes stain fluorescent red. However, initial tests demonstrated that PU presented strong background green auto fluorescence, deterring the use of SYTO 9 stain. As alternative, Hoechst 33342 (Molecular Probes, EUA) nucleic acid stain was used. This stain emits blue fluorescence when bound to dsDNA and so, fluorescence is produced by combining with the nucleus of living and dead cells. In Table 6, the different staining, stain ratios and general conditions tested for the viability assessment for different experiments performed for optimization can be found. Three different stains were tested. DAPI stains all bacteria blue and staining is preceded by a fixation protocol and so bacteria need to be dead for the staining to work. HCS NuclearMask Deep Red stain stains live and fixed cells red. And Hoechst that stains blue live and dead bacteria. After different optimization experiments the staining protocol adopted was as follows. A volume of 700 µL of Hoechst at a concentration of 5 µg/mL was added to each sample and incubated at 37° for 15 min, protected from light. Then samples were washed twice with PBS (1 mL) and mounted on microscope glass slides with a drop of 3 µL of PI 1,25 µg/mL placed on each sample. Samples were observed using an inverted fluorescence microscope Axiovert 200M (Zeiss, Germany) with the fluorescence levels set at 20% to minimize autofluorescence. Pictures of nine fields per sample were taken and analysed using the ImageJ software.

**Table 6** – Different conditions and stains tested for adherent bacteria viability assessment.

| Staining | Procedure |
|---|---|
| DAPI | 20min PFA 4%, Vectashield with DAPI |
| Syto9:PI | 4:1 with oil; 100µl, 10min, remove stain, mount |
| | 4:1 without oil; add 100µl stain and mount |
| | 3:1 without oil, on coverslip, add 50µl stain and mount on top of the drop |
| Hoechst (2,5µg/ml) + PI (1,25µg/ml) | without oil; add 10µl drop of mixed stains and mount |

| | |
|---|---|
| Hoechst (5µg/ml) | without oil; mount, 5µl, 15min, 37°C |
| PI (2,5µg/ml) | without oil; add 5µ stain and mount |
| HCS NuclearMask Deep Red stain | 700µl,30min, RT, protected from light, wash 1x with PBS and mount with oil |
| Hoechst (2,5µg/ml) + PI (1,25µg/ml) | 700µl, 15min, 37°C, protected from light, without washing, drop of 7ul of PI and mount |
| Hoechst (1,25µg/ml) + PI (1,25µg/ml) | add drop of 4µl of each and mount, 37°C, dark, 15min |
| Hoechst (2,5µg/ml) | add 7µl drop and mount, 37°C, dark, 15min |
| Hoechst (5µg/ml) + PI (1,25µg/ml) | 700µl, 15min, 37°C, dark, without washing, drop of 10 or 15µl of PI and mount |
| Hoechst (5µg/ml) + PI (1,25µg/ml) | 700µl, 15min, 37°C, protected from light, wash 2x PBS, 700µl of PI, 15min and mount with 5µl Vectashield |
| Hoechst (5µg/ml) + PI (1,25µg/ml) | 700µl, 15min, 37°C, protected from light, wash 2x PBS, 5µl of PI on coverslip and put sample on top, seal with varnish |

# CHAPTER IV:
# Results and Discussion

## 1. GNP-M dry powders and chemical oxidation

By SEM analysis of the GNP-M5 and GNP-M15 dry powders large platelets are observed with planar conformations constituted by single layer stacks with sharped edges (Figure 12 A-F).

Single graphene nanoplatelets were not found, which can be explained due to the fact that both GNP-M5 and GNP-15 powders were analysed as received and according to the manufacturer they present granular forms constituted by collections of individual platelets. This is visible at the lower magnification images (Figure 12 A and D). Complete and stable dispersions can only be achieved with the use of proper solvents and agitation. SEM images of the GNP-M5 and GNP-M15 powders show smooth surfaces with irregular and sharp particles. After oxidation, the platelets' planar conformation is lost and flakes appear wrinkled and the sharped edges possess now a folded form indicated by yellow arrows in Figure 12. This can occur due to the short dimensions of the flakes allowing the oxygen-containing functional groups present at the platelets' edges and basal planes to form intra-platelet hydrogen bonds and thus making the sheets look like a wrapped and folded paper[198]. The platelets closely associate with each other and form a disordered solid. These is explained by the inter-platelets hydrogen bonds that lead to a higher agglomeration of the materials observed in the lower magnification pictures (Figure 12 A, D, G, J and M). Both oxidation methods performed yielded

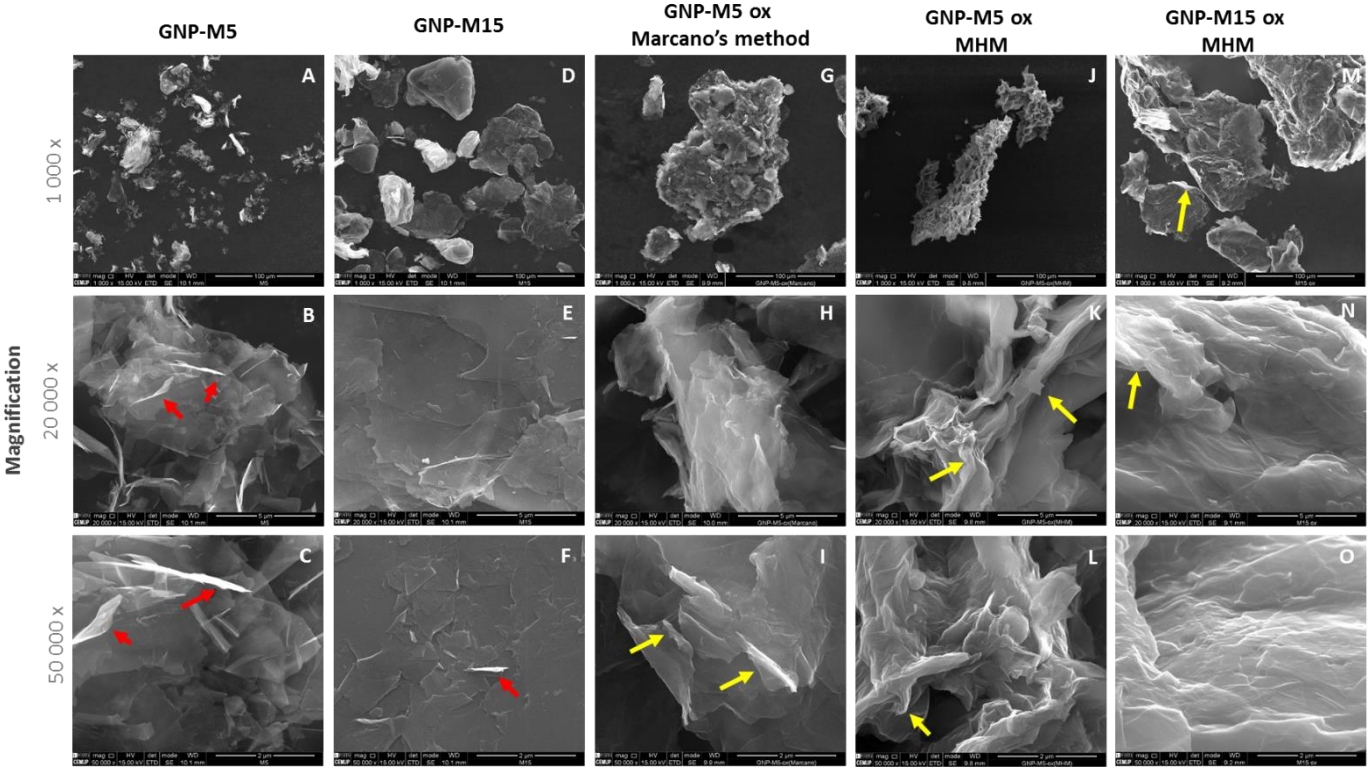


**Figure 12.** SEM images of dry powders of GNP-M5, GNP-M15 and their oxidised forms GNP-M5 oxidised by the MHM and by the Marcano's method, and GNP-M15 oxidised by the MHM. Sharped and folded edges are indicated by red and yellow arrows, respectively. Each row corresponds to magnifications of each material at 1 000 ×, 20 000 × and 50 000 × (scale bar = 100 µm, 5 µm and 2 µm, respectively).

highly wricked sheet conformation indicating that the GNPs were effectively oxidised. Comparing GNP-M5 oxidised by the Modified Hummer's Method to the GNP-M5 oxidised by Marcano's Method, MHM originated GNP with a more wrinkled surface. One can hypothesize that a more wrinkled surface and more folded edges indicate a more oxidative method, however further characterization is needed to effectively conclude that in this work the MHM produced more oxidised GNP.

XPS analysis was performed to confirm the oxidation of the GNPs. The relative atomic composition of the GBMs is described in Table 7. XPS results show that GNP-M5 and GNP-M15 have a low degree of oxidation (at.% of oxygen O 1s < 3%) which was expected since GNP are manufactured through non-oxidizing processes (microwave and ultrasonic treatment) despite still presenting some oxygen in the sheet edges. It was also shown that oxidation of GNP-M5 increases the oxygen content in the final product, increasing O 1s at.% to about 30 %. Marcano's method yielded an oxidised GNP-M5 with slightly higher O 1s at.% when compared to the Modified Hummer's Method.

The XPS spectra for C 1s is in accordance with the literature, with the same peaks and therefore functional groups being detected[59; 199; 200]. GNP-M5 and GNP-M15 exhibit two characteristic C1s peak assigned to the $sp^2$ and $sp^3$ carbon components, and a very small peak corresponding to the carbon atoms bound to oxygen in the hydroxyl (C-OH) and epoxy (C-O-C) functional groups (Figure 13 A and B). The C–C $sp^3$ relates to the interlayer bonding between pairs of graphene planes[201]. The oxidation is documented by increasing peaks belonging to oxygen-containing groups in XPS C1s. The oxidation process increases the content of hydroxyl (C-OH), epoxy (C-O-C), carboxyl (HO-C=O) and carbonyl (C=O) groups. The generation of these oxygenated functional groups breaks the carbon sigma bonds (C-C $sp^2$) and transforms them into single C-C or $sp^3$ bonds[202]. The Binding Energy (BE) for epoxy group is close to that for hydroxyl, and the BE for carbonyl is close to the carboxyl groups. Due to the difficulties to deconvolute heavily overlapping peaks, and as performed by others, two peaks for carbon–oxygen functionalities in C1s spectra of GNP-M5 ox were included: one for hydroxyl and epoxy groups, and one for carbonyl and carboxyl groups (Figure 13 C and D)[203]. The oxidation by the Modified Hummers Method lead to the formation of more epoxyls (C-O-C) and hydroxyls (C-OH) than the Marcano's method (Figure 13 D). XPS results also show that the total C-C ($sp^2$ and $sp^3$) is lower for GNP-M5 ox by MHM, despite the total C at.% being similar for both oxidation methods. This suggests a stronger oxidation with oxygen-containing functional groups distributed by more carbon atoms[198; 204]. Similarly, the dominance of epoxides and alcohols on the basal plane of GO has also been reported. GO is heavily oxygenated bearing hydroxyl and epoxy groups on $sp^3$ hybridized carbon on the basal plane, in addition to carbonyl and carboxyl groups already located at the sheet edges on $sp^2$ carbon[4].

The difference of O at% between the GNP-M5 oxidised by MHM and Marcano's method was not considered significant and taking into account that the total C-C was lower for the MHM, the method chosen and adopted for the present work was the Modified Hummer's Method because our research group is more experienced with this method and it has been used extensively with very good results[59; 162; 198].

**Table 7** - Surface atomic composition (%) of the GNP-M5, GNP-M15, GNP-M5 oxidised by the MHM and GNP-M5 oxidised by the Marcano's method calculated from high-resolution XPS spectra.

| Element Atomic Percentage (%) | GNP-M5 | GNP-M15 | GNP-M5 ox (MHM) | GNP-M5 ox (Marcano) |
|---|---|---|---|---|
| C 1s | 97.3 | 97.72 | 70.15 | 67.57 |
| O 1s | 2.7 | 2.28 | 29.85 | 32.43 |

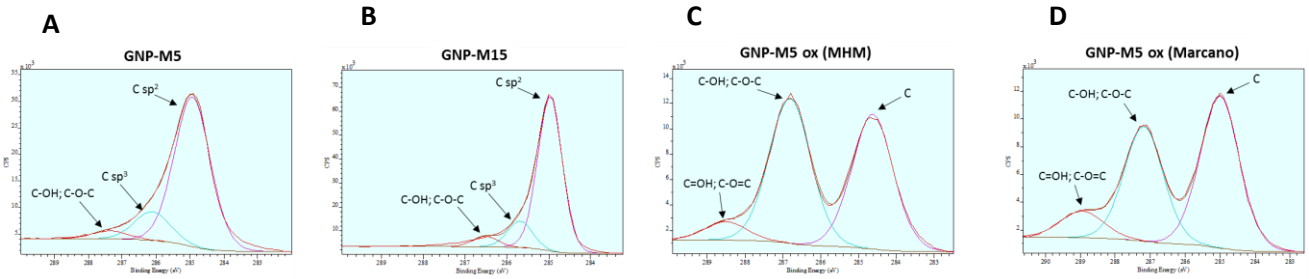


**E**

| *Functional Groups Percentage (%)* | *GNP-M5* | *GNP-M15* | *GNP-M5 ox (MHM)* | *GNP-M5 ox (Marcano)* |
|---|---|---|---|---|
| *C (285 eV)* | *95.65* | *94.72* | *45.25* | *51.67* |
| *C-OH; C-O-C (287 eV)* | *4.35* | *5.48* | *48.62* | *38.51* |
| *C=O; O-C=O (289 eV)* | - | - | *6.13* | *9.81* |

**Figure 13.** XPS spectra fitting for the core level C 1s of GNP-M5 (A), GNP-M15 (B) and GNP-M5 oxidised by the Modified Hummers Method (C) and Marcano's method (D). Table shows content of C 1s chemical groups resulting from XPS spectra fitting (E).

## 2. Antibacterial Activity of GNP and GNPox dispersions

The antibacterial activity of GBMs dispersions was assessed towards *S. epidermidis* and with concentrations ranging from 1 to 512 µg/ml. The bacteria populations were determined by cultivable method (CFUs) and metabolic bacteria measured in relative fluorescence units (RFUs). In all GNP dispersions tested reductions of metabolically active bacteria were detected (Figure 14 A and B). As the materials' concentration increased there is a tendency to lower metabolic activity, as such, the highest metabolic activity reduction was observed at the higher material concentrations of 512, 256 and 128 µg/ml. These higher concentrations were therefore chosen for further analysis by viable cell counting method to assess if, besides being metabolically less active, *S. epidermidis* viability was also affected and assess the cultivable bacteria. From the metabolic activity data, comparing GNP-M with different sizes, it can be observed that GNP-M5 lead to a higher decrease on the metabolic activity than GNP-M15. The same tendency was detected for the oxidized GNPs, where GNP-M5ox had a higher effect on the metabolic activity than GNP-M15ox (Figure 14 A-C). This is in accordance with studies that

describe smaller particles leading to lower bacterial viability than larger particles[9; 78; 92].. Although the GBMs used in such studies have been mostly GO and rGO, GNPs tested in this work behaved similarly. It is also clear that oxidized GNPs had greater effect than the non-oxidized GNPs.

In Figure 14 D the results from the cultivable method are represented and a general decrease, though not very consistent, of CFUs compared to the control (bacteria grown with no GNPs) can be observed. As seen from the metabolic activity results, the oxidized GNP dispersions have shown to have higher effect than the respective non-oxidized GNP dispersions on bacteria viability, leading to greater CFUs/mL reduction. This information is in accordance with studies that showed GO as having stronger antibacterial effect than rGO in dispersion[9; 75; 76; 77; 79; 83; 85]. GNP dispersions are unstable and contain large particles. This causes the settlement of the GNP particles in suspension due to the high concentration thus having fewer chances to mingle and diminishing the contact of GNPs with the bacteria[9]. This is less observed for the oxidized GNPs because the suspension is more stable due to the oxygen-containing groups present at the GNPox surface and edges. At the highest concentration (512 µg/mL), the oxidized GNPs caused a very significant decrease of cell viability compared to the control of bacteria growing without GNPs. Moreover, comparing the platelet size effect between the oxidized GNPs, it can be seen that GNP-M5 ox caused lower cell viability than GNP-M15 ox. An important aspect to have into account is the long incubation period during which the particles precipitate when the dispersions stand and a "GNP film" can be deposited at the bottom of the wells.

From these results, it can be concluded that from all the GNPs tested, GNP-M5 ox had a stronger antibacterial effect, seen by a more notorious decrease of both the metabolic activity (100%) and cultivable bacteria counting (82%). None of the tested concentrations completely inhibited *S. epidermidis* growth and hence a Minimal Bactericidal Concentration (MBC) value was not determined (MBC > 512 µg/mL). Nevertheless, these results indicate and confirm the antibacterial activity of GNPs in dispersion.

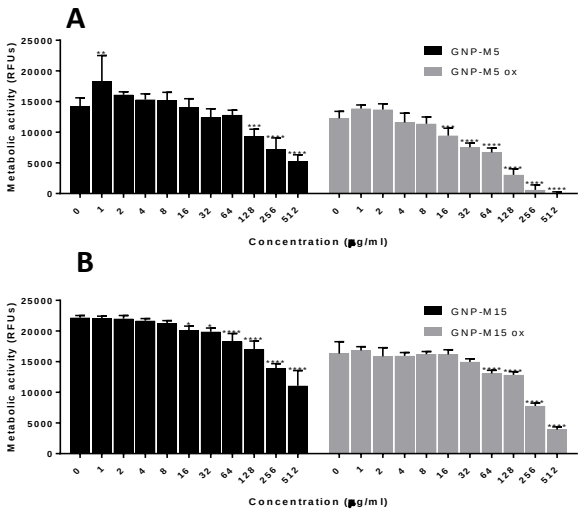


| C | Metabolic Activity Reduction (%) | | | |
|---|---|---|---|---|
| **Concentration (µg/mL)** | GNP-M5 | GNP-M5 ox | GNP-M15 | GNP-M15 ox |
| 512 | 63 | 100 | 50 | 76 |
| 256 | 49 | 95 | 37 | 52 |
| 128 | 34 | 75 | 23 | 21 |
| 64 | 10 | 45 | 18 | 20 |
| 32 | 13 | 38 | 10 | 8 |
| 16 | 1 | 23 | 9 | 1 |
| 8 | -7 | 7 | 4 | 1 |
| 4 | -8 | 5 | 2 | 2 |
| 2 | -13 | -12 | 1 | 3 |
| 1 | -29 | -13 | 1 | -3 |

D

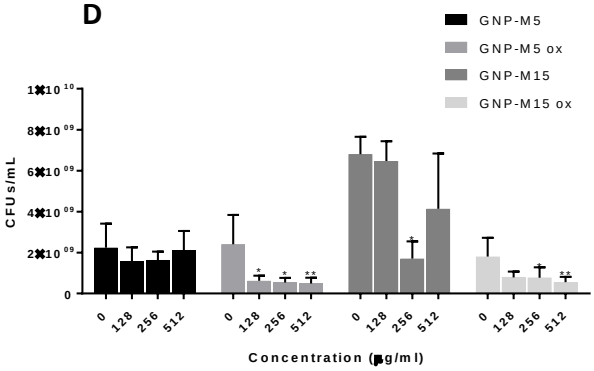


E

| Concentration (µg/mL) | CFUs/mL Reduction (%) | | | |
|---|---|---|---|---|
| | GNP-M5 | GNP-M5 ox | GNP-M15 | GNP-M15 ox |
| 512 | 5 | 82 | 46 | 69 |
| 256 | 27 | 78 | 75 | 57 |
| 128 | 30 | 74 | 5 | 56 |

**Figure 14.** *S.epidermidis* metabolic activity cultured for 24h with GNP-M5 and GNP-M5 ox (A), GNP-M15 and GNP-M15 ox (B) aqueous dispersions. Metabolic activity reduction calculated as percentage of the control (bacteria without GNPs) (C). Bacteria viability for all dispersions (D). CFU reduction calculated as percentage of the control of the bacteria grown without GBMs (E). For the metabolic activity data and CFUs/mL the statistical tests performed were the one way ANOVA and Kruskal Wallis ($P < 0.05$), respectively. *, *****, and **** statistically significant different from control (0 µg/mL) ($p \leq 0.05$, $p \leq 0.01$, $p \leq 0.001$ and $p \leq 0.0001$).

## 3. PU/GNP Composites

Melt-blending was used for preparing the composite material as this represents an economically attractive and industrially scalable method for efficiently dispersing nanofillers in thermoplastic polymers[205]. Moreover, this method doesn't involve the use of solvents and therefore represents an environmentally friendly method that avoids concerns with human health during processing and with toxicity of remaining solvent residues. Optimization was necessary to produce uniform and defect-free samples, both in neat PU and when increasing GNP content. Tests were performed by varying the melting temperature, the mold temperature and time and agitation parameters during melting (data not shown). The final conditions were applied for the production of all the samples, neat PU and PU/GNP composites (see PU/GNP Composites by Melt-Blending in CHAPTER III).

PU/GNP-M5 and PU/GNP-M15 composites were produced with 0.5, 1, 5 and 10 wt% GNP content. The GNP incorporation in the PU matrix is visually detected by an obvious change of colour from a colourless PU sample to completely black composites (Figure 15). This can be observed even with low GNP amounts (0.5 wt%) due to the high surface area of the GNP. According to the GNP manufacturers, the high aspect ratio of the nanoplatelets – which are much larger than thick – makes them effective at low loading levels.

The quality of filler dispersion in the matrix and surface of the composites obtained with the different GNP contents was further investigated by SEM.

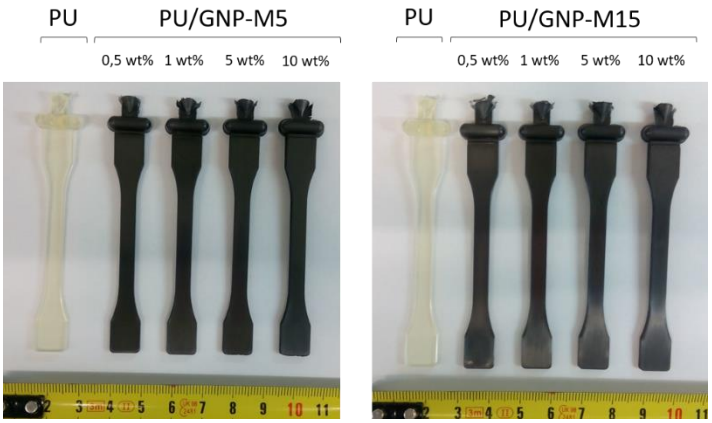


**Figure 15.** Digital pictures of the PU/GNP composites produced by melt-blending.

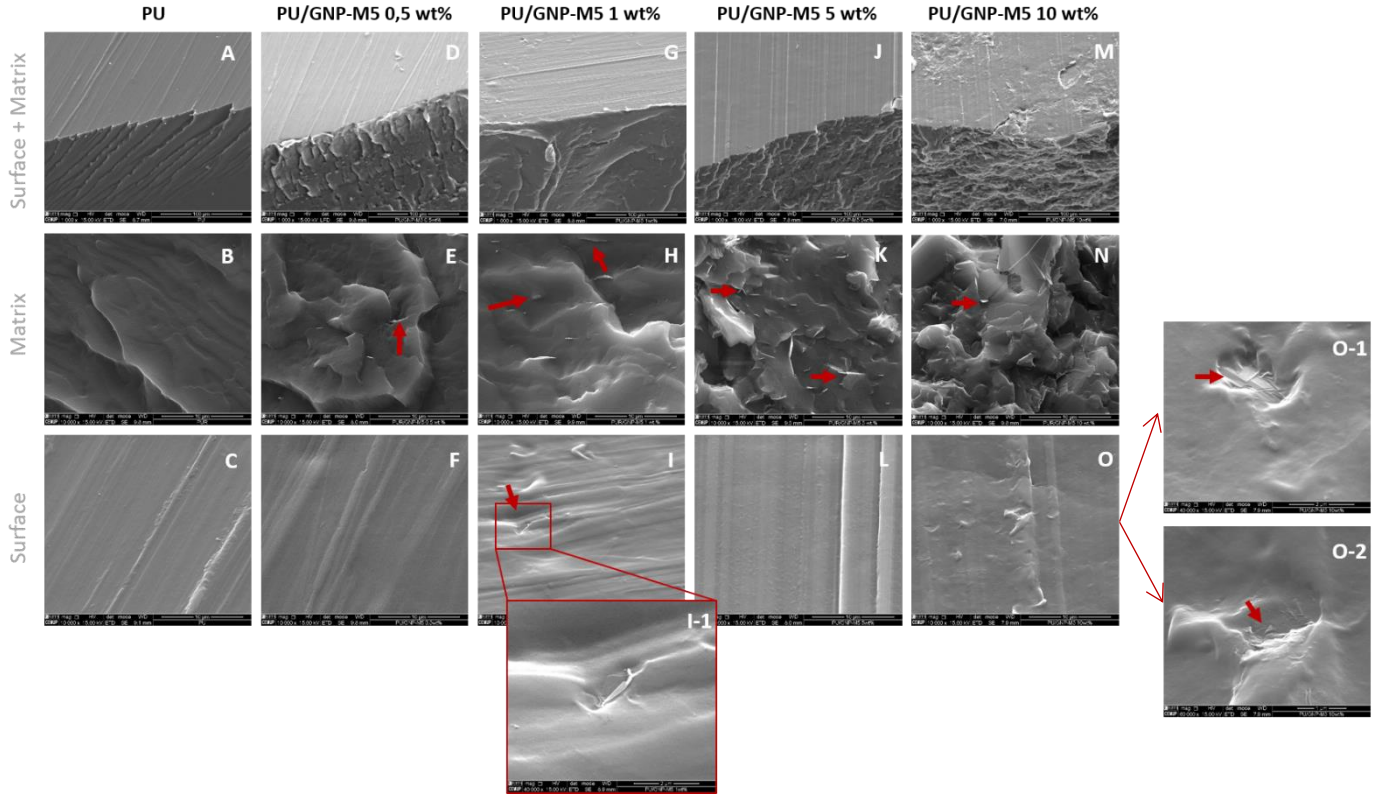


**Figure 16.** PU and PU/GNP-M5 composite SEM images at different magnifications. Lower magnification (1 000×) pictures were taken to see both the surface and the transversal fracture (Surface + Matrix) while higher magnification (10 000×) pictures were taken to the transversal fracture to analyse the composite matrix (Matrix) and to the composites' surface (Surface). Additional pictures with higher magnifications were taken when GNP was found exposed at the surface of PU/GNP-M5 1 wt% (I-1, 40 000×)) and PU/GNP-M5 10wt% (O-1, 40 000×, and O-2, 60 000×). Red arrows indicate the presence of GNP. (Scale bar = 100 µm, 10 µm, 2 µm and 1µm for 1 000×, 10 000×, 40 000× and 60 000× magnifications, respectively).

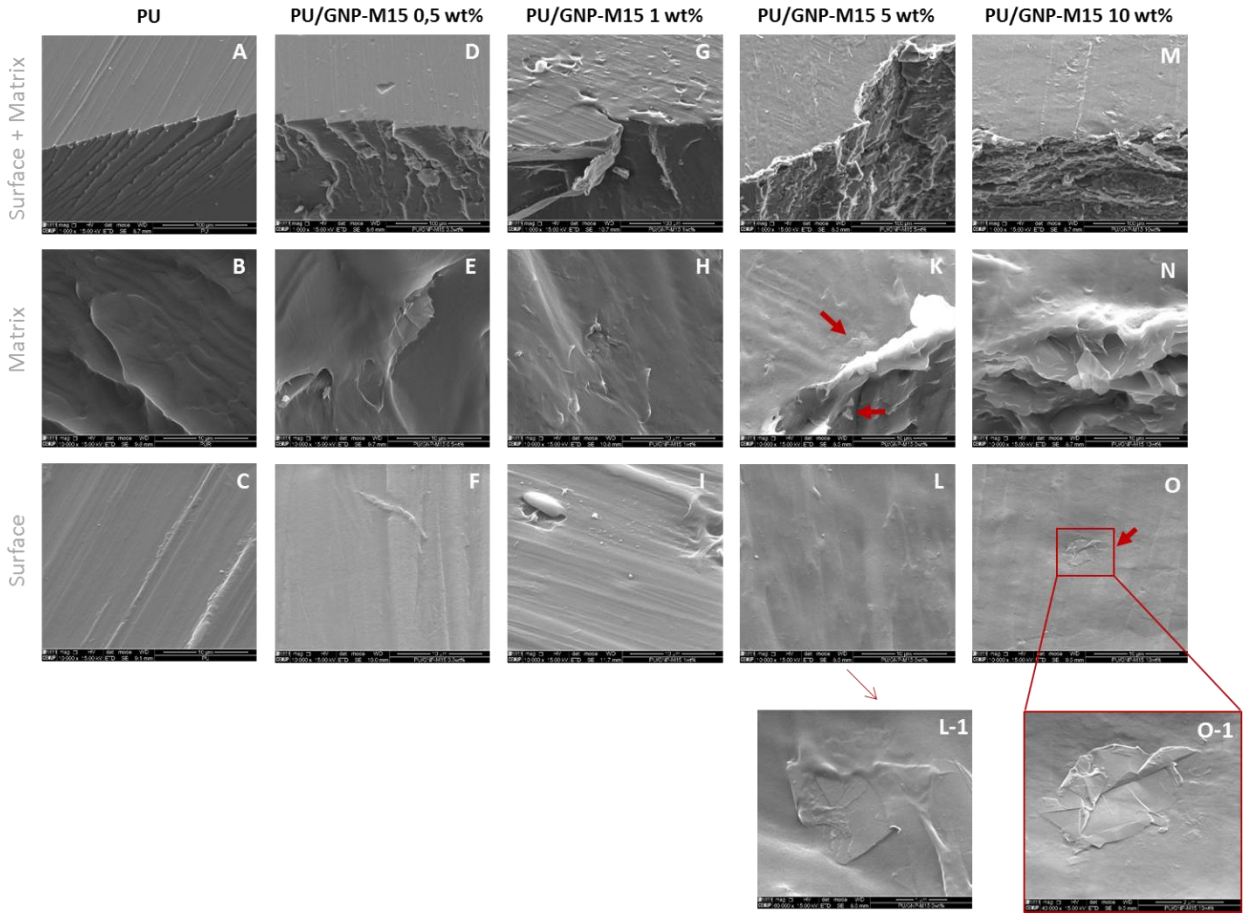


**Figure 17.** PU/GNP-M15 composite SEM images at different magnifications. Lower magnification (1 000×) images were taken to see both the surface and the transversal fracture (Surface + Matrix) while higher magnification (10 000×) images of the transversal fracture show the composite matrix (Matrix) and the composites' surface (Surface). Additional images with higher magnifications were taken when GNP was found exposed at the surface (L-1, 60 000× and O-1, 40 000×). Red arrows indicate the presence of GNP. (Scale bar = 100 µm, 10 µm, 2 µm and 1µm for 1 000×, 10 000×, 40 000× and 60 000× magnifications, respectively).

In Figure 16 and Figure 17, the fracture surface (corresponding to the matrix pictures) of the neat TPU is relatively smooth compared to the surfaces of the 0.5wt%, 1wt%, 5wt% and 10wt% PU/GNP-M5 and PU-GNP-M15 composites. Fracture surface roughness increases with GNP concentration, indicating that the filler incorporation enabled energy dissipating mechanisms during fracture[206]. The fracture surface of the 10wt% GNP content samples is therefore the roughest of all the samples (Figure 16 N and Figure 17 N) and more platelets are visible in the matrix. Identical results were obtained by Tang and co-workers, who described pure PU to have a smooth cross-section and surface, and PU incorporated with GO to be rougher and with apparent irregular stripes[207]. Matrix images show the presence of higher amounts of visible platelets as the GNP loading is increased. Some aggregates could be found, particularly in the 10 wt% samples. Therefore, increasing GNP concentration leads to larger aggregate size and higher probability that the GNPs will aggregate. However, GNP appears to be quite homogenously distributed throughout the samples' matrix. Kalaitzidou *et al.* reported agglomeration of GNP particle when dispersed in a polypropylene (PP) matrix and mentioned a screw design not optimized for nanoparticles[186]. This could explain the agglomerates observed

in the matrix' pictures particularly for high GNP content since identical equipments were used for melt-blending. The GNP manufacturer also indicates the use of specially designed screws for nanocomposites and the pre-mixing of the GNPs with powdered polymers, rather than pellets, to obtain better dispersion into a thermoplastic matrix.

An interface can be described as the linking region between the matrix and the dispersion phase, and is the link that bonds the constituting entities of a composite[208]. As such, it can be stated that in the produced composites there was good adhesion at the interface between the GNPs and the PU matrix.

In all of the samples the surface presents defects that appear like lines. This can be explained by the production method and the moisture levels during injection molding[209]. But since all samples were produced with the same conditions this aspect can be ignored when comparing the composites. Scanning the surface to find GNPs exposed was an exhaustive process and very few platelets were found at the PU/GNP-M5 composites' surface (Figure 16 F, I, L and O) and PU/GNP-M15 composites' surface (Figure 17 F, I, L and O). Moreover, the platelets which were found at the surface were not completely exposed, being partially or completely covered by a layer of polymer and were usually displayed in a planar orientation. This can be observed at the surface of PU/GNP-M5 1wt% (Figure 16 I-1), PU/GNP-M5 10wt% (Figure 16 O-1 and O-2), PU/GNP-M15 5wt% (Figure 17 L-1) and PU/GNP-M15 10wt% (Figure 17 O-1).

The water contact angle of the composites obtained by melt-blending was determined and results are shown in Figure 18.

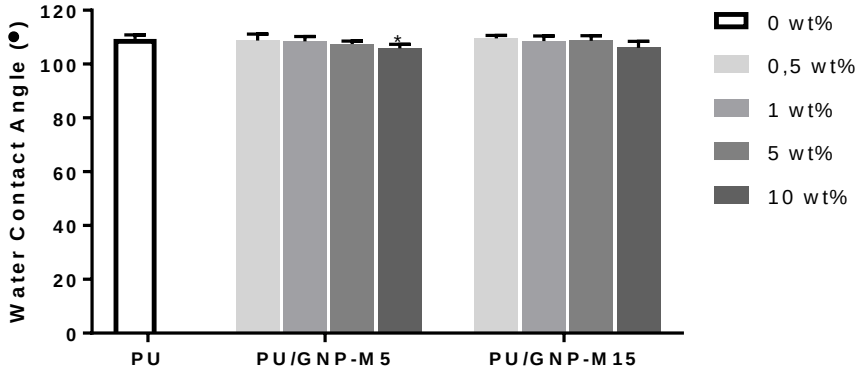


**Figure 18.** Water contact angle measurement for PU (control), PU/GNP-M5 and PU/GNP-M15 composites obtained by melt-blending. Statistic test performed was Kruskal Wallis and * indicates statistically significant different from control (PU) ($p \leq 0.05$).

All samples possess a water contact angle higher than 100°, demonstrating the high hydrophobicity of the samples. Comparing the composites with the PU control, statistical difference in the measured contact angles is only detected for PU/GNP-M5 composite with GNP content of 10 wt% (angle decrease about 4°). This may be due to platelet agglomeration within the polymer matrix, leading to a decrease in the exposed graphene area at the film surface. Our group has also reported that the water contact angle of poly(lactic acid)PLA/GO films decreased about 9° comparing with pristine PLA films[59]. Different studies using PU Tecothane report different water contact angles. Zhao and co-workers reported unmodified PU films as being relatively hydrophobic with a contact angle of 90° and Stachelek *et al.* reported an angle of 73°[210; 211]. In both studies PU films were produced by casting but using

different solvents, DMF in the first and THF in the second. It is possible that the production method alters the material's properties and affects the water contact angle, with melt-blending producing materials with higher hydrophobicity. Moreover, since this method evaluates only the materials surface, the degree of GNP exposure at the surface is crucial to obtain differences in the contact angle.

Taken the characterization results together, it can be concluded that the composites preparation by melt-blending resulted on GNP effectively dispersed on the polymer matrix, but this is not a good method when the purpose is to expose GNP at the surface and consequently achieve polyurethane's surface modification.

## 3.1. Antibacterial Properties of PU/GNP composites

To determine the antibacterial activity of PU/GNP composites and the behaviour of bacteria when in contact with the composite's surface, a method that induces the contact of the bacteria tested, *S.epidermidis*, and the surface was performed according to the ISO 22196 guidelines. Since the GBM's mechanism of action is yet to be completely enlightened, it was important to evaluate different parameters. Moreover, despite the testing performed facilitated the bacteria to contact with the surface, there is still a small volume between the surface and the polypropylene film used to force bacteria contact (see Figure 11 B). So, the bacteria present on the suspension is not always and not at all moments in contact with the surface, can fluctuate between the surface and the supernatant. Therefore it was important to evaluate both the bacteria that effectively adhered to the surface (sessile bacteria) and the bacteria that remained on the supernatant (planktonic bacteria) after the 24 h contact incubation. For the planktonic bacteria, the metabolic activity and the cultivable bacteria assessments were performed. While the bacteria adhered to the surfaces were assessed also by metabolic activity determination and by counting of total and live cells. Initially LIVE/DEAD Backlight kit was tested for fluorescent staining and counting of the red stained dead bacteria and green stained live bacteria. This kit has shown to be inappropriate for PU samples as there was a lot of background in the green fluorescence channel due to autofluorescence of the polyurethane (Figure 19).

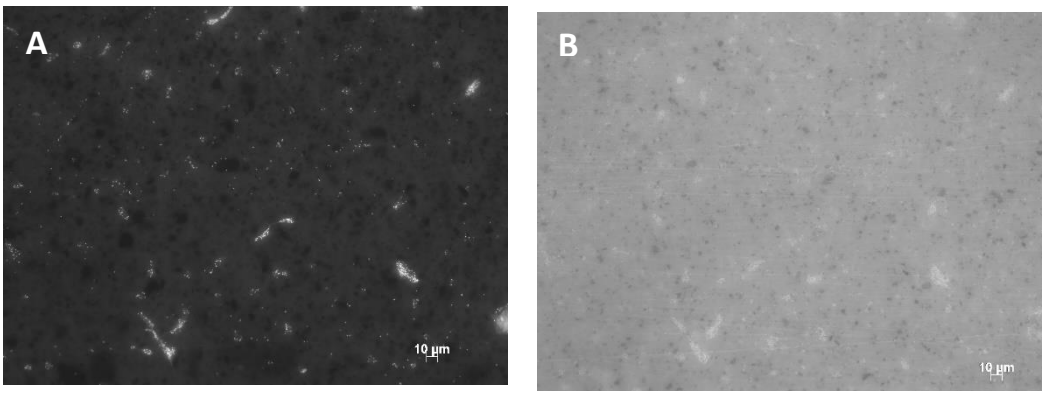


**Figure 19.** Representative fluorescence pictures of PU/GNP-M5 0,5 wt% stained with propidium iodide (PI) (A) and Syto9 (B). Magnification of 40×.

In fact, polyurethane belongs to a group of few polymers that show an autofluorescence effect for visible light excitation (488nm) and its fluorescent effect has already been reported[212; 213]. Therefore, alternatively, adhered bacteria were stained with two fluorescent

stains separately: Hoechst, that stains all bacteria (live and dead), and the same propidium iodide (PI) present in the LIVE/DEAD kit that only stains dead bacteria.

From planktonic bacteria evaluation, statistically significant differences on cultivable bacteria were only found comparing all the samples with S. *epidermidis* cultured on PP film (Figure 20 B). No difference was found comparing the composite containing GNP-M5 and neat PU sample. In terms of metabolic activity no effect was detected (Figure 20 A). As such, the surface of PU/GNP-M5 composite didn't possess antibacterial activity towards planktonic bacteria. Analysing the sessile bacteria, there seems to be a slight decrease on the metabolic active bacteria however this is not accompanied by an increase in the percentage of dead bacteria (Figure 21). Representative images of the total and dead bacteria can be found in Figure A 3 (APPENDIX). Moreover, comparing the total number of adhered bacteria there is no significant difference between the different samples (Figure 21 B). Bacteria can be less metabolically active when in contact with PU containing GNP-M5 but they are still alive. The incorporation of GNP-M5 didn't decrease bacterial adhesion nor increased bactericidal activity of PU.

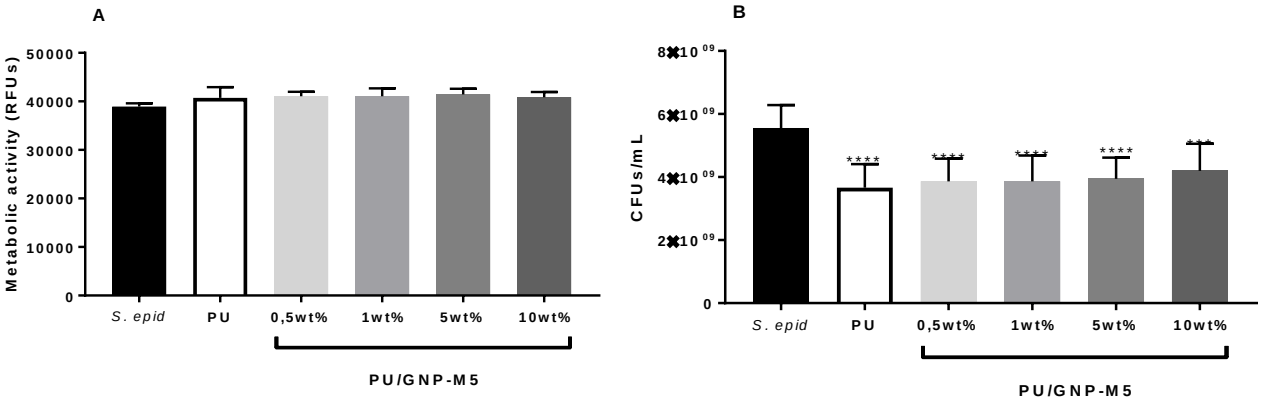


**Figure 20. Planktonic Bacteria.** Metabolic activity (A) and cultivable bacteria counting (B) of planktonic *S.epidermidis* cultured with PU/GNP-M5 composites. Statistical analysis of CFUs/mL performed with one-way ANOVA and Metabolic Activity with Kruskal Wallis tests. Statistical difference (*****) was only observed comparing with the CFUs/mL value of the control of S.epidermidis cultured on PP film *($p \leq 0.0001$)*

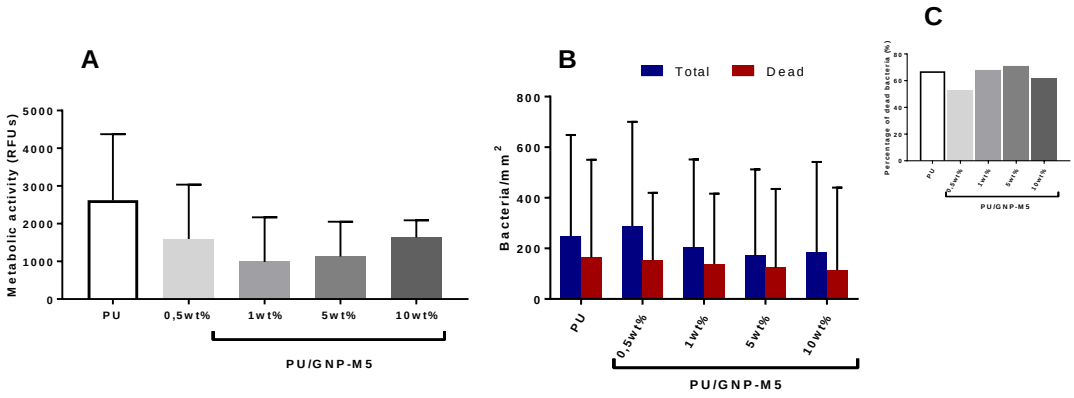

**Figure 21. Adherent Bacteria.** Metabolic activity of adhered bacteria (A) and comparison between the total and the dead adhered bacteria (B) on PU/GNP-M5 composites produced by melt-blending. Figure C represents the percentage of dead bacteria. No significant differences were detected.

PU/GNP-M15 composite antibacterial assessment for planktonic bacteria retrieve similar results to the PU/GNP-M5 composite (Figure 22). A slight decrease of metabolic activity is only found comparing the PU/GNP-M15 10 wt% composite with the neat PU sample. However, this decrease in the metabolic active planktonic bacteria is not accompanied with a decrease in cultivable bacteria, on the contrary no significant differences were observed comparing the bacteria cultured on neat PU and on the composite samples. In terms of sessile bacteria, the decrease of metabolic activity observed for PU/GNP-M5 is not observed for PU/GNP-M15. Again no significant difference is observed on the number of adhered bacteria (Figure 23 B) and the percentage of dead bacteria is also identical on the PU/GNP-M15 comparing to the neat PU surface (Figure 23 C). Representative images of the total and dead bacteria can be found in Figure A 4.

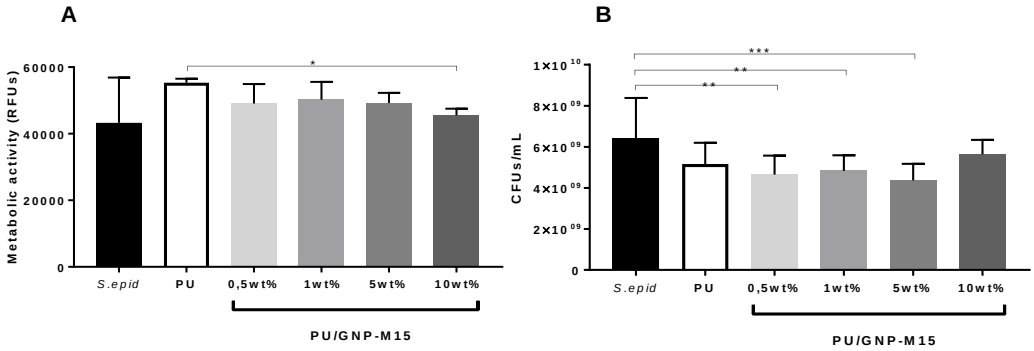


**Figure 22. Planktonic Bacteria.** Metabolic activity (A) and cultivable bacteria counting (B) of planktonic *S.epidermidis* cultured with PU/GNP-M15 composite. Statistical analysis of CFUs/mL performed with one-way ANOVA and Metabolic Activity with Kruskal Wallis tests and differences between samples are indicated with * ($p \leq 0.05$), ** ($p \leq 0.01$) and *** ($p \leq 0.001$).

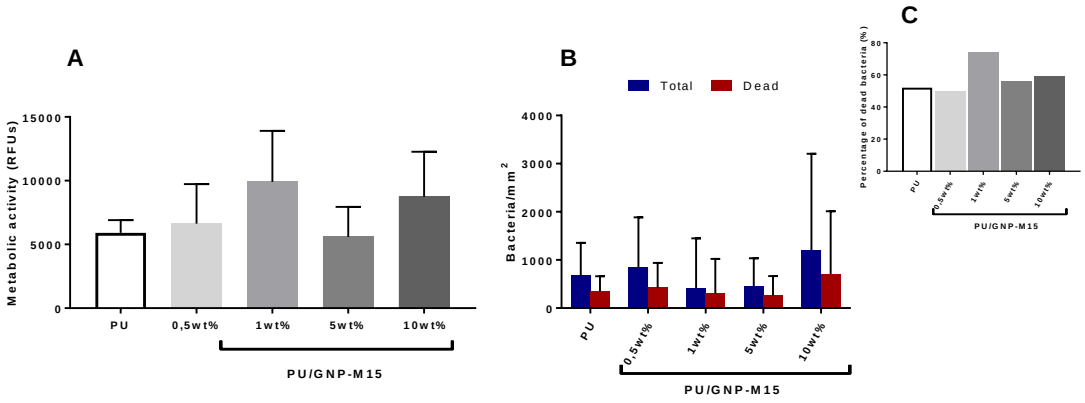


**Figure 23. Adherent Bacteria.** Metabolic activity of adhered bacteria (A) and comparison between the total and the dead adhered bacteria (B) on PU/GNP-M15 composites produced by melt-blending. Figure C represents the percentage of dead bacteria. No statistically significant differences were detected.

For PU/GNP-M5 and PU/GNP-M15 composites produced by melt-blending it was observed that GNP incorporation on PU matrix didn't yield a material with significant antibacterial activity. The surfaces didn't prevent *S.epidermidis* attachment and didn't exhibit biocidal activity. These results lead to the conclusion that the PU surface was not effectively modified and GNPs present at the surface were not enough to develop any effect on the bacteria that contact it. Moreover, in Figure A 9, it is possible to see the adhesion of bacteria around the borders of GNP-M5 at the surface of 0.5 wt% PU/GNP-M5 composite. These images were taken in preliminary tests in which after 24h incubation, the bacteria were fixed and stained with DAPI. So, bacteria also adhered and grew preferentially at the borders of the GNP, however it is not possible to conclude if the GNP was in fact exposed or covered by a polymer layer. If it were covered by polymer, a possible explanation is that rougher surfaces increase bacterial adhesion, and the areas where GNP is present at the surface have substantial roughness. This can be interesting, since the roughness induced by GBMs promotes bacterial adhesion and the subsequent contact can trigger the antibacterial activity of the GBMs, if effectively exposed.

These results contrast with some studies reporting that incorporation of GBMs increased the antibacterial activity of neat polymers. Yadav and co-workers reported the inhibition of *E. coli* growth (about 50%) when cultured for 24 h with a composite of polyurethane with carbon nanotubes[214]. In a different study the incorporation of 5% GO into PLA/PU composite reduced *E. coli* and *S. aureus* growth up to 100%[185]. Incorporation of GO has also shown to decrease the number of adherent *E. coli* and *S.aureus* on polyethylene (PE) films[179]. Melt-blending method did in fact produce composites with increasing GNP-M content relatively well dispersed on the PU matrix, however the GNP incorporation didn't lead to surface modification. The surface of the materials didn't present exposed GNP, as seen by SEM, and the wettability was not modified. The incorporation of the oxidized GNP (GNP-M5ox and GNP-M15ox) on PU by melt-blending was not performed due to the less encouraging results obtained with the non-oxidised materials. Therefore a different strategy was proposed – the development of GNP-containing coatings for application on polyurethane substrates.

# 4. PU/GNP Coatings

Different coatings containing GNP-M5, GNP-M5ox, GNP-M15 and GNP-M15ox were developed. These coatings consisted on a mixture of PU and GNPs produced by solvent mixing. In this technique the polymer and the GNPs were dissolved in the same solvent in parallel, and then the dispersions were mixed and applied on surfaces, namely glass or PU.

## 4.1. PU/GNP-M coatings on glass coverslips

In Figure 24, the visual aspect of the glass coverslips coated with PU/GNP composites can be found. It is noted, as it was reported for composites produced by melt-bending, that the GNP contents used (12 wt% of GNP in PU or PU:GNP weight ratio of 8:1) lead to a drastic change of colour from transparent PU to black or brownish colour, if GNP or oxidised GNP was incorporated, respectively. It is also visible to the naked eye that the surface is not completely uniform, with a pattern observed with the incorporation of non-oxidised GNPs and with visible GNP agglomerates particularly with GNPox incorporation. This can be

explained by a fast solvent evaporation and GNP dispersions not being completely homogeneous before the dip-coating. It was also concluded that glass was not a good substrate because dip-coating films easily detached from the glass coverslip. Glass can, however, be a good substrate if the purpose is to simply get a free-standing PU/GNP film and not to produce an adhered coating.

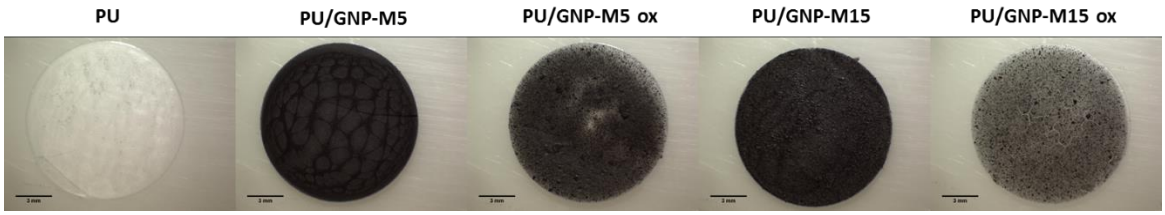


**Figure 24.** Pictures of the PU/GNP composite coatings on glass coverslips (scale bar represents 3 mm for all images).

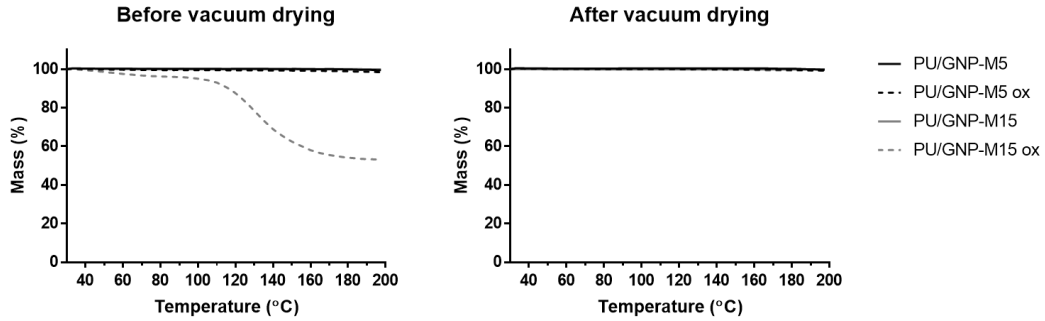


**Figure 25.** Thermogravimetry analysis of PU/GNP coatings obtained on glass coverslips before and after vacuum drying.

TG analysis (Figure 25) demonstrated that before vacuum drying there was no mass variation when increasing the temperature up to 200 °C for all the samples except for PU/GNP-M15ox coating. The decrease of mass around 100 °C indicates that the PU/GNP-M15ox coating contained some water probably due to an incomplete drying process of GNP-M15ox powder after the washing steps performed following the oxidation process. This water is eliminated during vacuum drying, as seen by no mass variation during the TG analysis. However, after drying, PU/GNP-M15ox coating had cracks and when detached from the glass coverslip it broke into small pieces. Therefore, it is essential that the powders used are completely dried or that there is no residual water. Room temperature drying for 24 h is enough for THF evaporation since no mass variation was observed for the other coatings.

Analysing the coating surface by SEM, an irregular topography with different sized wholes randomly distributed is observed for all the samples (Figure 26 C, F, I, L and O). In the matrix of the coatings the presence of GNPs is confirmed by the presence of stacked sheets and big agglomerates (yellow arrows). However, GNP is not evenly distributed and dispersed in this matrix. Moreover, GNP was hardly found at the surface and bubble-like defects were found. Energy-dispersive X-ray spectroscopy (EDS) was performed to determine the chemical composition of these surface defects (Figure 27). It was found a peak of sulphur on this bubble-like structures which indicates contamination or remaining residues from the acids used for the GNP oxidation process. The coating's thickness ranged from 17 µm to 46 µm (values obtained by analysis of the images using ImageJ software). These values and the

images at lower amplifications (Figure 26) indicate that this method produces coatings with irregular thickness. It can be concluded that this coating formulation was not effective for GNP exposure at the surface and further improvements are needed to produce uniform coatings.

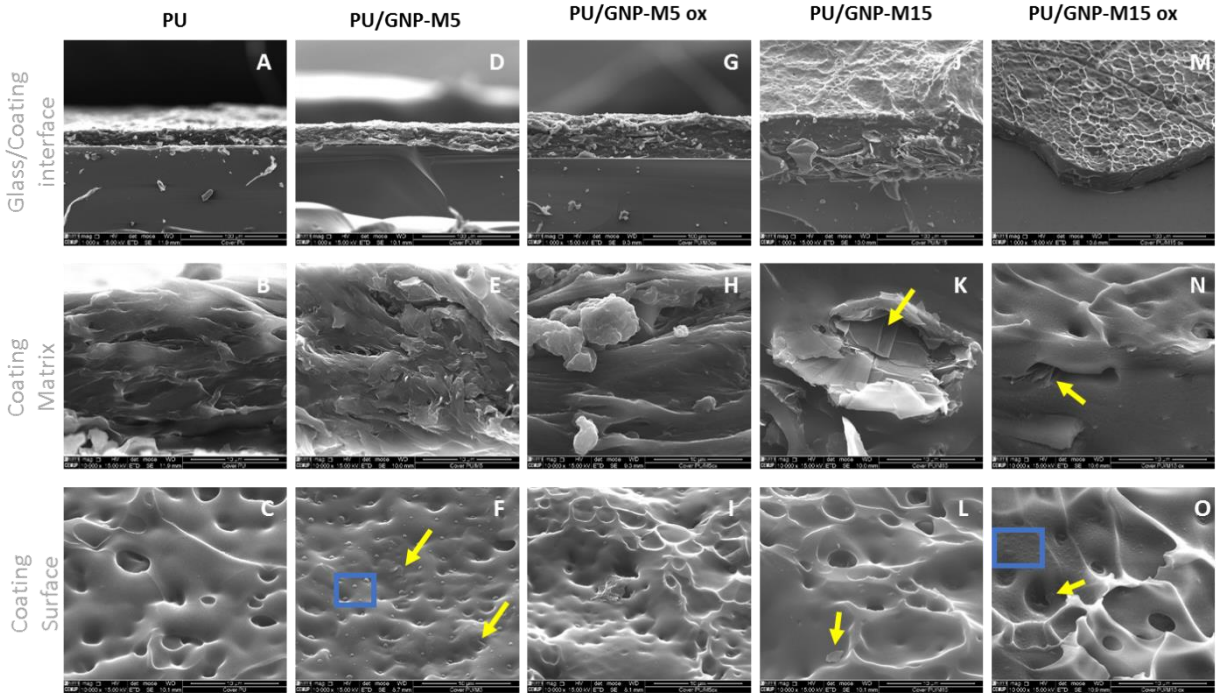


**Figure 26.** SEM images of PU and PU/GNP coatings on glass coverslips. In the lower magnification (1 000×) images the interface between the coating and the glass coverslip is visible (A, D, G, J and M). Higher magnification (10 000×) pictures were taken to the coatings' matrix (B, E, H, K and N) and surface (C, F, I, L and O). Yellow arrows indicate the presence of GNP and blue squares indicate observed bubbles at the surface. (Scale bar = 100 µm and 10 µm for 1 000×, and 10 000× magnifications, respectively).

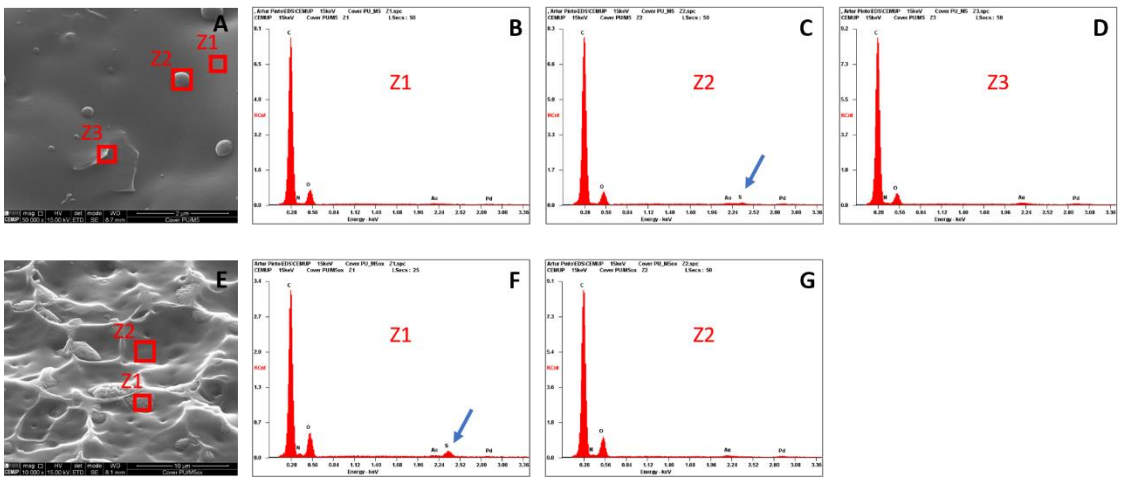

**Figure 27.** Energy-dispersive X-ray spectroscopy (EDS) was performed at different areas of the PU/GNP-M5 and PU/GNP-M5 ox coatings' surface on glass. Blue arrow indicates the presence of sulphur (S). Pictures B, C and D represent the EDS spectrums of zones Z1, Z2 and Z3 of the PU/GNP-M5 coating (A), respectively. While pictures F and G represent the EDS spectrums of zones Z1 and Z2 of the PU/GNP-M5ox coating (B), respectively.

## 4.2. PU/GNP-M coatings on PU films

The coating formulation applied on glass coverslips was also applied on neat PU samples obtained by melting and consequent injection molding of the PU pellets, to see if the fact of using glass as substrate influenced the coatings' surface. Identical surface topography was observed and exposed GNP was almost not found at the coatings' surface (Figure 28). Taking these results into account it was suggested that slow and gradual solvent evaporation together with better dispersion of GNP could yield more uniform coated surfaces. Gradual solvent evaporation should minimize the holes observed at the surfaces while a better GNP dispersion should improve its distribution on the entire surface.

For the coating formulation, the GNPs had been dispersed in tetrahydrofuran (THF), so a different solvent was tested to address if more homogeneous GNP dispersions could be achieved and thus lead to more uniform coatings. First GNP-M5, GNPM-15 and respective oxidized forms obtained by the MHM were dispersed in dimethylformamide (DMF) and THF. These solvents are both recommended by the materials manufacturer and are commonly used in various studies for graphene-based materials (GBMs) dispersion and composites preparation[171; 175; 176; 177; 185; 208]. GNP-M5, GNP-M15, GNP-M5ox and GNP-M15ox dispersions in DMF and THF were produced at different concentrations (2 wt%, 5 wt% and 10 wt%). The stability of the dispersions was assessed by subjecting the dispersions to the same preparation conditions and inspected at different times up to 4 days. Figure 30 illustrates the GNP dispersions after settling for 24 h.

Firstly, the oxidised GNPs produce a solution with a brownish colour while the GNPs solutions are black. This difference derives from the hydrophilic functional groups on the surface of GNP oxidised platelets. Time-dependent precipitation of the materials occurred in all of the dispersions, however to a higher extent in the non-oxidised materials. This is explained by the intersheet hydrophobic interactions that cause them to aggregate[215]. None of the dispersions remained visually homogeneous and stable after 1 day with GNP sedimentation observed in all (Figure 30). However, even in a smaller period of time, after 2h (Figure 29), a clear distinction can be observed between DMF dispersions and THF dispersions. The GNP dispersed in DMF exhibited higher dispersion stability than in THF after 2h. This might be explained due to the higher polarity of DMF compared to THF, the first having a dielectric constant of 38 while THF's dielectric constant is 7.6. Moreover, more sedimentation of macroscopic agglomerates was visible in the dispersions with higher loadings. Taking this information together, DMF was the solvent selected to disperse GNPs in the following work progress.

For optimization of the dip-coating formulation a large number of PU substrates were needed and since extrusion and injection molding were very time consuming processes and glass demonstrated not to be a proper substrate, neat PU films produced by casting were used. To improve the exposure of GNPs at the coating surface DMF was used as solvent for the mixture production. This solvent created better GNP dispersions, as discussed before and, according to the manufacturers, polyurethane is completely dissolved in DMF. Different GBMs concentrations and PU/GBMs ratios were tested to evaluate which mixture would induce more

exposed platelets at the coating surface and, importantly, with good interface between the two components. The purpose was to obtain well adhered GNPs exposed at the surface. To prove the concept, the GBMs used for the next sample production were GNP-M5 and GNP-M5 ox. GNP concentration was varied in order to understand if there was a direct relation between GNP concentration and GNP exposure at the surface. Also, by diminishing the ratio of PU to GNP on the coating formulation the question posed was if the PU content could be lowered to the minimum necessary to ensured GNP adherence to the substrate without "covering" it.

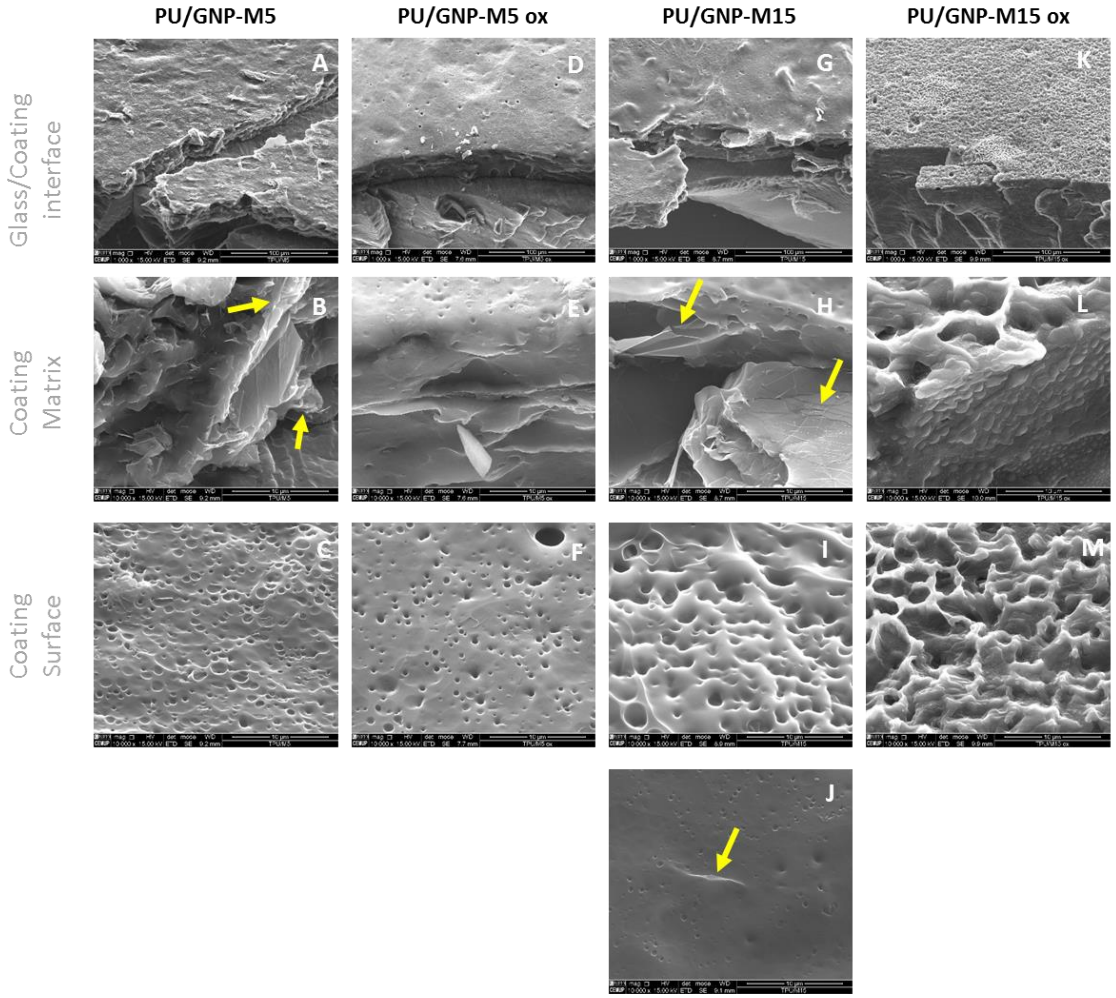


**Figure 28.** SEM images of PU/GNP coatings applied on PU obtained from extrusion-injection molding method. In the lower magnification (1 000×) pictures the interface between the coating and the PU is visible (A, D, G and K). Higher magnification (10 000×) pictures were taken to see in detail the coatings' matrix (B, E, H and L) and surface (C, F, I, J and M). Pictures I and J are from the same PU/GNP-M15 coating but in zones that present distinct topography. Yellow arrows indicate the presence of GNP. (Scale bar = 100 µm and 10 µm for 1 000× and 10 000× magnifications, respectively).

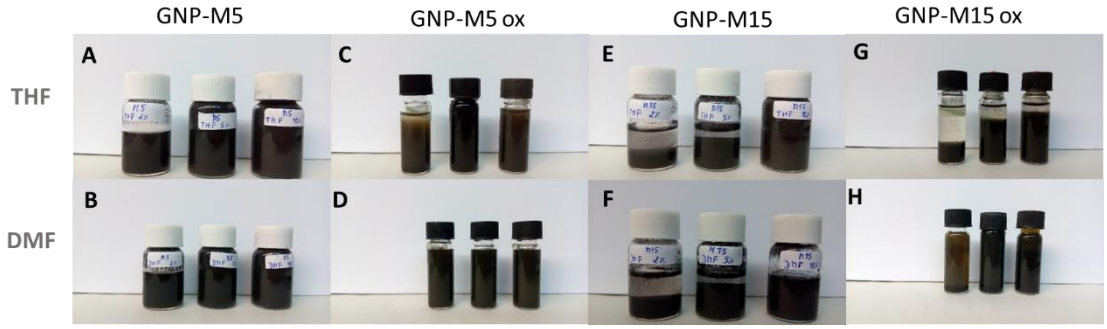


**Figure 29.** 2 wt%, 5 wt% and 10 wt% (left to right) GNP dispersions after 2h settling: GNP-M5 in THF (A) and DMF (B); GNP-M5 ox in THF (C) and DMF (D); GNP-M15 in THF (E) and DMF (F); GNP-M15 ox in THF (G) and DMF(H).

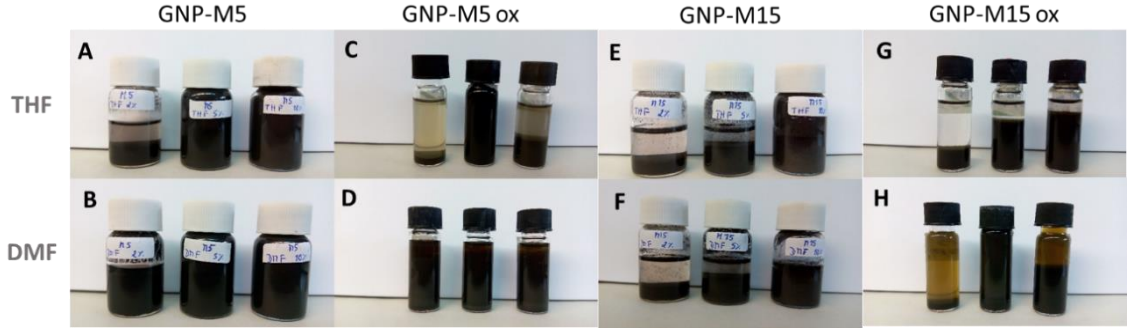


**Figure 30.** 2 wt%, 5 wt% and 10 wt% (left to right) GNP dispersions after 1 day settling: GNP-M5 in THF (A) and DMF (B); GNP-M5 ox in THF (C) and DMF (D); GNP-M15 in THF (E) and DMF (F); GNP-M15 ox in THF (G) and DMF(H).

Colour change is visible for all samples with increasingly darker aspect as the GNP-M5 and GNP-M5ox concentration increased (Figure 31). To the naked eye no difference is observed between the different PU/GNP ratios for the same concentrations. Rubbing with an eraser was performed three times for each sample as a test to evaluate the platelets adherence to the surface (Figure A 5). All of the samples completely resisted to the rubbing, meaning that no difference was observed at the coating surface nor change of colour was observed at the eraser, except for the PU/GNP-M5 coatings with the highest GNP content (1 mg/mL). For GNP-M5 coating at 1 mg/mL, resistance decreased as the PU:GNP ratio decreased from 1:1 to 1:4, where in the last case (1 mg/mL 1:4) the white eraser used turned black. This result is not surprising, it is reasonable to conclude that if the PU content is decreased, GNP is not so well adhered to the material because less interactions exist between the two. PU molecule chains contain many N-H groups that establish strong interactions with the oxygen-containing groups existent in the GNPs structure and at more extent in their oxidised forms[185].

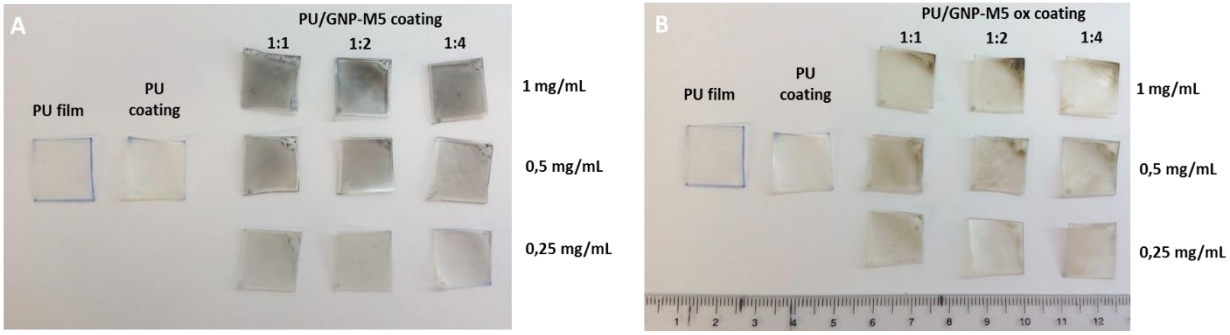


**Figure 31.** Images of the different samples obtained: PU film produced by casting and PU coating on PU film (control), PU/GNP-M5 (A) and PU/GNP-M5 ox coatings (B) on PU film

Isopropanol (IPA) was also tested for GNP-M5 dispersion and the coating produced seemed to have less GNP content, visible by a very bright colour compared to the coating produced at the same experimental conditions but using DMF as solvent (Figure A 6). This might be explained by the different PU Tecothane® solubility in DMF and IPA, according to the suppliers PU is completely dissolved in DMF but not in IPA. Thus, the interaction between the solvent used and the PU of the substrate is very important, but further studies are need to reach a solid conclusion.

Compared to the composites obtained by melt-blending, the coatings produced by these dip-coating formulations present much more GNP platelets exposed at the surface (Figure 32). Agglomerations can be seen in the lower magnification pictures and the surfaces produced have areas with high concentration of GNPs and areas with more distributed GNP. All surfaces present a mesh appearance, even the control obtained by dip-coating the PU casted films into a neat PU solution in DMF. This can be induced by the solvent evaporation and consequent PU precipitation. In PU/GNP-M5 coatings many graphene platelets were found at the surface and in different orientations; the sharp edges of the platelets seem to emerge or burst from the composite matrix. These sharp edges can be observed in pictures of higher magnification (Figure 32 right pictures). Thin platelets are found with random orientation, it is possible to see a platelet in an almost complete transversal position (Figure 32 G3). Some of the platelets observed at the surface are partially or completely covered with polyurethane (blue arrow in Figure 32 C3).

As can be seen in Figure 33, the surface of the PU/GNP-M5ox is very different. Platelet-like forms suggesting the presence of GNP at the surface were not visible, however the entire surface had areas with a rough topography similar to the GNP-Mox powders (Figure 12 G-O). It is also visible the formation of spherical agglomerates with a highly wrinkled topography. The size of these spheres decreases with decreasing GNP-M5ox concentration. This might be explained by strong physical interactions between PU and GNP-M5ox. In the liquid-phase mixing method used, when PU is mixed with oxidized GNP sheets they will preferentially stick together, causing agglomerated GNPox/PU structures to be formed upon solvent evaporation, instead of a thin film spreading over the surface[185]. The surface is more uniform, with spheres better distributed at the lowest GNP-M5ox concentration tested (0.25 µg/mL) possibly due to better dispersions at lower GNP contents. It can also be seen that decreasing the PU content in the coating mixture (PU:GNP ratio decrease from 1:1 to 1:4, maintaining the GNP concentration in DMF) the surface acquires a more mesh-like topography. This can be explained because PU exists in lower quantities and is not enough for complete uniform surface coverage, but enough to allow the coating to stick to the PU film substrate and to guarantee the presence of GNP at the surface.

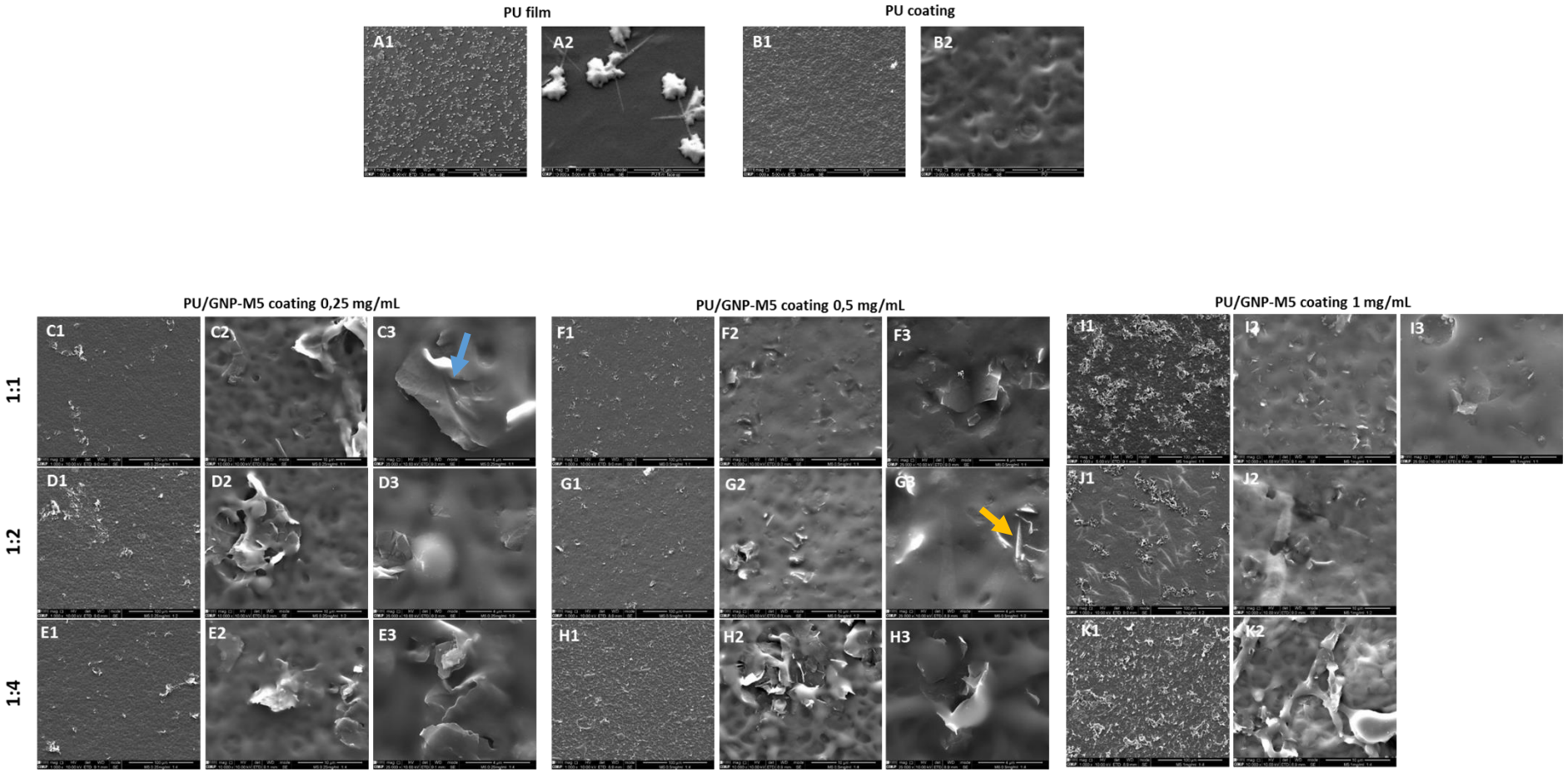


**Figure 32.** SEM images of the PU film produced by casting, PU coating on PU film (control) and PU/GNP-M5 coatings on PU film at different GNP concentrations and PU:GNP ratios tested. Pictures at 1 000× (picture 1), 10 000× (picture 2) and 25 000× (picture 3) magnifications were taken. Blue arrow indicates GNP partially covered with polymer and yellow arrow pints to GNP transversely oriented. (Scale bar = 100 µm, 10 µm and 4 µm for 1 000×, 10 000× and 25 000× magnifications, respectively).

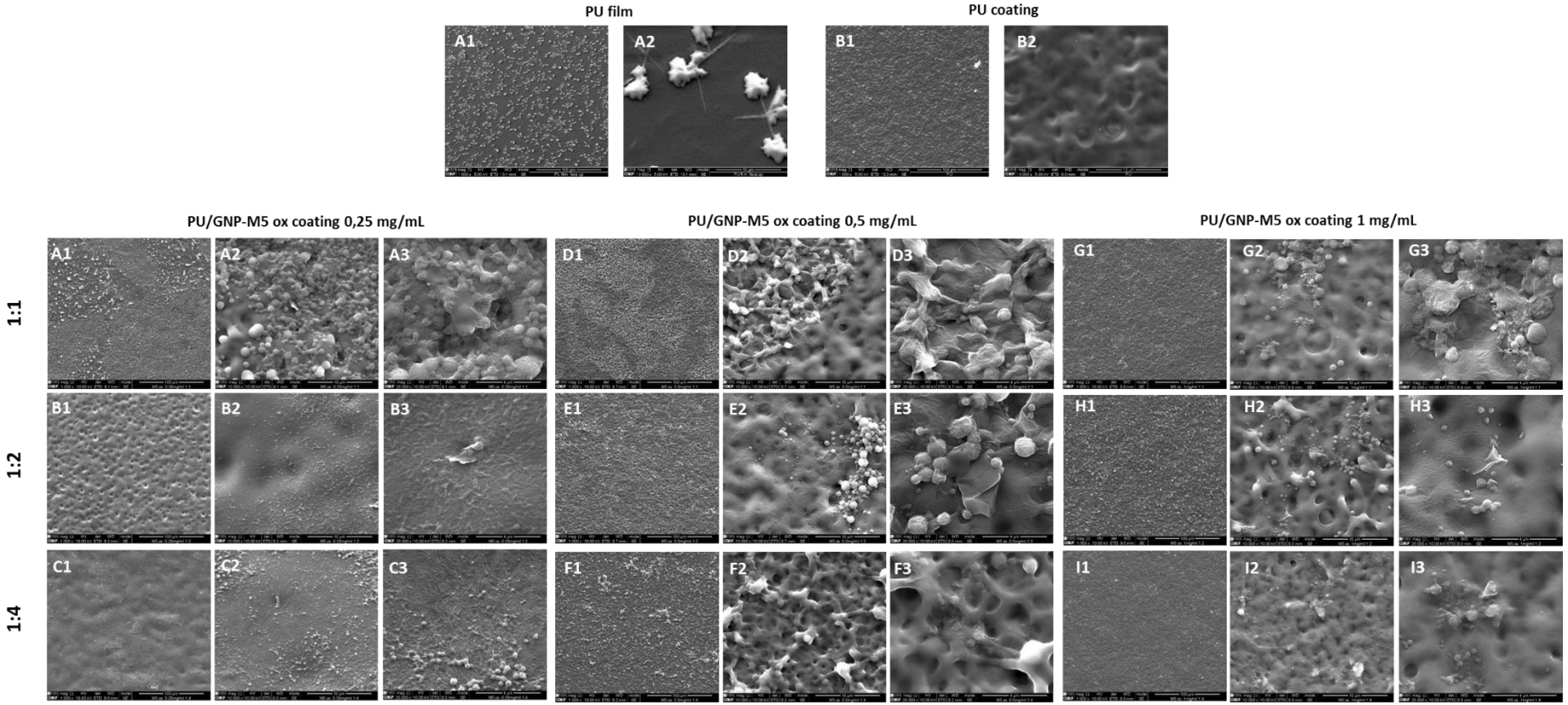


**Figure 33.** SEM images of the PU film produced by casting, PU coating on PU film (control) and PU/GNP-M5ox coatings on PU film at different GNP concentrations and PU:GNP ratios tested. Pictures at 1 000× (picture 1), 10 000× (picture 2) and 25 000× (picture 3) magnifications were taken. (Scale bar = 100 µm, 10 µm and 4 µm for 1 000×, 10 000× and 25 000× magnifications, respectively).

Coatings' wettability was analysed by water contact angle measurements and results are depicted in Figure 34. PU casted film and PU coating on PU film had a water contact angle of 85°. This value is in accordance with Zhao *et al.* work, in which PU Tecothane films produced by casting from a 5% (w/v) solution in DMF had a contact angle of 90◦[210]. In PU/GNP-M5 coating, there seems to be a slight tendency for contact angle increase with increasing GNP concentration maintaining the PU:GNP ratio. Varying the PU:GNP ratio and maintaining the same GNP concentration there is only a visible effect for the 1:4 ratio, where the highest GNP-M5 concentration (1mg/mL) had a higher contact angle compared to the lowest concentration (0.25 mg/mL). Therefore, wettability change was only detected at the sample of PU/GNP-M5 coating with 1 mg/mL GNP concentration and 1:4 PU:GNP ratio, with the water contact angle of PU increased to about 100°. The higher hydrophobicity is justified by the presence of more GNPs exposed at the surface and in agglomerates, forming hydrophobic sites. Identical results were demonstrated for poly(vinyl acetate) (PVAc) with incorporation of 0.1 wt% GNPs[216]. For the PU/GNP-M5ox coatings the water contact angle was roughly the same for all samples with no obvious tendency observed. It would be expected that GNP-M5ox slightly decreased the water contact angle and hence increased the hydrophilicity of the surface[59]. However, wettability is affected not only by the chemical composition but also by the surface roughness. Surface roughness will enhance the wettability caused by the chemistry of the surface. So the contact angles measured cannot be directly correlated with the GNPs presence at the surface because the different topography and the degree of surface roughness has to be taken in consideration.

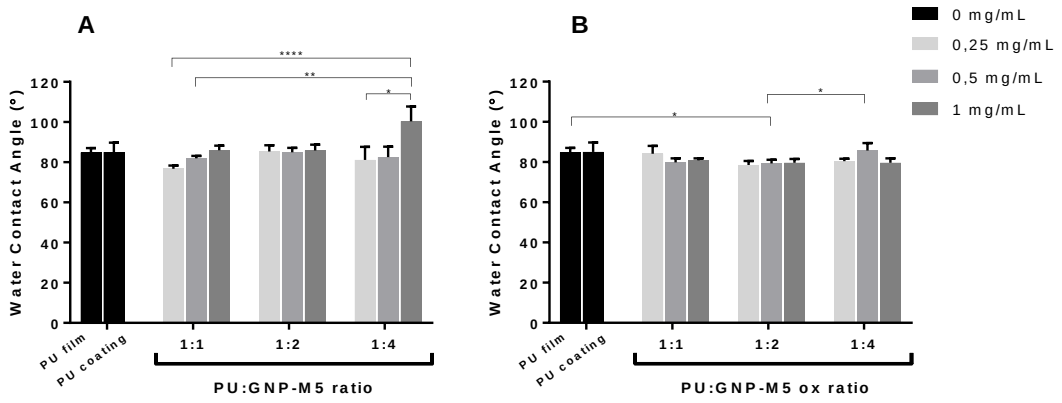


**Figure 34.** Water contact angle measurement for PU film obtained by casting, PU coating, PU/GNP-M5 (A) and PU/GNP-M5 ox (B) coatings applied on PU casting film. Statistic test performed was Kruskal Wallis and statistically significant differences are indicated with * ($p \leq 0.05$), ** ($p \leq 0.01$), *** ($p \leq 0.001$) and **** ($p \leq 0.0001$).

This method of solvent mixing PU and GNP, and applying this mixture by dip-coating produced PU surfaces with exposed GNP, and thus one of the goals was achieved. Due to time constraints, for antibacterial activity assessment, some of the tested conditions had to be selected, otherwise the number of samples to analyse would be excessive and unfeasible. The intermediate GNP concentration of 0.5 mg/mL was chosen to assess the effect of PU:GNP ratio and, to assess the GNP concentration effect, all samples at PU:GNP ratio of 1:2 were analysed. Therefore, for PU/GNP-M5 coatings the samples tested were: 1mg/mL 1:2, 0.5 mg/mL 1:1, 0.5 mg/mL 1:2, 0.5 mg/mL 1:4 and 0.25 mg/mL 1:2. For PU/GNP-M5ox coatings the same samples were analysed and 0.25 mg/mL 1:1 was also analysed because it was the surface where more

spherical composite structures were observed. The square samples were cut into circular shapes with 14 mm diameter (Figure 35) and sterilized with ethanol prior to antibacterial activity assessment.

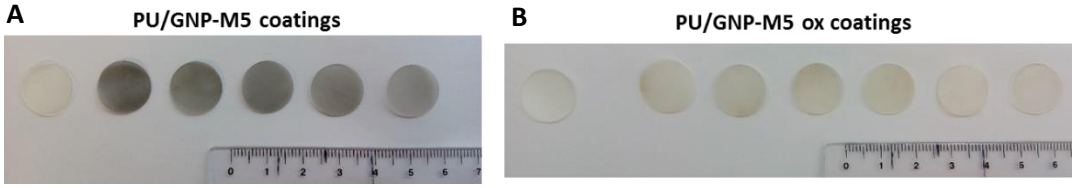


**Figure 35.** Circular samples (14 mm diameter) obtained by cutting the dip-coated squares with a puncher. A- PU coating and PU/GNP-M5 1mg/mL 1:2, 0.5 mg/mL 1:1, 0.5 mg/mL 1:2, 0.5 mg/mL 1:4 and 0.25 mg/mL 1:2 coatings from left to right. B- PU coating and PU/GNP-M5 ox 1mg/mL 1:2, 0.5 mg/mL 1:1, 0.5 mg/mL 1:2, 0.5 mg/mL 1:4, 0.25 mg/mL 1:1 and 0.25 mg/mL 1:2 coatings from left to right.

## 4.3. Antibacterial Properties of PU/GNP coatings

The antibacterial activity was assessed in coatings by measuring the metabolic active bacteria (Alamar blue assay) and cultivable bacteria (CFUs counting) of the supernatant after inoculation with *S. epidermidis* and 24h incubation. Metabolic activity of the bacteria adhered to the coatings was also evaluated, and the counting of the total and dead cells was further performed through fluorescent staining with Hoechst and PI stains, respectively.

In Figure 36 A, it is possible to see that the contact of bacteria with the GNP-M5 containing coatings didn't inhibit the growth of bacteria. Moreover, instead of a decrease of cultivable bacteria there was in fact a slight increase comparing with the control of neat PU. The highest increase of viable bacteria was about 30% and it was when incubated with 0.25 mg/mL 1:2 and 1 mg/mL 1:2 PU/GNP-M5 coatings. However, the order of magnitude is the same (2-4 x $10^9$ CFUs/mL) for all samples, which in terms of bacterial growth is not significant. In terms of metabolic activity there were no significant differences observed, except for a slight decrease on 0.5 mg/mL 1:1 PU/GNP-M5 coating comparing with neat PU coating (Figure 36 B). And interestingly the slight increase of viable bacteria on 0.25 mg/mL 1:2 and 1 mg/mL 1:2 PU/GNP-M5 coatings (Figure 36 A) is accompanied by a slight increase of metabolic activity (Figure 36 B). Anti-planktonic activity for PU/GNP-M5 coatings was not verified, though 0.25 mg/mL 1:2 and 1 mg/mL 1:2 PU/GNP-M5 coatings seem to have the opposite effect to the desired. The bacteria collected from the samples washings were metabolically active, as seen by no difference comparing with the controls, and they remained viable.

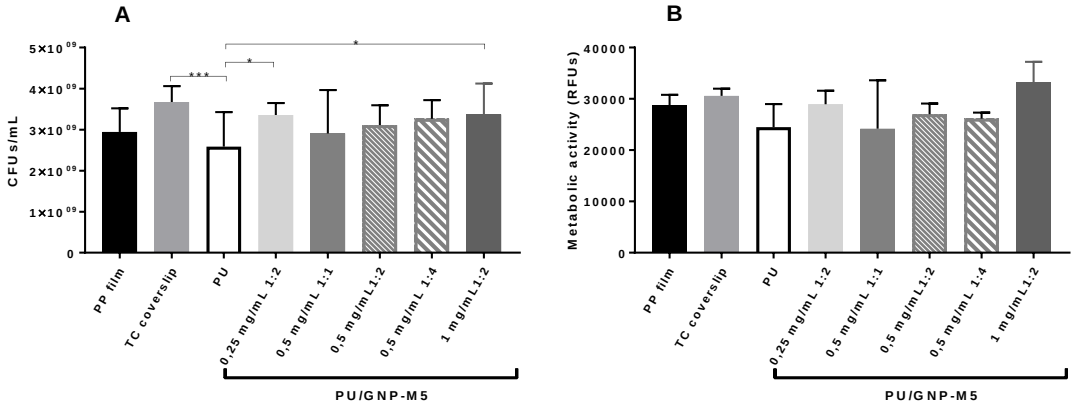


**Figure 36. Planktonic Bacteria.** Metabolic activity and cultivable bacteria counting of planktonic *S.epidermidis* cultured on PU/GNP-M5 coatings on PU. Statistical analysis of CFUs/mL performed with one-way ANOVA and Metabolic Activity with Kruskal Wallis tests and differences are indicated with * ($p \leq 0.05$), ** ($p \leq 0.01$) and *** ($p \leq 0.001$).

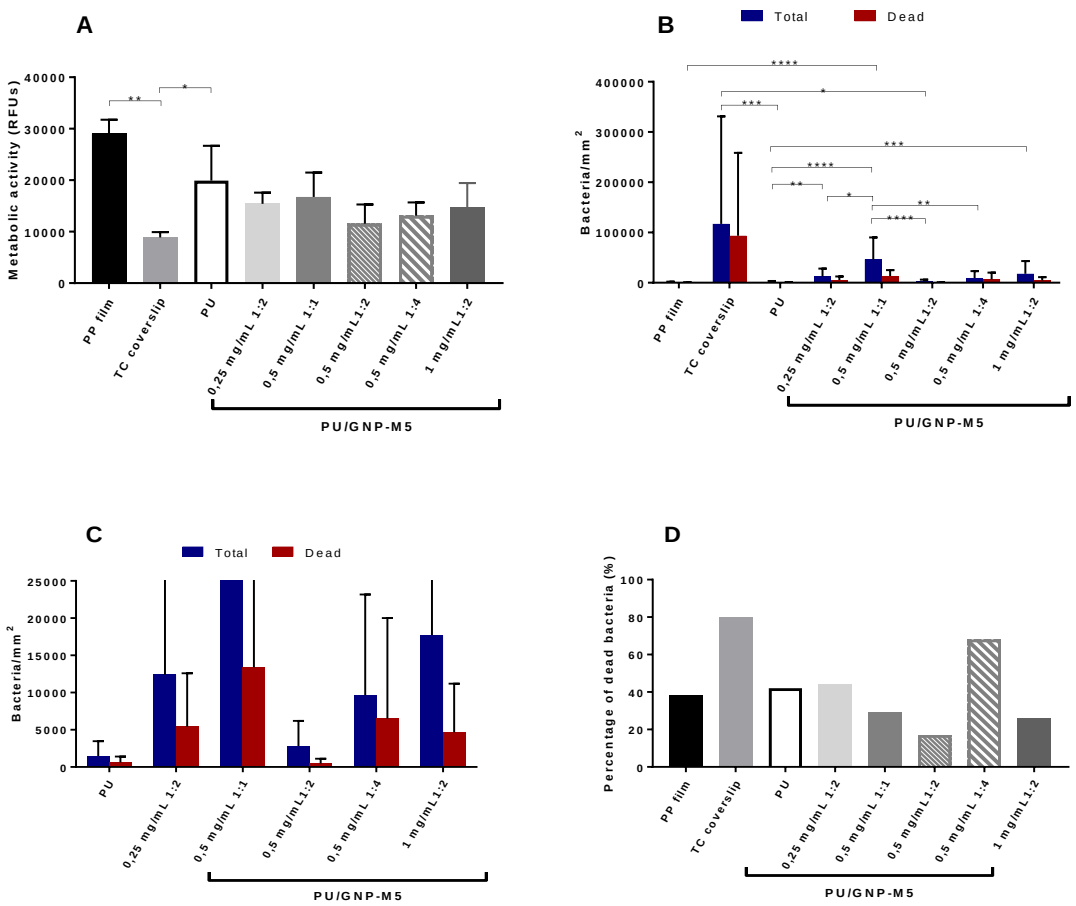


**Figure 37. Adherent Bacteria.** Metabolic activity of adhered bacteria (A) and comparison between the total and the dead adhered bacteria (B) on PU/GNP-M5 coatings on PU. Figure C, is a zoomed Figure B and excluding the controls PP film and TC coverslips to better compare the PU/GNP-M5 coatings with neat PU coating. The percentage of dead bacteria for each sample is described at D. Statistical analysis performed with Kruskal Wallis test and differences are indicated with * ($p \leq 0.05$), ** ($p \leq 0.01$), *** ($p \leq 0.001$) and **** ($p \leq 0.0001$).

Analysing the anti-sessile effects of GNP-M5 coatings there were differences comparing with the effects on planktonic bacteria. In terms of metabolic activity, comparing with neat PU coating, there is a decrease of 23, 16, 42, 34 and 26% on 0.25 mg/mL 1:2, 0.5 mg/mL 1:1, 0.5 mg/mL 1:2, 0.5 mg/mL 1:4 and 1 mg/mL 1:2 PU/GNP-M15 coating surfaces, respectively (Figure 37 A). The intermediate GNP concentration (0.5 mg/mL) yielded the lowest metabolic activity at the PU:GNP ratio of 1:2. None of the coatings tested showed anti-attachment activity when compared with the PU coating, since they all had more bacteria adhered (Figure 37 C). The sample that had more attached bacteria was the 0.5 mg/mL 1:1 however they were not metabolic active, otherwise an increase had to be detected on Figure 37 A. In fact, the increased number of adherent bacteria was not accompanied by an increase in the metabolic activity, which can indicate that bacteria in contact with the surfaces were metabolically less active. The PU/GNP-M5 coating with the lowest adhered bacteria was the 0.5 mg/mL 1:2 PU/GNP-M5 (total number of bacteria identical to neat PU sample), however the percentage of dead bacteria was low (Figure 37 C and D). So it is possible that this surface has antifouling properties but no bactericide activity, however this surface seemed to behave similarly to the neat PU coating. While 0.5 mg/mL 1:4 PU/GNP-M5 coating had the highest percentage of dead bacteria, around 68%. This surface can act not by preventing bacteria attachment but by killing the bacteria that adhere.

This results suggest that, as expected, the surfaces modified with GNP-M5 act by contact and they exert no effect on planktonic bacteria. The 0.5 mg/mL 1:4 PU/GNP-M5 seemed to have better activity than the other tested surfaces, however further experiments ought to be performed to confirm these results. This antibacterial activity can be explained by the characteristics of the surface. As seen by SEM (Figure 32), this surface had GNP-M5 better dispersed at the surface and with many platelets exposed. It leads to the conclusion that increasing the GNP concentration (to 1 mg/mL) is not favourable because it can lead to the platelets agglomeration which will ultimately lead to less GNP exposed by surface area. And decreasing the amount of PU in the coating solution allows higher GNP-M5 exposure and consequently incubated bacteria can contact with more platelets and suffer from their antibacterial activity.

For PU/GNP-M5ox coatings there were no differences in terms of viable bacteria present in the supernatant (Figure 38 A). However there is a decrease on the metabolic activity on the PU/GNP-M5ox coatings at the GNP concentrations of 0.25 mg/mL and 0.5 mg/mL comparing with PU. This effect is more significant for the 0.25 mg/mL 1:1 and 0.5 mg/mL 1:4 samples. Hence, oxidised GNP-M5 had an effect on the planktonic bacteria whereas the non-oxidised material didn’t. These coatings had a very irregular surface and wrinkled aspect (Figure 32) which may lead to a higher surface area for bacteria to contact with the oxidised GNP spread on the surface.

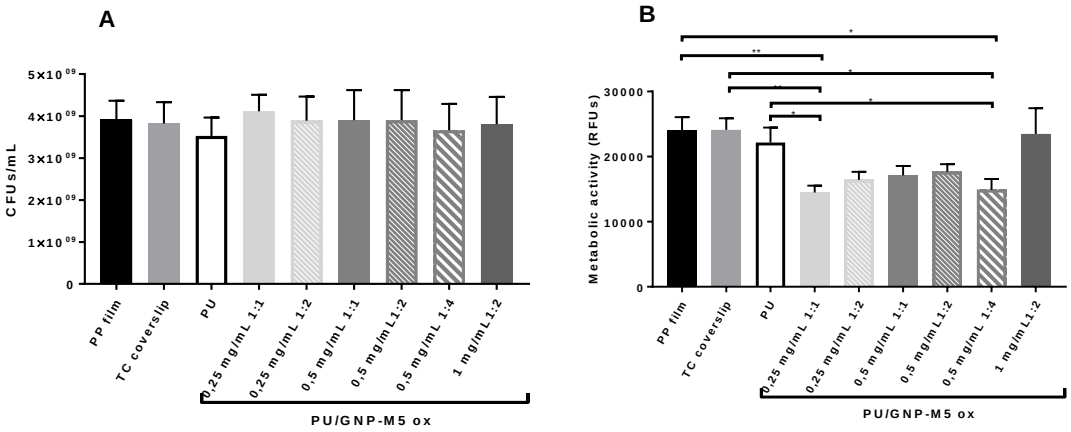


**Figure 38. Planktonic Bacteria.** Metabolic activity and cultivable bacteria counting of planktonic *S.epidermidis* cultured on PU/GNP-M5ox coatings on PU. Statistical analysis of CFUs/mL performed with one-way ANOVA and Metabolic Activity with Kruskal Wallis tests. Statistically significant differences are indicated with * ($p \leq 0.05$) and ** ($p \leq 0.01$).

In terms of the metabolic activity of the adherent bacteria, a decrease is only suggested for 0.25 mg/mL 1:2 and 0.5 mg/mL 1:1 samples PU/GNP-M5ox coatings comparing with PU coating, though not statistically significant (Figure 39 A). *S. epidermidis* attachment was prevented for 0.5 mg/mL 1:1 and 0.5 mg/mL 1:2 coatings (Figure 39 C). These surfaces exerted an antifouling effect on S. epidermidis and hindered the bacteria adhesion and biofilm formation by more than 80% comparing with PU coating. However the adherent bacteria were still metabolically active. So these two coatings, GNP-M5ox 0.5 mg/mL 1:1 and 0.5 mg/mL 1:2, have an anti-adhesive effect possibly due to a better distribution of platelets at the surface (see Figure A 7), while GNP-M5ox at higher concentration yields a surface with GNP big agglomerates that consist on an accumulation of platelets with killing potential (Figure 39 D). In fact 1 mg/mL 1:2 PU/GNP-M5ox coating had a substantial increase of adhered bacteria but almost 100 % of them were dead. At the lowest concentration (0.25 mg/mL), graphene platelets were more uniformly distributed and probably more covered with polymer hindering the direct contact of GNP with bacteria, and the surface topography favoured bacteria adherence.

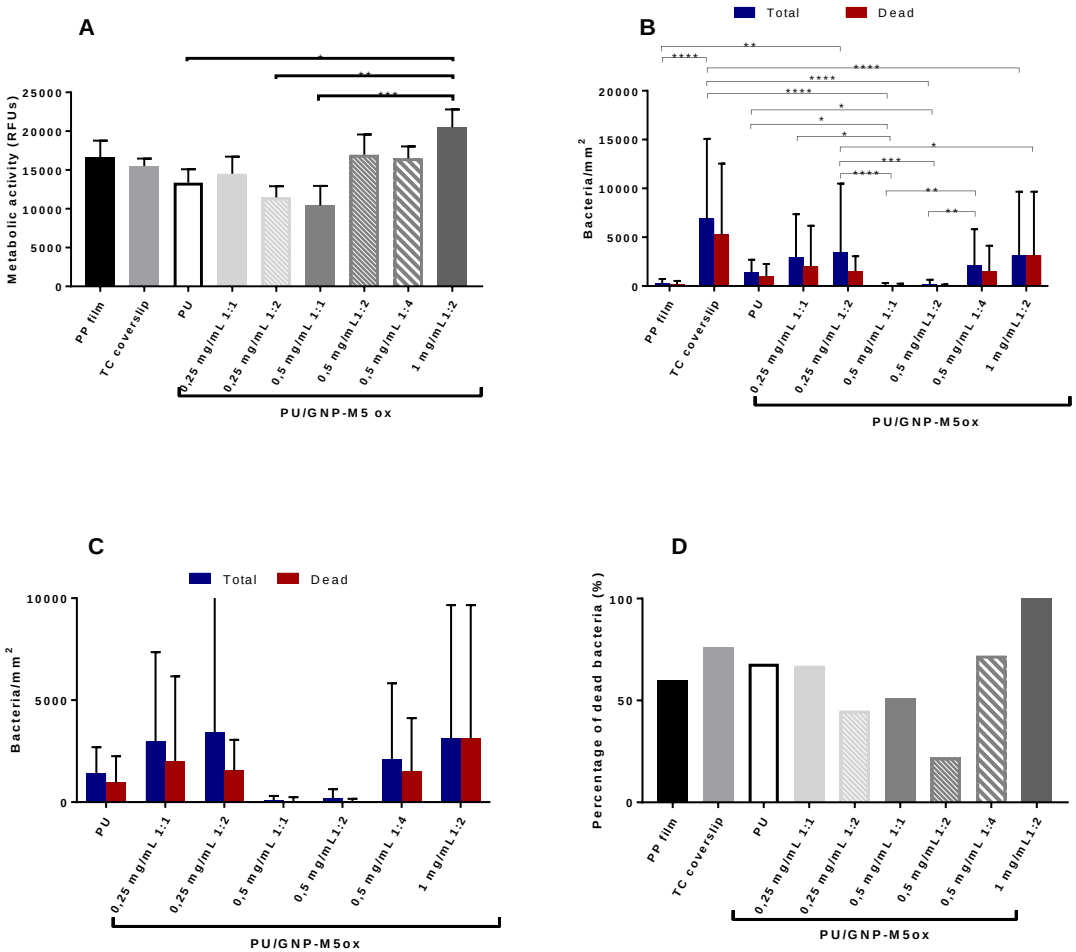


**Figure 39. Adherent Bacteria.** Metabolic activity of adhered bacteria (A) and comparison between the total and the dead adhered bacteria (B) on PU/GNP-M5ox coatings on PU. Figure C, is a zoomed Figure B and excluding the controls PP film and TC coverslips to better compare the PU/GNP-M5 coatings with neat PU coating. The percentage of dead bacteria for each sample is described at D. Statistical analysis performed with Kruskal Wallis test and differences are indicated with * ($p \leq 0.05$), ** ($p \leq 0.01$), *** ($p \leq 0.001$) and **** ($p \leq 0.0001$).

Comparing PU/GNP-M5 and PU/GNP-M5ox coatings, there is indication that the surface modified with oxidised GNP rendered better antibacterial activity by either antifouling or killing effects, depending on the GNP concentration. In view of the application for catheter-infection prevention, a surface that inhibited bacteria attachment would be ideal since it acts at the frontline as a prevention measure and not as a counteragent. Thus, PU/GNP-M5ox 0.5 mg/mL 1:1 and 1:2 coatings are the most promising. In the representative fluorescence pictures (Figure A 7 and Figure A 8), it is shown that bacteria seemed to adhere preferentially to the area around the platelets and on top of the platelets. So the roughness caused by GNP incorporation on the coatings leads to more bacterial adhesion and the effects of their contact is later demonstrated by bacteria death, particularly seen for PU/GNP-M5ox 1 mg/mL 1:2 coating.

Evaluation of the adherent bacteria was found to be difficult with fluorescent staining. PU samples possess autofluorescence hindering a clear and background-free image, and dip-coating produces coatings with a non-uniform thickness making it difficult to mount the samples for microscope observation. Moreover, since the incubation time is long (24h) *S.*

*epidermidis* adheres and grows to form biofilm. Hence, the growth of the bacteria happens also in a three-dimensional (3D) fashion since biofilm has a 3D structure, therefore hampering a perfect focus when acquiring the microscope images. Confocal microscopy could be used however, it is an even more time-consuming technique, making it more difficult to analyse the high number of samples resulting from these assays. A proposed alternative is the recovery of the adherent bacteria by washings and sonication. However this has also disadvantages because there is always the possibility of not being recovered the totality of the bacteria or even killing some upon sonication[197].

Ruiz *et al.* reported GO-coated filters lacking bacteriostatic activity and even supported *E. coli* growth[94]. These results were attributed to GO lying flat on the substrate with few exposed edges. Li *et al.* evaluated the interaction of graphene films on different substrates and observed no growth of *S. aureus* and *E. coli* when graphene was applied on conducting and semiconducting surfaces, presenting therefore bactericidal activity[105]. It seems clear that, as the interaction of bacteria with GBMs is dependent on the orientation of the surface relative to the bacteria, the way GBMs are deposited onto surfaces can influence the antimicrobial properties. In fact, Pham and co-workers reported increased numbers of attached *P. aeruginosa* and *S. aureus* cells on graphite surfaces with greater smoothness and that cells remained viable, while increased density of graphene edges lead to bactericidal activity[113]. In this work, it was also proposed that the decreased density of graphene edges allowed *S. aureus* cells to colonize the surface of graphene nanosheets. Liu *et al.* also reported that GO sheets could aggregate *E. coli* cells together and didn't kill them[80]. Identical behaviour was observed in the present work, with *S. epidermidis* adhering preferentially to the surface of GNPs.

The dip coating demonstrated to be a useful way to produce a GNP coating on polyurethane surface, however this technique resulted in non-uniform coating thickness on substrate and aggregation of GNP and GNPox. During the blending, the polymer coats the surface of the stacked sheets and interconnects them after the organic solvents are removed, resulting in inhomogeneous distribution of sheets in polymer matrix[4].

Due to time restrictions and since the coating strategy appeared at a later stage of the work, the results reported come from non-repeated experiments and hence repetition is essential to confirm and clarify the antibacterial effects of the surfaces.

# CHAPTER V:
# Conclusion and Future Work

## 1. Conclusion

Oxidation of the graphene nanoplatelets M5 and M15 used yielded platelets with a more wrapped-like aspect and with more oxygen-containing groups at the surface and edges. Aqueous dispersions of the non-oxidised and oxidised GNPs have shown to decrease *S. epidermidis* metabolic activity and viability, with oxidized GNPs having stronger antibacterial effect than the non-oxidized GNPs, independently of the platelets size.

GNP-M and GNP-Mox were for the first time incorporated into thermoplastic polyurethane to produce a material with antibacterial properties. Different strategies were followed, namely the production by melt-blending of polyurethane composites with GNP-M5 and GNP-M15 as nanofillers, and the application of a composite coating onto a glass or polyurethane surface by dip-coating from GNP dispersions containing dissolved PU.

For both the composites produced and for the coatings it was seen that the behaviour of the interface between the matrix and the dispersion phase is one of the parameters that restrain a homogenous dispersion of the nanofillers and causes GNPs agglomeration. The composites produced by melt-blending showed a good dispersion of GNPs in the polyurethane matrix but no significant modification of the surface. Very few GNPs were found exposed at the surface, and they were distributed in a planar conformation with no edges exposed and mostly covered with polymer. Antibacterial assessment confirmed that the GNPs present at the surface were not sufficient to effectively contact bacteria and no effects were detected on bacteria attachment, metabolic activity or viability. Dip coating was performed to produce PU films coated with GNP-M and GNP-Mox. It was verified that good dispersions and solvent evaporation are critical factors to fabricate uniform and homogeneous coatings. The solvent has to evaporate at a slow rate to avoid GNPs agglomeration and the formation of bubbles or holes at the surface. The application of either PU/GNP-M or GNP-Mox coatings on PU using different GNP concentrations and PU:GNP ratios effectively increased the exposure of GNPs at the surface comparing with the melt blending composites. The surfaces were analysed by SEM and demonstrated to be very irregular and with high roughness, due to holes formed upon solvent evaporation and due to the GNPs. Exposed GNPs had different orientations, with many oriented transversally to the surface. Moreover, the PU/GNPox coatings presented different topography from the PU/GNP coatings. The surface was much more wrinkled and spherical structures were observed for all PU/GNPox coatings with different sizes and distribution depending on the GNP concentration and PU ratio. Comparing with the neat polyurethane control, the coatings didn't present striking antibacterial activity, despite some surfaces presenting interesting effects. For planktonic bacteria only the PU/GNP-M5ox coating seemed to decrease *S. epidermidis* metabolic activity. In terms of adherent bacteria, results obtained suggest PU/GNP-M5ox coatings as having stronger effect than PU/GNP-M5, either by inhibiting bacteria attachment or by increased bactericidal activity. The PU/GNP-M5ox coatings produced with GNP concentration of 0.5 mg/mL demonstrated to have an anti-

adhesive effect possibly due to a better distribution of platelets at the surface. On the other hand, 1 mg/mL 1:2 PU/GNP-M5ox coatings had an increased bacterial adhesion but a very high bactericide activity.

This work has demonstrated the potential of GNP incorporation to develop PU with antibacterial properties, however further studies should be performed to confirm and clarify the properties of these surfaces.

## 2. Future Work

The results obtained still leave a lot of questions to answer and work to be done. On the dip coating technique, measures of surface roughness and viscosity of the different solutions used should be performed. It would be interesting to see if these solutions are homogeneous, because to the naked eye all the solutions are black and there is no real awareness on the homogeneity of the dispersions. For that, since we work with organic solvents, a technique that could be performed is Cryo-SEM. This would give information on the homogeneity of the dispersions and if this correlates with the homogeneity of the surfaces obtained. Due to time restrictions this was not performed but it is something to do in the short-term. GNP-M15 and GNP-M15 ox are also going to be used for the production of dip coating samples onto PU films. In fact, the samples are already being produced and antibacterial testing is on the agenda. The dip-coating method performed needs optimization since the coatings' surface was not uniform, with areas with GNP aggregation and different roughness. Here, different dipping times and different viscosities could be tested by varying the solvent content of the mixture. Even the drying process could be optimized to obtain a more homogeneous drying over the entire surface area. Also, samples were dried vertically which could induce flowing of the solvent mixture and accumulation at the lower part of the sample.

It would also be useful to see if a surface of pure GNP-M5, GNP-M5ox, GNP-M15 and GNP-M15ox present antibacterial activity. This would give information on the effects of GNPs in direct contact with bacteria. The antibacterial activity of structurally flat GNPs is an interesting topic to investigate. Besides dip coating, other methods can be tested to form GBMs films on PU like spraying, Langmuir–Blodgett (LB) technique, spin coating and drop casting. These last two methods allow the control of the evaporation time which can, consequently, control the GNP distribution along the coating. GNP surface can also be functionalized to improve its dispersibility in organic solvents.

Finally, besides *S. epidermidis,* it is obviously important to test other bacteria involved in catheter-related infections in the future.

# REFERENCES


[1] Chee, W., Lim, H., Huang, N., & Harrison, I. (2015). Nanocomposites of graphene/polymers: a review. *RSC Advances, 5*(83), 68014-68051.

[2] Kim, H., Abdala, A. A., & Macosko, C. W. (2010). Graphene/Polymer Nanocomposites. *Macromolecules, 43*(16), 6515-6530. doi:10.1021/ma100572e

[3] Potts, J. R., Dreyer, D. R., Bielawski, C. W., & Ruoff, R. S. (2011). Graphene-based polymer nanocomposites. *Polymer, 52*(1), 5-25.

[4] Singh, V., Joung, D., Zhai, L., Das, S., Khondaker, S. I., & Seal, S. (2011). Graphene based materials: Past, present and future. *Progress in Materials Science, 56*(8), 1178-1271. doi:10.1016/j.pmatsci.2011.03.003

[5] Lee, G., & Bishop, P. (2012). *Microbiology and infection control for health professionals*: Pearson Higher Education AU.

[6] Gloukhoff Wentling, A. (2004). Hemodialysis catheters: materials, design and manufacturing *Hemodialysis vascular access and peritoneal dialysis access* (Vol. 142, pp. 112-127): Karger Publishers.

[7] Ma, N., Petit, A., Huk, O. L., Yahia, L. H., & Tabrizian, M. (2003). Safety issue of re-sterilization of polyurethane electrophysiology catheters: a cytotoxicity study. *Journal of Biomaterials Science, Polymer Edition, 14*(3), 213-226.

[8] Diseases, N. I. o. D. a. D. a. K. (Producer). (2014, 25/08/2016). Vascular Access for Hemodialysis. Retrieved from https://www.niddk.nih.gov/health-information/health-topics/kidney-disease/vascular-access-for-hemodialysis/Pages/index.aspx

[9] Liu, S., Zeng, T. H., Hofmann, M., Burcombe, E., Wei, J., Jiang, R., . . . Chen, Y. (2011). Antibacterial activity of graphite, graphite oxide, graphene oxide, and reduced graphene oxide: Membrane and oxidative stress. *ACS Nano, 5*(9), 6971-6980. doi:10.1021/nn202451x

[10] Levey, A. S., Coresh, J., Balk, E., Kausz, A. T., Levin, A., Steffes, M. W., . . . Eknoyan, G. (2003). National Kidney Foundation practice guidelines for chronic kidney disease: evaluation, classification, and stratification. *Annals of internal medicine, 139*(2), 137-147.

[11] Parmar, M. S. (2002). Chronic renal disease. *BMJ: British Medical Journal, 325*(7355), 85.

[12] Coentrão, L., Santos-Araújo, C., Dias, C., Neto, R., & Pestana, M. (2012). Effects of starting hemodialysis with an arteriovenous fistula or central venous catheter compared with peritoneal dialysis: a retrospective cohort study. *BMC nephrology, 13*(1), 88.

[13] Daugirdas, J. T., Blake, P. G., & Ing, T. S. (2012). *Handbook of dialysis*: Lippincott Williams & Wilkins.

[14] Sinnakirouchenan, R., & Holley, J. L. (2011). Peritoneal dialysis versus hemodialysis: risks, benefits, and access issues. *Advances in chronic kidney disease, 18*(6), 428-432.

[15] O'Grady, N. P., Alexander, M., Burns, L. A., Dellinger, E. P., Garland, J., Heard, S. O., . . . Pearson, M. L. (2011). Guidelines for the prevention of intravascular catheter-related infections. *Clinical infectious diseases, 52*(9), e162-e193.

[16] Konner, K. (2001). Vascular access in the 21st century. *Journal of nephrology, 15*, S28-32.

[17] Manns, B., Tonelli, M., Yilmaz, S., Lee, H., Laupland, K., Klarenbach, S., . . . Murphy, B. (2005). Establishment and maintenance of vascular access in incident hemodialysis patients: a prospective cost analysis. *Journal of the American Society of Nephrology, 16*(1), 201-209.

[18] Pisoni, R. L., Young, E. W., Dykstra, D. M., Greenwood, R. N., Hecking, E., Gillespie, B., . . . Held, P. J. (2002). Vascular access use in Europe and the United States: results from the DOPPS. *Kidney international, 61*(1), 305-316.

[19] Maki, D. G., Stolz, S. M., Wheeler, S., & Mermel, L. A. (1997). Prevention of central venous catheter-related bloodstream infection by use of an antiseptic-impregnated catheter: a randomized,

controlled trial. *Annals of internal medicine, 127*(4), 257-266.

[20] Tal, M. G., & Ni, N. (2008). Selecting optimal hemodialysis catheters: material, design, advanced features, and preferences. *Techniques in vascular and interventional radiology, 11*(3), 186-191.

[21] Taylor, G., Gravel, D., Johnston, L., Embil, J., Holton, D., Paton, S., . . . Committee, C. H. E. (2004). Incidence of bloodstream infection in multicenter inception cohorts of hemodialysis patients. *American journal of infection control, 32*(3), 155-160.

[22] Besarab, A. (2006). Clinical Practice Guidelines for Vascular Access. *American Journal of Kidney Diseases, 48*, S176-S247. doi:10.1053/j.ajkd.2006.04.029

[23] Little, M. A., O'Riordan, A., Lucey, B., Farrell, M., Lee, M., Conlon, P. J., & Walshe, J. J. (2001). A prospective study of complications associated with cuffed, tunnelled haemodialysis catheters. *Nephrology Dialysis Transplantation, 16*(11), 2194-2200.

[24] Fan, P.-Y. (1994). Acute vascular access: New advances. *Adv Ren Replace Ther, 1*(2), 90-98.

[25] Martins, M., Rodrigues, A., Pedrosa, J. M., Carvalho, M. J., Cabrita, A., & Oliveira, R. (2013). Update on the challenging role of biofilms in peritoneal dialysis. *Biofouling, 29*(8), 1015-1027.

[26] Torreggiani, M., Scaramuzzi, M. L., Manini, A., Castoldi, F., Serpieri, N., Maggi, N., . . . Montagna, F. (2013). Hemodialysis vascular access: everything you always wanted to know about it (but were afraid to ask). *J Nephrol, 26*(5), 836-847.

[27] Lok, C. E., & Mokrzycki, M. H. (2011). Prevention and management of catheter-related infection in hemodialysis patients. *Kidney international, 79*(6), 587-598.

[28] Timsit, J.-F., Dubois, Y., Minet, C., Bonadona, A., Lugosi, M., Ara-Somohano, C., . . . Schwebel, C. (2011). New materials and devices for preventing catheter-related infections. *Annals of intensive care, 1*(1), 34.

[29] Patil, H. V., Patil, V. C., Ramteerthkar, M., & Kulkarni, R. (2011). Central venous catheter-related bloodstream infections in the intensive care unit. *Indian Journal of Critical Care Medicine, 15*(4), 213.

[30] Rogers, K. L., Fey, P. D., & Rupp, M. E. (2009). Coagulase-negative staphylococcal infections. *Infectious disease clinics of North America, 23*(1), 73-98.

[31] Malmsten, M. (2014). Nanomaterials as Antimicrobial Agents *Handbook of Nanomaterials Properties* (pp. 1053-1075): Springer.

[32] Sharma, V. K., Yngard, R. A., & Lin, Y. (2009). Silver nanoparticles: green synthesis and their antimicrobial activities. *Advances in colloid and interface science, 145*(1), 83-96.

[33] Muranyi, P., Schraml, C., & Wunderlich, J. (2010). Antimicrobial efficiency of titanium dioxide-coated surfaces. *Journal of applied microbiology, 108*(6), 1966-1973.

[34] Kang, S., Pinault, M., Pfefferle, L. D., & Elimelech, M. (2007). Single-walled carbon nanotubes exhibit strong antimicrobial activity. *Langmuir, 23*(17), 8670-8673.

[35] O'Toole, G., Kaplan, H. B., & Kolter, R. (2000). Biofilm formation as microbial development. *Annual Reviews in Microbiology, 54*(1), 49-79.

[36] Vuong, C., & Otto, M. (2002). Staphylococcus epidermidis infections. *Microbes and infection, 4*(4), 481-489.

[37] Rupp, M. E., & Archer, G. L. (1994). Coagulase-negative staphylococci: pathogens associated with medical progress. *Clinical infectious diseases*, 231-243.

[38] Ratner, B. D., Hoffman, A. S., Schoen, F. J., & Lemons, J. E. (2004). *Biomaterials science: an introduction to materials in medicine*: Academic press.

[39] CDC. (2004). National Nosocomial Infections Surveillance (NNIS) system report, data summary from January 1992 through June 2004, issued October 2004. *Am J Infect Control*(32), 470-485. doi:doi:10.1016/j.ajic.2004.10.001

[40] Otto, M. (2009). Staphylococcus epidermidis—the'accidental'pathogen. *Nature Reviews Microbiology, 7*(8), 555-567.

[41] Miragaia, M., Thomas, J., Couto, I., Enright, M., & De Lencastre, H. (2007). Inferring a population structure for Staphylococcus epidermidis from multilocus

sequence typing data. *Journal of bacteriology, 189*(6), 2540-2552.

[42] Szycher, M. (1991). *High Performance Biomaterials: A Complete Guide to Medical and Pharmceutical Applications*: CRC Press.

[43] Park, J., & Lakes, R. S. (2007). *Biomaterials: an introduction*: Springer Science & Business Media.

[44] McKeen, L. (2012). 13 - Elastomers *The Effect of Sterilization on Plastics and Elastomers (Third Edition)* (pp. 319-353). Boston: William Andrew Publishing.

[45] Linder, L., Curelaru, I., Gustavsson, B., Hansson, H., Stenqvist, O., & Wojciechowski, J. (1983). Material thrombogenicity in central venous catheterization: a comparison between soft, antebrachial catheters of silicone elastomer and polyurethane. *JPEN. Journal of parenteral and enteral nutrition, 8*(4), 399-406.

[46] Harper, C. A. (2000). *Modern Plastics Handbook: handbook*: McGraw-Hill Professional.

[47] Henrich, W. L. (2012). *Principles and practice of dialysis*: Lippincott Williams & Wilkins.

[48] Geim, A. K., & Novoselov, K. S. (2007). The rise of graphene. *Nature materials, 6*(3), 183-191.

[49] Sanchez, V. C., Jachak, A., Hurt, R. H., & Kane, A. B. (2011). Biological interactions of graphene-family nanomaterials: an interdisciplinary review. *Chemical research in toxicology, 25*(1), 15-34.

[50] Liu, J., Tang, J., & Gooding, J. J. (2012). Strategies for chemical modification of graphene and applications of chemically modified graphene. *Journal of Materials Chemistry, 22*(25), 12435-12452.

[51] Pinto, A. M., Gonçalves, I. C., & Magalhães, F. D. (2013). Graphene-based materials biocompatibility: A review. *Colloids and Surfaces B: Biointerfaces, 111*, 188-202. doi:10.1016/j.colsurfb.2013.05.022

[52] Choi, W., Lahiri, I., Seelaboyina, R., & Kang, Y. S. (2010). Synthesis of graphene and its applications: a review. *Critical Reviews in Solid State and Materials Sciences, 35*(1).

[53] Wei, D., Liu, Y., Wang, Y., Zhang, H., Huang, L., & Yu, G. (2009). Synthesis of N-doped graphene by chemical vapor deposition and its electrical properties. *Nano letters, 9*(5), 1752-1758.

[54] Enoki, T., Kobayashi, Y., & Fukui, K.-I. (2007). Electronic structures of graphene edges and nanographene. *International Reviews in Physical Chemistry, 26*(4), 609-645.

[55] Dhand, V., Rhee, K. Y., Kim, H. J., & Jung, D. H. (2013). A comprehensive review of graphene nanocomposites: research status and trends. *Journal of Nanomaterials, 2013*, 158.

[56] Dong, H., & Qi, S. (2015). Realising the potential of graphene-based materials for biosurfaces–A future perspective. *Biosurface and Biotribology*.

[57] Kuila, T., Bose, S., Mishra, A. K., Khanra, P., Kim, N. H., & Lee, J. H. (2012). Chemical functionalization of graphene and its applications. *Progress in Materials Science, 57*(7), 1061-1105. doi:10.1016/j.pmatsci.2012.03.002

[58] Mao, S., Pu, H., & Chen, J. (2012). Graphene oxide and its reduction: modeling and experimental progress. *RSC Advances, 2*(7), 2643-2643. doi:10.1039/c2ra00663d

[59] Pinto, A. M., Moreira, S., Gonçalves, I. C., Gama, F. M., Mendes, A. M., & Magalhães, F. D. (2013). Biocompatibility of poly(lactic acid) with incorporated graphene-based materials. *Colloids and Surfaces B: Biointerfaces, 104*, 229-238. doi:10.1016/j.colsurfb.2012.12.006

[60] Sundar, S., & Prajapati, V. K. (2012). Drug targeting to infectious diseases by nanoparticles surface functionalized with special biomolecules. *Current medicinal chemistry, 19*(19), 3196.

[61] Bao, H., Pan, Y., & Li, L. (2012). Recent advances in graphene-based nanomaterials for biomedical applications. *Nano Life, 2*(01), 1230001.

[62] Yang, K., Zhang, S., Zhang, G., Sun, X., Lee, S.-T., & Liu, Z. (2010). Graphene in mice: ultrahigh in vivo tumor uptake and efficient photothermal therapy. *Nano letters, 10*(9), 3318-3323.

[63] Notley, S. M., Crawford, R. J., & Ivanova, E. P. (2013). Bacterial interaction with graphene particles and surfaces. *Advances in Graphene Science*.

[64] Chung, C., Kim, Y.-K., Shin, D., Ryoo, S.-R., Hong, B. H., & Min, D.-H. (2013). Biomedical applications of graphene and graphene oxide. *Accounts of chemical research, 46*(10), 2211-2224.

[65] Shen, H., Zhang, L., Liu, M., & Zhang, Z. (2012). Biomedical applications of graphene. *Theranostics, 2*(3), 283.

[66] Ivanova, E. P., Hasan, J., Webb, H. K., Truong, V. K., Watson, G. S., Watson, J. A., . . . Tobin, M. J. (2012). Natural bactericidal surfaces: mechanical rupture of Pseudomonas aeruginosa cells by cicada wings. *Small, 8*(16), 2489-2494.

[67] Hasan, J., Crawford, R. J., & Ivanova, E. P. (2013). Antibacterial surfaces: the quest for a new generation of biomaterials. *Trends in biotechnology, 31*(5), 295-304.

[68] Pankey, G., & Sabath, L. (2004). Clinical relevance of bacteriostatic versus bactericidal mechanisms of action in the treatment of Gram-positive bacterial infections. *Clinical infectious diseases, 38*(6), 864-870.

[69] Jastrzębska, A. M., Kurtycz, P., & Olszyna, A. R. (2012). Recent advances in graphene family materials toxicity investigations. *Journal of Nanoparticle Research, 14*(12), 1-21.

[70] Santos, C. M., Mangadlao, J., Ahmed, F., Leon, A., Advincula, R. C., & Rodrigues, D. F. (2012). Graphene nanocomposite for biomedical applications: fabrication, antimicrobial and cytotoxic investigations. *Nanotechnology, 23*(39), 395101-395101. doi:10.1088/0957-4484/23/39/395101

[71] Wang, K., Ruan, J., Song, H., Zhang, J., Wo, Y., Guo, S., & Cui, D. (2011). Biocompatibility of graphene oxide. *Nanoscale Res Lett, 6*(8), 1-8.

[72] Martynková, G. S., & Valášková, M. (2014). Antimicrobial nanocomposites based on natural modified materials: A review of carbons and clays. *Journal of nanoscience and nanotechnology, 14*(1), 673-693.

[73] Seabra, A. B., Paula, A. J., de Lima, R., Alves, O. L., & Duran, N. (2014). Nanotoxicity of graphene and graphene oxide. *Chemical research in toxicology, 27*(2), 159-168.

[74] Yang, K., Li, Y., Tan, X., Peng, R., & Liu, Z. (2013). Behavior and toxicity of graphene and its functionalized derivatives in biological systems. *Small, 9*(9-10), 1492-1503.

[75] Hu, W., Peng, C., Luo, W., Lv, M., Li, X., Li, D., . . . Fan, C. (2010). Graphene-Based Antibacterial Paper. *ACS Nano, 4*(7), 4317-4323. doi:10.1021/nn101097v

[76] Chen, J., Wang, X., & Han, H. (2013). A new function of graphene oxide emerges: Inactivating phytopathogenic bacterium Xanthomonas oryzae pv. Oryzae. *Journal of Nanoparticle Research, 15*(5). doi:10.1007/s11051-013-1658-6

[77] Gurunathan, S., Han, J. W., Dayem, A. A., Eppakayala, V., Park, M.-R., Kwon, D.-N., & Kim, J.-H. (2013). Antibacterial activity of dithiothreitol reduced graphene oxide. *Journal of Industrial and Engineering Chemistry, 19*(4), 1280-1288. doi:10.1016/j.jiec.2012.12.029

[78] Liu, S., Hu, M., Zeng, T. H., Wu, R., Jiang, R., Wei, J., . . . Chen, Y. (2012). Lateral dimension-dependent antibacterial activity of graphene oxide sheets. *Langmuir, 28*(33), 12364-12372.

[79] Gurunathan, S., Han, J. W., Dayem, A. A., Eppakayala, V., & Kim, J.-H. (2012). Oxidative stress-mediated antibacterial activity of graphene oxide and reduced graphene oxide in Pseudomonas aeruginosa. *International journal of nanomedicine, 7*, 5901.

[80] Liu, L., Liu, J., Wang, Y., Yan, X., & Sun, D. D. (2011). Facile synthesis of monodispersed silver nanoparticles on graphene oxide sheets with enhanced antibacterial activity. *New Journal of Chemistry, 35*(7), 1418-1423.

[81] Krishnamoorthy, K., Navaneethaiyer, U., Mohan, R., Lee, J., & Kim, S.-J. (2011). Graphene oxide nanostructures modified multifunctional cotton fabrics. *Applied Nanoscience, 2*(2), 119-126. doi:10.1007/s13204-011-0045-9

[82] Bykkam, S., Rao, K., Chakra, C., & Thunugunta, T. (2013). Synthesis and characterization of graphene oxide and its

antimicrobial activity against klebseilla and staphylococus. *International Journal of Advanced Biotechnology Research, 4*, 142-146.

[83] Kurantowicz, N., Sawosz, E., Jaworski, S., Kutwin, M., Strojny, B., Wierzbicki, M., . . . Koziński, R. (2015). Interaction of graphene family materials with Listeria monocytogenes and Salmonella enterica. *Nanoscale research letters, 10*(1), 1-12.

[84] Chen, J., Peng, H., Wang, X., Shao, F., Yuan, Z., & Han, H. (2014). Graphene oxide exhibits broad-spectrum antimicrobial activity against bacterial phytopathogens and fungal conidia by intertwining and membrane perturbation. *Nanoscale, 6*(3), 1879-1889.

[85] Wang, X., Liu, X., & Han, H. (2013). Evaluation of antibacterial effects of carbon nanomaterials against copper-resistant Ralstonia solanacearum. *Colloids and Surfaces B: Biointerfaces, 103*, 136-142.

[86] Efremova, L. V., Vasilchenko, A. S., Rakov, E. G., & Deryabin, D. G. (2014). Toxicity of Graphene Shells, Graphene Oxide, and Graphene Oxide Paper Evaluated with Escherichia coli Biotests. *BioMed Research International*.

[87] Hui, L., Piao, J.-G., Auletta, J., Hu, K., Zhu, Y., Meyer, T., . . . Yang, L. (2014). Availability of the basal planes of graphene oxide determines whether it is antibacterial. *ACS applied materials & interfaces, 6*(15), 13183-13190.

[88] Krishnamoorthy, K., Veerapandian, M., Zhang, L.-H., Yun, K., & Kim, S. J. (2012). Antibacterial efficiency of graphene nanosheets against pathogenic bacteria via lipid peroxidation. *The Journal of Physical Chemistry C, 116*(32), 17280-17287.

[89] Kumar, S., Ghosh, S., Munichandraiah, N., & Vasan, H. (2013). 1.5 V battery driven reduced graphene oxide–silver nanostructure coated carbon foam (rGO–Ag–CF) for the purification of drinking water. *Nanotechnology, 24*(23), 235101.

[90] Krishnamoorthy, K., Jeyasubramanian, K., Premanathan, M., Subbiah, G., Shin, H. S., & Kim, S. J. (2014). Graphene oxide nanopaint. *Carbon, 72*, 328-337.

[91] Sawangphruk, M., Srimuk, P., Chiochan, P., Sangsri, T., & Siwayaprahm, P. (2012). Synthesis and antifungal activity of reduced graphene oxide nanosheets. *Carbon, 50*(14), 5156-5161.

[92] Perreault, F., de Faria, A. F., Nejati, S., & Elimelech, M. (2015). Antimicrobial properties of graphene oxide nanosheets: why size matters. *ACS Nano, 9*(7), 7226-7236.

[93] Tu, Y., Lv, M., Xiu, P., Huynh, T., Zhang, M., Castelli, M., . . . Fang, H. (2013). Destructive extraction of phospholipids from Escherichia coli membranes by graphene nanosheets. *Nature nanotechnology, 8*(8), 594-601.

[94] Ruiz, O. N., Fernando, K. A. S., Wang, B., Brown, N. A., Luo, P. G., McNamara, N. D., . . . Bunker, C. E. (2011). Graphene Oxide: A Nonspecific Enhancer of Cellular Growth. *ACS Nano, 5*(10), 8100-8107. doi:10.1021/nn202699t

[95] Xu, W.-P., Zhang, L.-C., Li, J.-P., Lu, Y., Li, H.-H., Ma, Y.-N., . . . Yu, S.-H. (2011). Facile synthesis of silver@ graphene oxide nanocomposites and their enhanced antibacterial properties. *J. Mater. Chem., 21*(12), 4593-4597.

[96] Tang, J., Chen, Q., Xu, L., Zhang, S., Feng, L., Cheng, L., . . . Peng, R. (2013). Graphene oxide–silver nanocomposite as a highly effective antibacterial agent with species-specific mechanisms. *ACS applied materials & interfaces, 5*(9), 3867-3874.

[97] Das, M. R., Sarma, R. K., Saikia, R., Kale, V. S., Shelke, M. V., & Sengupta, P. (2011). Synthesis of silver nanoparticles in an aqueous suspension of graphene oxide sheets and its antimicrobial activity. *Colloids and Surfaces B: Biointerfaces, 83*(1), 16-22. doi:10.1016/j.colsurfb.2010.10.033

[98] Lim, H. N., Huang, N. M., & Loo, C. (2012). Facile preparation of graphene-based chitosan films: Enhanced thermal, mechanical and antibacterial properties. *Journal of Non-Crystalline Solids, 358*(3), 525-530.

[99] Zhang, D., Liu, X., & Wang, X. (2011). Green synthesis of graphene oxide sheets decorated by silver nanoprisms and their

anti-bacterial properties. *Journal of inorganic biochemistry, 105*(9), 1181-1186.

[100] Ma, J., Zhang, J., Xiong, Z., Yong, Y., & Zhao, X. (2011). Preparation, characterization and antibacterial properties of silver-modified graphene oxide. *Journal of Materials Chemistry, 21*(10), 3350-3352.

[101] Carpio, I. E. M., Santos, C. M., Wei, X., & Rodrigues, D. F. (2012). Toxicity of a polymer–graphene oxide composite against bacterial planktonic cells, biofilms, and mammalian cells. *Nanoscale, 4*(15), 4746-4756.

[102] Wei, Y., Zuo, X., Li, X., Song, S., Chen, L., Shen, J., . . . Fang, S. (2014). Dry plasma synthesis of graphene oxide–Ag nanocomposites: A simple and green approach. *Materials Research Bulletin, 53*, 145-150.

[103] Xie, A.-G., Cai, X., Lin, M.-S., Wu, T., Zhang, X.-J., Lin, Z.-D., & Tan, S. (2011). Long-acting antibacterial activity of quaternary phosphonium salts functionalized few-layered graphite. *Materials Science and Engineering: B, 176*(15), 1222-1226.

[104] Thakur, S., Barua, S., & Karak, N. (2015). Self-healable castor oil based tough smart hyperbranched polyurethane nanocomposite with antimicrobial attributes. *RSC Advances, 5*(3), 2167-2176.

[105] Li, J., Wang, G., Zhu, H., Zhang, M., Zheng, X., Di, Z., . . . Wang, X. (2014). Antibacterial activity of large-area monolayer graphene film manipulated by charge transfer. *Scientific reports, 4*.

[106] Parra, C., Dorta, F., Jimenez, E., Henríquez, R., Ramírez, C., Rojas, R., & Villalobos, P. (2015). A nanomolecular approach to decrease adhesion of biofouling-producing bacteria to graphene-coated material. *Journal of nanobiotechnology, 13*(1), 1-10.

[107] Akhavan, O., & Ghaderi, E. (2010). Toxicity of graphene and graphene oxide nanowalls against bacteria. *ACS Nano, 4*(10), 5731-5736. doi:10.1021/nn101390x

[108] Akhavan, O., & Ghaderi, E. (2012). Escherichia coli bacteria reduce graphene oxide to bactericidal graphene in a self-limiting manner. *Carbon, 50*(5), 1853-1860.

[109] Park, S., Mohanty, N., Suk, J. W., Nagaraja, A., An, J., Piner, R. D., . . . Ruoff, R. S. (2010). Biocompatible, Robust Free-Standing Paper Composed of a TWEEN/Graphene Composite. *Advanced Materials, 22*(15), 1736-1740.

[110] Santos, C. M., Tria, M. C. R., Vergara, R. A. M. V., Ahmed, F., Advincula, R. C., & Rodrigues, D. F. (2011). Antimicrobial graphene polymer (PVK-GO) nanocomposite films. *Chemical Communications, 47*(31), 8892-8894.

[111] Vecitis, C. D., Zodrow, K. R., Kang, S., & Elimelech, M. (2010). Electronic-structure-dependent bacterial cytotoxicity of single-walled carbon nanotubes. *ACS Nano, 4*(9), 5471-5479.

[112] Liu, S., Ng, A. K., Xu, R., Wei, J., Tan, C. M., Yang, Y., & Chen, Y. (2010). Antibacterial action of dispersed single-walled carbon nanotubes on Escherichia coli and Bacillus subtilis investigated by atomic force microscopy. *Nanoscale, 2*(12), 2744-2750.

[113] Pham, V. T., Truong, V. K., Quinn, M. D., Notley, S. M., Guo, Y., Baulin, V. A., . . . Ivanova, E. P. (2015). Graphene induces formation of pores that kill spherical and rod-shaped bacteria. *ACS Nano, 9*(8), 8458-8467.

[114] Bao, Q., Zhang, D., & Qi, P. (2011). Synthesis and characterization of silver nanoparticle and graphene oxide nanosheet composites as a bactericidal agent for water disinfection. *Journal of Colloid And Interface Science, 360*(2), 463-470. doi:10.1016/j.jcis.2011.05.009

[115] Dallavalle, M., Calvaresi, M., Bottoni, A., Melle-Franco, M., & Zerbetto, F. (2015). Graphene can wreak havoc with cell membranes. *ACS applied materials & interfaces, 7*(7), 4406-4414.

[116] Romero-Vargas Castrillón, S., Perreault, F. o., de Faria, A. F., & Elimelech, M. (2015). Interaction of Graphene Oxide with Bacterial Cell Membranes: Insights from Force Spectroscopy. *Environmental Science & Technology Letters, 2*(4), 112-117.

[117] Mao, J., Guo, R., & Yan, L.-T. (2014). Simulation and analysis of cellular internalization pathways and membrane perturbation for graphene nanosheets. *Biomaterials, 35*(23), 6069-6077.

[118] Oberdörster, G., Oberdörster, E., & Oberdörster, J. (2005). Nanotoxicology: an emerging discipline evolving from studies of ultrafine particles. *Environmental health perspectives*, 823-839.

[119] Stone, V., Johnston, H., & Schins, R. P. (2009). Development of in vitro systems for nanotoxicology: methodological considerations. *Critical reviews in toxicology, 39*(7), 613-626.

[120] Tian, T., Shi, X., Cheng, L., Luo, Y., Dong, Z., Gong, H., . . . Liu, Z. (2014). Graphene-based nanocomposite as an effective, multifunctional, and recyclable antibacterial agent. *ACS applied materials & interfaces, 6*(11), 8542-8548.

[121] Wu, M.-C., Deokar, A. R., Liao, J.-H., Shih, P.-Y., & Ling, Y.-C. (2013). Graphene-based photothermal agent for rapid and effective killing of bacteria. *ACS Nano, 7*(2), 1281-1290.

[122] Yan, L., Zhao, F., Li, S., Hu, Z., & Zhao, Y. (2011). Low-toxic and safe nanomaterials by surface-chemical design, carbon nanotubes, fullerenes, metallofullerenes, and graphenes. *Nanoscale, 3*(2), 362-382.

[123] Wang, H., Liu, J., Wu, X., Tong, Z., & Deng, Z. (2013). Tailor-made Au@ Ag core–shell nanoparticle 2D arrays on protein-coated graphene oxide with assembly enhanced antibacterial activity. *Nanotechnology, 24*(20), 205102.

[124] Zhang, Z., Zhang, J., Zhang, B., & Tang, J. (2013). Mussel-inspired functionalization of graphene for synthesizing Ag-polydopamine-graphene nanosheets as antibacterial materials. *Nanoscale, 5*(1), 118-123.

[125] Sreeprasad, T., Maliyekkal, M. S., Deepti, K., Chaudhari, K., Xavier, P. L., & Pradeep, T. (2011). Transparent, luminescent, antibacterial and patternable film forming composites of graphene oxide/reduced graphene oxide. *ACS applied materials & interfaces, 3*(7), 2643-2654.

[126] Cai, X., Tan, S., Lin, M., Xie, A., Mai, W., Zhang, X., . . . Liu, Y. (2011). Synergistic antibacterial brilliant blue/reduced graphene oxide/quaternary phosphonium salt composite with excellent water solubility and specific targeting capability. *Langmuir : the ACS journal of surfaces and colloids, 27*(12), 7828-7835. doi:10.1021/la201499s

[127] Pandey, H., Parashar, V., Parashar, R., Prakash, R., Ramteke, P. W., & Pandey, A. C. (2011). Controlled drug release characteristics and enhanced antibacterial effect of graphene nanosheets containing gentamicin sulfate. *Nanoscale, 3*(10), 4104-4108. doi:10.1039/c1nr10661a

[128] Mondal, T., Bhowmick, A. K., & Krishnamoorti, R. (2012). Chlorophenyl pendant decorated graphene sheet as a potential antimicrobial agent: synthesis and characterization. *Journal of Materials Chemistry, 22*(42), 22481-22487.

[129] Kavitha, T., Gopalan, A. I., Lee, K.-P., & Park, S.-Y. (2012). Glucose sensing, photocatalytic and antibacterial properties of graphene–ZnO nanoparticle hybrids. *Carbon, 50*(8), 2994-3000.

[130] Cai, X., Tan, S., Yu, A., Zhang, J., Liu, J., Mai, W., & Jiang, Z. (2012). Sodium 1-naphthalenesulfonate-functionalized reduced graphene oxide stabilizes silver nanoparticles with lower cytotoxicity and long-term antibacterial activity. *Chemistry, an Asian journal, 7*(7), 1664-1670. doi:10.1002/asia.201200045

[131] Dai, C., Yang, X., & Xie, H. (2011). One-step synthesis of reduced graphite oxide–silver nanocomposite. *Materials Research Bulletin, 46*(11), 2004-2008.

[132] He, G., Wu, H., Ma, K., Wang, L., Sun, X., Chen, H., & Wang, X. (2013). Photosynthesis of Multiple Valence Silver Nanoparticles on Reduced Graphene Oxide Sheets With Enhanced Antibacterial Activity. *Synthesis and Reactivity in Inorganic, Metal-Organic, and Nano-Metal Chemistry, 43*(4), 440-445.

[133] He, T. T., Zhou, Y. Z., Yang, J., & Shi, H. F. (2013). *Characterization of Antibacterial Effects of Novel Silver Nanoparticles: A Case Study on Pseudomonas as a Model for Gram-Negative Bacteria.* Paper presented at the Advanced Materials Research.

[134] Jiang, B., Tian, C., Song, G., Chang, W., Wang, G., Wu, Q., & Fu, H. (2013). A novel Ag/graphene composite: facile fabrication and enhanced antibacterial properties.

*Journal of Materials Science, 48*(5), 1980-1985.

[135] de Faria, A. F., Martinez, D. S. T., Meira, S. M. M., de Moraes, A. C. M., Brandelli, A., Souza Filho, A. G., & Alves, O. L. (2014). Anti-adhesion and antibacterial activity of silver nanoparticles supported on graphene oxide sheets. *Colloids and Surfaces B: Biointerfaces, 113*, 115-124.

[136] Zhou, Y., Yang, J., He, T., Shi, H., Cheng, X., & Lu, Y. (2013). Highly Stable and Dispersive Silver Nanoparticle–Graphene Composites by a Simple and Low-Energy-Consuming Approach and Their Antimicrobial Activity. *Small, 9*(20), 3445-3454.

[137] Das, M. R., Sarma, R. K., Borah, S. C., Kumari, R., Saikia, R., Deshmukh, A. B., . . . Boukherroub, R. (2013). The synthesis of citrate-modified silver nanoparticles in an aqueous suspension of graphene oxide nanosheets and their antibacterial activity. *Colloids and Surfaces B: Biointerfaces, 105*, 128-136.

[138] Kumar, S. V., Huang, N. M., Lim, H. N., Marlinda, A., Harrison, I., & Chia, C. H. (2013). One-step size-controlled synthesis of functional graphene oxide/silver nanocomposites at room temperature. *Chemical Engineering Journal, 219*, 217-224.

[139] Chook, S. W., Chia, C. H., Zakaria, S., Ayob, M. K., Chee, K. L., Huang, N. M., . . . Rahman, R. M. F. R. A. (2012). Antibacterial performance of Ag nanoparticles and AgGO nanocomposites prepared via rapid microwave-assisted synthesis method. *Nanoscale research letters, 7*(1), 1-7.

[140] Shen, J., Li, T., Shi, M., Li, N., & Ye, M. (2012). Polyelectrolyte-assisted one-step hydrothermal synthesis of Ag-reduced graphene oxide composite and its antibacterial properties. *Materials Science and Engineering: C, 32*(7), 2042-2047.

[141] Shen, J., Shi, M., Li, N., Yan, B., Ma, H., Hu, Y., & Ye, M. (2010). Facile synthesis and application of Ag-chemically converted graphene nanocomposite. *Nano research, 3*(5), 339-349.

[142] Nguyena, V. H., Kim, B.-K., Jo, Y.-L., & Shim, J.-J. (2012). Preparation and antibacterial activity of silver nanoparticles-decorated graphene composites. *The Journal of Supercritical Fluids, 72*, 28-35.

[143] Cai, X., Lin, M., Tan, S., Mai, W., Zhang, Y., Liang, Z., . . . Zhang, X. (2012). The use of polyethyleneimine-modified reduced graphene oxide as a substrate for silver nanoparticles to produce a material with lower cytotoxicity and long-term antibacterial activity. *Carbon, 50*(10), 3407-3415.

[144] Li, T., Shen, J., Li, N., & Ye, M. (2014). Facile in situ synthesis of hydrophilic RGO–CD–Ag supramolecular hybrid and its enhanced antibacterial properties. *Materials Science and Engineering: C, 39*, 352-358.

[145] Ocsoy, I., Paret, M. L., Ocsoy, M. A., Kunwar, S., Chen, T., You, M., & Tan, W. (2013). Nanotechnology in plant disease management: DNA-directed silver nanoparticles on graphene oxide as an antibacterial against Xanthomonas perforans. *ACS Nano, 7*(10), 8972-8980.

[146] Liu, L., Liu, J., & Sun, D. D. (2012). Graphene oxide enwrapped Ag 3 PO 4 composite: towards a highly efficient and stable visible-light-induced photocatalyst for water purification. *Catalysis Science & Technology, 2*(12), 2525-2532.

[147] Liu, J., Liu, L., Bai, H., Wang, Y., & Sun, D. D. (2011). Gram-scale production of graphene oxide–TiO 2 nanorod composites: towards high-activity photocatalytic materials. *Applied Catalysis B: Environmental, 106*(1), 76-82.

[148] Cao, B., Cao, S., Dong, P., Gao, J., & Wang, J. (2013). High antibacterial activity of ultrafine TiO 2/graphene sheets nanocomposites under visible light irradiation. *Materials Letters, 93*, 349-352.

[149] Ko, T. Y., Kim, S. Y., Kim, H. G., Moon, G.-S., & In, I. (2013). Antibacterial Activity of Chemically Reduced Graphene Oxide Assembly with Chitosan through Noncovalent Interactions. *Chemistry Letters, 42*(1), 66-67.

[150] Li, P., Sun, S., Dong, A., Hao, Y., Shi, S., Sun, Z., . . . Chen, Y. (2015). Developing of a novel antibacterial agent by functionalization of graphene oxide with guanidine polymer with enhanced

antibacterial activity. *Applied Surface Science, 355*, 446-452.

[151] Wang, X., Zhou, N., Yuan, J., Wang, W., Tang, Y., Lu, C., . . . Shen, J. (2012). Antibacterial and anticoagulation properties of carboxylated graphene oxide–lanthanum complexes. *Journal of Materials Chemistry, 22*(4), 1673-1678.

[152] Some, S., Ho, S.-M., Dua, P., Hwang, E., Shin, Y. H., Yoo, H., . . . Lee, H. (2012). Dual functions of highly potent graphene derivative–poly-L-lysine composites to inhibit bacteria and support human cells. *ACS Nano, 6*(8), 7151-7161.

[153] Ouyang, Y., Cai, X., Shi, Q., Liu, L., Wan, D., Tan, S., & Ouyang, Y. (2013). Poly-l-lysine-modified reduced graphene oxide stabilizes the copper nanoparticles with higher water-solubility and long-term additively antibacterial activity. *Colloids and Surfaces B: Biointerfaces, 107*, 107-114.

[154] Santos, C. M., Mangadlao, J., Ahmed, F., Leon, A., Advincula, R. C., & Rodrigues, D. F. (2012). Graphene nanocomposite for biomedical applications: fabrication, antimicrobial and cytotoxic investigations. *Nanotechnology, 23*(39), 395101.

[155] Tai, Z., Ma, H., Liu, B., Yan, X., & Xue, Q. (2012). Facile synthesis of Ag/GNS-g-PAA nanohybrids for antimicrobial applications. *Colloids and Surfaces B: Biointerfaces, 89*, 147-151.

[156] Kholmanov, I. N., Stoller, M. D., Edgeworth, J., Lee, W. H., Li, H., Lee, J., . . . Akinwande, D. (2012). Nanostructured hybrid transparent conductive films with antibacterial properties. *ACS Nano, 6*(6), 5157-5163.

[157] Akhavan, O., & Ghaderi, E. (2009). Photocatalytic reduction of graphene oxide nanosheets on TiO2 thin film for photoinactivation of bacteria in solar light irradiation. *The Journal of Physical Chemistry C, 113*(47), 20214-20220.

[158] Wang, Y., Zhang, D., Bao, Q., Wu, J., & Wan, Y. (2012). Controlled drug release characteristics and enhanced antibacterial effect of graphene oxide–drug intercalated layered double hydroxide hybrid films. *Journal of Materials Chemistry, 22*(43), 23106-23113.

[159] Mittal, V. (2014). Functional polymer nanocomposites with graphene: A review. *Macromolecular Materials and Engineering, 299*(8), 906-931.

[160] Pan, Y., Wu, T., Bao, H., & Li, L. (2011). Green fabrication of chitosan films reinforced with parallel aligned graphene oxide. *Carbohydrate Polymers, 83*(4), 1908-1915. doi:10.1016/j.carbpol.2010.10.054

[161] Zhang, X., Liu, X., Zheng, W., & Zhu, J. (2012). Regenerated cellulose/graphene nanocomposite films prepared in DMAC/LiCl solution. *Carbohydrate Polymers, 88*(1), 26-30.

[162] Pinto, A. M., Cabral, J., Tanaka, D. a. P., Mendes, A. M. A. M., Magalhães, F. D., & Magalhaes, F. D. (2013). Effect of incorporation of graphene oxide and graphene nanoplatelets on mechanical and gas permeability properties of poly(lactic acid) films. *Polymer International, 62*(1), 33-40. doi:10.1002/pi.4290

[163] Yang, J., Wu, M., Chen, F., Fei, Z., & Zhong, M. (2011). Preparation, characterization, and supercritical carbon dioxide foaming of polystyrene/graphene oxide composites. *The Journal of Supercritical Fluids, 56*(2), 201-207.

[164] Yang, X., Li, L., Shang, S., & Tao, X.-m. (2010). Synthesis and characterization of layer-aligned poly (vinyl alcohol)/graphene nanocomposites. *Polymer, 51*(15), 3431-3435.

[165] Lahiri, D., Dua, R., Zhang, C., de Socarraz-Novoa, I., Bhat, A., Ramaswamy, S., & Agarwal, A. (2012). Graphene nanoplatelet-induced strengthening of ultrahigh molecular weight polyethylene and biocompatibility in vitro. *ACS applied materials & interfaces, 4*(4), 2234-2241. doi:10.1021/am300244s

[166] Pan, Y., Bao, H., Sahoo, N. G., Wu, T., & Li, L. (2011). Water-Soluble Poly (N-isopropylacrylamide)–Graphene Sheets Synthesized via Click Chemistry for Drug Delivery. *Advanced Functional Materials, 21*(14), 2754-2763.

[167] Song, P., Cao, Z., Cai, Y., Zhao, L., Fang, Z., & Fu, S. (2011). Fabrication of exfoliated graphene-based polypropylene nanocomposites with enhanced mechanical

and thermal properties. *Polymer, 52*(18), 4001-4010. doi:10.1016/j.polymer.2011.06.045

[168] Gao, J., Chen, F., Wang, K., Deng, H., Zhang, Q., Bai, H., & Fu, Q. (2011). A promising alternative to conventional polyethylene with poly(propylene carbonate) reinforced by graphene oxide nanosheets. *Journal of Materials Chemistry, 21*(44), 17627-17627. doi:10.1039/c1jm14300j

[169] Bian, J., Lin, H. L., He, F. X., Wei, X. W., Chang, I.-T., & Sancaktar, E. (2013). Fabrication of microwave exfoliated graphite oxide reinforced thermoplastic polyurethane nanocomposites: Effects of filler on morphology, mechanical, thermal and conductive properties. *Composites Part A: Applied Science and Manufacturing, 47*, 72-82.

[170] Zhang, J. L., Guo, L., Chen, L., Li, S. H., & Wu, G. (2014). *Graphene Oxide Reinforced Degradable Polyurethane for Anterior Cruciate Ligament Tissue Engineering.* Paper presented at the Advanced Materials Research.

[171] Choi, J. T., Kim, D. H., Ryu, K. S., Lee, H.-i., Jeong, H. M., Shin, C. M., . . . Kim, B. K. (2011). Functionalized graphene sheet/polyurethane nanocomposites: effect of particle size on physical properties. *Macromolecular Research, 19*(8), 809-814.

[172] Raghu, A. V., Lee, Y. R., Jeong, H. M., & Shin, C. M. (2008). Preparation and physical properties of waterborne polyurethane/functionalized graphene sheet nanocomposites. *Macromolecular Chemistry and Physics, 209*(24), 2487-2493.

[173] Pan, H., Wang, X., Zhang, Y., Yu, L., & Zhang, Z. (2014). Graphene oxides reduced and modified by hydramines–Potentials as electrode materials of supercapacitors and reinforcing agents of waterborne polyurethane. *Materials Research Bulletin, 59*, 117-124.

[174] Hu, X., Tian, M., Qu, L., Zhu, S., & Han, G. (2015). Multifunctional cotton fabrics with graphene/polyurethane coatings with far-infrared emission, electrical conductivity, and ultraviolet-blocking properties. *Carbon, 95*, 625-633.

[175] Kim, H., Miura, Y., & Macosko, C. W. (2010). Graphene/polyurethane nanocomposites for improved gas barrier and electrical conductivity. *Chemistry of Materials, 22*(11), 3441-3450.

[176] Li, X., Deng, H., Li, Z., Xiu, H., Qi, X., Zhang, Q., . . . Fu, Q. (2015). Graphene/thermoplastic polyurethane nanocomposites: Surface modification of graphene through oxidation, polyvinyl pyrrolidone coating and reduction. *Composites Part A: Applied Science and Manufacturing, 68*, 264-275.

[177] Pokharel, P. (2014). High performance polyurethane nanocomposite films prepared from a masterbatch of graphene oxide in polyether polyol. *Chemical Engineering Journal, 253*, 356-365.

[178] Pant, H. R., Pokharel, P., Joshi, M. K., Adhikari, S., Kim, H. J., Park, C. H., & Kim, C. S. (2015). Processing and characterization of electrospun graphene oxide/polyurethane composite nanofibers for stent coating. *Chemical Engineering Journal, 270*, 336-342.

[179] Jin, S., Xu, D., Zhou, N., Yuan, J., & Shen, J. (2013). Antibacterial and anticoagulation properties of polyethylene/geneO-MPC nanocomposites. *Journal of Applied Polymer Science, 129*(2), 884-891.

[180] Mazaheri, M., Akhavan, O., & Simchi, A. (2014). Flexible bactericidal graphene oxide–chitosan layers for stem cell proliferation. *Applied Surface Science, 301*, 456-462.

[181] Lu, B., Li, T., Zhao, H., Li, X., Gao, C., Zhang, S., & Xie, E. (2012). Graphene-based composite materials beneficial to wound healing. *Nanoscale, 4*(9), 2978-2982.

[182] Hong, B., Jung, H., & Byun, H. (2013). Preparation of Polyvinylidene Fluoride Nanofiber Membrane and Its Antibacterial Characteristics with Nanosilver or Graphene Oxide. *Journal of nanoscience and nanotechnology, 13*(9), 6269-6274.

[183] Fan, Z., Liu, B., Wang, J., Zhang, S., Lin, Q., Gong, P., . . . Yang, S. (2014). A Novel Wound Dressing Based on Ag/Graphene Polymer Hydrogel: Effectively Kill Bacteria and Accelerate Wound Healing. *Advanced Functional Materials, 24*(25), 3933-3943.

[184] Cao, Y.-C., Wei, W., Liu, J., You, Q., Liu, F., Lan, Q., . . . Zhao, J. (2015). The

Preparation of Graphene Reinforced Poly (vinyl alcohol) Antibacterial Nanocomposite Thin Film. *International Journal of Polymer Science, 2015*.

[185] An, X., Ma, H., Liu, B., & Wang, J. (2013). Graphene oxide reinforced polylactic acid/polyurethane antibacterial composites. *Journal of Nanomaterials, 2013*, 18.

[186] Kalaitzidou, K., Fukushima, H., & Drzal, L. T. (2007). Mechanical properties and morphological characterization of exfoliated graphite–polypropylene nanocomposites. *Composites Part A: Applied Science and Manufacturing, 38*(7), 1675-1682.

[187] Marcano, D. C., Kosynkin, D. V., Berlin, J. M., Sinitskii, A., Sun, Z., Slesarev, A., . . . Tour, J. M. (2010). Improved synthesis of graphene oxide. *ACS Nano, 4*(8), 4806-4814.

[188] MAGALHÃES, M. A. M., & Pacheco, T. D. A. (2013). Composite grapheno-metal oxide platelet method of preparation and applications: Google Patents.

[189] Martins, M., Wang, D., Ji, J., Feng, L., & Barbosa, M. (2003). Albumin and fibrinogen adsorption on PU–PHEMA surfaces. *Biomaterials, 24*(12), 2067-2076.

[190] Fowkes, F. M., & Zisman, W. A. (1964). Contact angle, wettability, and adhesion.

[191] Earnest, C. M. (1988). *Compositional analysis by thermogravimetry*.

[192] Andrews, J. M. (2001). Determination of minimum inhibitory concentrations. *Journal of antimicrobial Chemotherapy, 48*(suppl 1), 5-16.

[193] Wiegand, I., Hilpert, K., & Hancock, R. E. (2008). Agar and broth dilution methods to determine the minimal inhibitory concentration (MIC) of antimicrobial substances. *Nature protocols, 3*(2), 163-175.

[194] Hodgson, S. D., Greco-Stewart, V., Jimenez, C. S., Sifri, C. D., Brassinga, A. K. C., & Ramirez-Arcos, S. (2014). Enhanced pathogenicity of biofilm-negative Staphylococcus epidermidis isolated from platelet preparations. *Transfusion, 54*(2), 461-470.

[195] Cavaliere, E., De Cesari, S., Landini, G., Riccobono, E., Pallecchi, L., Rossolini, G. M., & Gavioli, L. (2015). Highly bactericidal Ag nanoparticle films obtained by cluster beam deposition. *Nanomedicine: Nanotechnology, Biology and Medicine, 11*(6), 1417-1423.

[196] Pallavicini, P., Taglietti, A., Dacarro, G., Diaz-Fernandez, Y. A., Galli, M., Grisoli, P., . . . Zanoni, R. (2010). Self-assembled monolayers of silver nanoparticles firmly grafted on glass surfaces: Low Ag+ release for an efficient antibacterial activity. *Journal of Colloid And Interface Science, 350*(1), 110-116.

[197] Barros, J., Grenho, L., Fernandes, M., Manuel, C., Melo, L., Nunes, O., . . . Ferraz, M. (2015). Anti-sessile bacterial and cytocompatibility properties of CHX-loaded nanohydroxyapatite. *Colloids and Surfaces B: Biointerfaces, 130*, 305-314.

[198] Pinto, A. M., Gonçalves, C., Sousa, D. M., Ferreira, A. R., Moreira, J. A., Gonçalves, I. C., & Magalhães, F. D. (2016). Smaller particle size and higher oxidation improves biocompatibility of graphene-based materials. *Carbon, 99*, 318-329.

[199] Dimiev, A. M., Ceriotti, G., Metzger, A., Kim, N. D., & Tour, J. M. (2015). Chemical Mass Production of Graphene Nanoplatelets in∼ 100% Yield. *ACS Nano, 10*(1), 274-279.

[200] Li, J., Kim, J.-K., & Sham, M. L. (2005). Conductive graphite nanoplatelet/epoxy nanocomposites: effects of exfoliation and UV/ozone treatment of graphite. *Scripta Materialia, 53*(2), 235-240.

[201] Park, J., Mitchel, W. C., Elhamri, S., Grazulis, L., Hoelscher, J., Mahalingam, K., . . . Lee, J. (2015). Observation of the intrinsic bandgap behaviour in as-grown epitaxial twisted graphene. *Nature communications, 6*.

[202] Geng, Y., Wang, S. J., & Kim, J.-K. (2009). Preparation of graphite nanoplatelets and graphene sheets. *Journal of Colloid And Interface Science, 336*(2), 592-598.

[203] Bouša, M., Frank, O., Jirka, I., & Kavan, L. (2013). In situ Raman spectroelectrochemistry of graphene oxide. *physica status solidi (b), 250*(12), 2662-2667.

[204] Dreyer, D. R., Park, S., Bielawski, C. W., & Ruoff, R. S. (2010). The chemistry of

graphene oxide. *Chemical Society Reviews, 39*(1), 228-240.

[205] Gonçalves, C., Pinto, A., Machado, A. V., Moreira, J., Gonçalves, I. C., & Magalhães, F. (2016). Biocompatible reinforcement of poly (Lactic acid) with graphene nanoplatelets. *Polymer Composites*.

[206] Freddy Arce, D. P., Ica Manas-Zloczower. (2016). *THERMOPLASTIC POLYURETHANE CHITOSAN / CELLULOSE NANOCRYSTALS COMPOSITES FOR WOUND HEALING APPLICATIONS*. Retrieved from SPE ANTEC™ Indianapolis 2016: http://leaders.4spe.org/spe/conferences/antec2016/papers/525.pdf

[207] Tang, X.-Z., Mu, C., Zhu, W., Yan, X., Hu, X., & Yang, J. (2016). Flexible polyurethane composites prepared by incorporation of polyethylenimine-modified slightly reduced graphene oxide. *Carbon, 98*, 432-440.

[208] Ma, J., Meng, Q., Michelmore, A., Kawashima, N., Izzuddin, Z., Bengtsson, C., & Kuan, H.-C. (2013). Covalently bonded interfaces for polymer/graphene composites. *Journal of Materials Chemistry A, 1*(13), 4255-4264.

[209] Walder, A. *Characteristics of Processing Thermoplastic Polyurethanes Resins into Medical Devices*. Retrieved from Lubrizol Advanced Materials:

[210] Zhao, T., Chen, H., Zheng, J., Yu, Q., Wu, Z., & Yuan, L. (2011). Inhibition of protein adsorption and cell adhesion on PNIPAAm-grafted polyurethane surface: Effect of graft molecular weight. *Colloids and Surfaces B: Biointerfaces, 85*(1), 26-31.

[211] Stachelek, S. J., Alferiev, I., Choi, H., Kronsteiner, A., Uttayarat, P., Gooch, K. J., . . . Levy, R. J. (2005). Cholesterol-derivatized polyurethane: Characterization and endothelial cell adhesion. *Journal of Biomedical Materials Research Part A, 72*(2), 200-212.

[212] Kim, M. S., & Sung, C. S. P. (2005). Intrinsic UV reflection and fluorescence studies for water sorption in polycarbonate, polyurethane and poly (ethylene terephthalate) films. *Fibers and Polymers, 6*(2), 127-130.

[213] Heckmann, W. (2005). Characterization of Polymer Materials by Fluorescence Imaging. *Microscopy and Microanalysis, 11*(S02), 2036-2037.

[214] Yadav, S. K., Mahapatra, S. S., & Cho, J. W. (2012). Synthesis of mechanically robust antimicrobial nanocomposites by click coupling of hyperbranched polyurethane and carbon nanotubes. *Polymer, 53*(10), 2023-2031.

[215] Stankovich, S., Dikin, D. A., Piner, R. D., Kohlhaas, K. A., Kleinhammes, A., Jia, Y., . . . Ruoff, R. S. (2007). Synthesis of graphene-based nanosheets via chemical reduction of exfoliated graphite oxide. *Carbon, 45*(7), 1558-1565.

[216] Pinto, A. M., Martins, J., Moreira, J. A., Mendes, A. M., & Magalhães, F. D. (2013). Dispersion of graphene nanoplatelets in poly(vinyl acetate) latex and effect on adhesive bond strength. *Polymer International, 62*(February), 928-935. doi:10.1002/pi.4379

# APPENDIX

**Table A 1 -** Effects of Functionalized-GBMs on bacteria.

| Ref | GBM | Production method | Properties | Investigated Bacteria | Cell viability | Membrane damage | Other |
|---|---|---|---|---|---|---|---|
| 94 | Ag-GO paper | GO(MHM + 7 days dialysis) + sonochemical method + filtration on PVDF membrane | Average size of Ag on GO surface=8nm | *E.Coli* | Large growth inhibition zones | - | - |
| 126 | BB-rGO | MHM + BB direct sonication + Hr | n/s | E. coli<br>S. aureus | *E.coli* MIC=1200 µg/mL<br>*S.aureus* MIC=800 µg/mL | Yes | - |
| | BB-rGO-TTP | BB-rGO+TTP direct addition + dialysis | | | *E.coli*, MIC:<br>BB-rGO-TTP-1 (13.5 wt% of TTP) =650 mg $L^{-1}$; BB-rGO-TTP-2 (20.7 wt% of TTP) =400 mg $L^{-1}$; BB-rGO-TTP-3 (23.2 wt% of TTP) =250 mg $L^{-1}$<br>*S.aureus*, MIC:<br>BB-rGO-TTP-1 =400 mg $L^{-1}$; BB-rGO-TTP-2 =250 mg $L^{-1}$; BB-rGO-TTP-3 =150 mg $L^{-1}$ | | |
| 130 | NA-rGO | MHM + NA direct sonication + Hr | t ≈ 0.6 nm | *E. coli*<br>*S. aureus* | *E.coli* ≈ 92.5% (1000 µg/mL, 6h)<br>No effect (100 µg $mL^{-1}$, 6h)<br>*S.aureus* ≈ 88.8 % (≈1000 µg mL-1, 6h)<br>No effect (100 µg $mL^{-1}$, 6h) | - | - |
| | AgNP-NA-rGO | MHM + NA and AgNO3 direct sonication + Hr | 3–20 nm diameter AgNPs anchored on the NA-rGO nanosheets. | | *E.coli*<br>AgNP-NA-rGO≈ 7.6% (100 µg $mL^{-1}$, 6h)<br>*S.aureus*<br>AgNP-NA-rGO≈ 3.1% (100 µg $mL^{-1}$, 6h) | | |
| 127 | Methanol derived graphene (MDG) | NaOH and $CH_3OH$ supersaturated solution heated | t ≈ 3.5 nm | *E. coli* | ≈ 70% (20 µg $mL^{-1}$, 2h)<br>≈ 55% (40 µg $mL^{-1}$, 2h) | - | - |
| 80 | Ag-GO | Ag nanoparticles: reducing $AgNO_3$ in toluene<br>GO: MHM + 1h sonication + Ag nanoparticles (stirred 12 h, RT) | Ag highly monodispersed with a uniform size = 6nm<br>GO sheets uniformly covered by Ag NPs | *E. coli* | Decreases with time and concentration<br>Colony forming count (2h, 37 ºC): 80 µg $mL^{-1}$= 1%; 100 µg $mL^{-1}$= 0%<br>LIVE/DEAD (100 mg $mL^{-1}$, 2h): Nearly all cells dead | Yes | - |
| 95 | rGO-Ag | GO (MHM) + Hr in the presence of graphene-poly(sodium 4-styrenesulfonate) ($H_2O$, 60 ºC, 30 min) + $AgNO_3$ stirred 10 h | Ag@rGO 0.02 wt.% (Ag/rGO)<br>Ag NPs size = several nm<br>Ag@rGO 0.2 wt.%<br>Ag NPs size ≈ 40 nm | *E. coli* | MIC:<br>Ag = 50 µg $mL^{-1}$<br>Ag@rGO 0.02 wt.% = 25 µg $mL^{-1}$<br>Ag@rGO 0.2 wt.% = 12.5 µg $mL^{-1}$ | - | - |
| 96 | Ag-GO | $AgNO_3$ reduction by sodium citrate in the presence of GO (MHM) suspension | For Ag:GO = 0.65:1 or 1:1<br>$d_{average}$ ≈ 46 nm<br>For Ag:GO = 2:1<br>$d_{average}$ ≈ 68 nm | *E. coli*<br>*S. aureus* | GO-Ag(1:1) (2.5 h, 37°C, $H_2O$, shaking) = highest antibacterial activity<br>MTT assay, 10 µg $mL^{-1}$: E.coli = 20%; S.aureus = 24%<br>CFU counting, 10 µg $mL^{-1}$: E.coli = 6%; S.aureus = 26%<br>MIC: E.coli = 4 µg $mL^{-1}$; S.aureus = 14 µg $mL^{-1}$ | *E. coli*: Yes<br>*S. aureus* Few | No DNA damage for both. Cell division inhibition of *S. aureus* (division time ↑1.5 fold) |
| 97 | Ag–GO | GO: Hummer and Offeman method (HM) + ultrasonication for 3 h<br>Reduction of $AgNO_3$ in GO suspension with $NaBH_4$ as redutor | Ag NPs diameter = 5–25nm with variable shape | *E. coli*<br>*Pseudomonas aeruginosa* | Maximum growth inhibition zone:<br>Sensitivity to $AgNO_3$ concentrations for Ag NPs synthesis:<br>$1\times10^{-3}$ mol $dm^{-3}$: *E. c* = 7 mm; *P. s* = 16 mm<br>$2\times10^{-3}$ mol $dm^{-3}$: *E. c* = 10 mm; *P. s* = 19 mm<br>$4\times10^{-3}$ mol $dm^{-3}$: *E. c* = 13 mm; *P. s* = 23 mm | | |

| | | | | | | | |
|---|---|---|---|---|---|---|---|
| | | | | | $8\times10^{-3}$ mol $dm^{-3}$: *E. c* = 18 mm; *P. s* =26 mm | | |
| 137 | Ag-GO | GO: Hummer and Offeman method (HM) + ultrasonication for 3 h<br>Reduction of $AgNO_3$ with $NaBH_4$ in the presence of trisodium citrate acting as stabilizing agent | Ag NPs size = 2–25 nm<br><br>GO= thin nanosheets | *S. aureus*<br><br>*B. subtilis* | (24 h, 35 ◦C for S. aureus and 30 ◦C for B. subtilis)<br>Zones of inhibition = 9-21 mm<br>Sensitivity to $AgNO_3$ concentrations for Ag NPs synthesis:<br>$5\times10^{-4}$ mol $dm^{-3}$: *B. s* = 0 mm; *S. a* = 10 mm<br>$1\times10^{-3}$ mol $dm^{-3}$: *B. s* = 0 mm; *S. a* = 12 mm<br>$2\times10^{-3}$ mol $dm^{-3}$: *B. s* = 5 mm; *S. a* = 14 mm<br>$4\times10^{-3}$ mold $m^{-3}$: *B. s* = 6 mm; *S. a* = 17 mm<br>$8\times10^{-3}$ mol $dm^{-3}$: *B. s* = 16 mm; *S. a* = 21<br><br>With $2\times10^{-3}$ mol $dm^{-3}$ $AgNO_3$: MIC = 100 µL for S. aureus and 120 µL for B. subtilis; MBC = 150 µL for both | Leakage of sugars and proteins from the cell wall, increased with incubation time. | - |
| 141 | Ag-rGO | GO: MHM + 30min sonication + 1h high-speed stirring<br>Ag-rGO: GO/ ethylene glycol mixture + $AgNO_3$ + reduction with $NaBH_4$ | GO: large sheets (a few hundred $nm^2$)<br>t = 1.2 nm<br>Ag-rGO: Ag NPs size average ≈ 6-8 nm<br>t = mostly single or few layers of rGO | *Colibacillus*<br>*Staphylococcus aureus*<br>*Canidia albicans* | CFU counting (36h)<br><br>Ag-rGO (50 µg/mL) ≈ 0% | - | - |
| 157 | rGO/$TiO_2$ thin films | $TiO_2$ thin film : dip-coating method<br>GO: MHM + exfoliation by heat<br>GO suspension spread onto $TiO_2$ thin film + dried at 60 °C in air for 24h + Post annealing (400°C, 30min) + UV-visible light-induced photocatalytic reduction | GO:<br>t = 1.7 nm<br><br>t = 1.1 nm | *E.Coli* | GO/$TiO_2$ thin film annealed at 400 °C<br>↑25% antibacterial activity<br>of the bare $TiO_2$ thin film under sunlight irradiation.<br>After the photocatalytic reduction:<br>for 0.5 h, rGO/$TiO_2$ = ↑60% antibacterial activity; for 4 h antibacterial activity↑7.5 times | | |
| 155 | Ag/rGO-g-PAA | rGO:MHM + Hr + 30min sonication + in situ poly(acrylic acid) (PAA) grafting + attachment of Ag nanocrystals ($AgNO_3$) | rGO: t = 0.8 nm (single-layer)<br>Ag NPs size = 4–8 nm | *S. aureus*<br><br>*E. coli* | (37ºC, 24 h)<br>Diameters of the inhibition zones:<br>S. aureus = 11.4 mm<br>E. coli = 9.9 mm | - | - |
| 147 | GO–$TiO_2$ nanorods | GO (MHM + 1h sonication)<br>$TiO_2$ NRs (two-phase hydrothermal method)<br>Mix GO and $TiO_2$ NRs at a two-phase water-toluene interface | GO: l =1–2 µm ( single and double layer)<br><br>$TiO_2$ NPs size = 4–5 nm | *E. coli* | Photocatalytic irradiation (100 W/$m^2$, 37ºC, 2 h)<br>Decreases with increasing time of solar irradiation<br>10% viability: $TiO_2$ NPs = 97 min; $TiO_2$ NRs = 87 min; GO–$TiO_2$ NPCs = 52 min; GO–$TiO_2$ NRC = 27 min<br>0% viability: GO–$TiO_2$ NRC = 2h | - | - |
| 146 | GO enwrapped $Ag_3PO4$ (GO–$Ag_3PO4$) | GO (MHM + 2h sonication) + ion-exchange method of $CH_3COOAg$ and $Na_2HPO_4$ in the presence of GO sheets | GO: mainly single-layer sheets<br>$Ag_3PO_4$ particles average diameter=500nm | *E. coli* | (20 µg/mL, gentle shaking, 2h, 37ºC)<br>$Ag_3PO4$ = 0%<br>GO–$Ag_3PO4$ = 0% | Yes | - |
| 121 | GO | MHM + sonication | magnetic NPs size= 5-8 nm | *S. aureus*<br><br>*E. coli* | (10 min, 80 ppm)<br>under dark<br>MRGO: *S. aureus* = 143%; *E. coli* = 117%<br>MRGOGA: *S. aureus* = 147%; *E. coli* = 108%<br>NIR laser irradiation<br>MRGO: *S. aureus* = 45%; *E. coli* = 39%<br>MRGOGA: *S. aureus* = 0.4%; *E. coli* = 0.1% | - | - |
| | rGO functionalized with magnetic NPs (MRGO) | Iron(III) chloride hexahydrate and iron(II) chloride tetrahydrate addition + Hr | | | | | |
| | MRGO functionalized with glutaraldehyde (GA) (MRGOGA) | MRGO dispersion in DI water by sonication + GA addition | | | | | |
| 99 | Ag-GO | Addition of $AgNO_3$ to gelatin solution and stirring for 12h + Mix with GO (MHM + 2h sonication) | n/s | *E. coli* | Growth inhibition rates: Ag/GO 1 ppm = 73.1%; Ag/GO 5 ppm = 85%; Ag/GO 10 ppm = 99.9% | - | - |
| 148 | GO-$TiO_2$ | titanium trichloride added to HCl solution + | Grain sizes = 5.3, 6.1, 7.2, and | *E. coli* | (37º, 12h, indoor natural light irradiation)<br>Pure $TiO_2$ = 91.2% | - | - |

| | | | | | | | |
|---|---|---|---|---|---|---|---|
| | | mix with GO (MHM) + sonication | 5.2 nm (pure $TiO_2$, $TiO_2$/1.4 wt% GSs, $TiO_2$/4.2 wt% GSs, and $TiO_2$/7 wt% GSs, respectively) | | $TiO_2$/1.4 wt% GO = 24.8%<br>$TiO_2$/4.2 wt% GO = 9.5%<br>$TiO_2$/7 wt% GO = 37.6%<br>without light irradiation $TiO_2$/4.2% GO ≈ 100% | | |
| 138 | Functional graphene oxide/silver nanocomposites (FGO/Ag) | FGO (MHM + 1h ultrasonication + silylation with TETA) FGO+$AgNO_3$ in an alkaline medium by a simple RT stirring method | FGO: single layers, l>1µm<br>Ag size (nm): (≠pH)<br>FGO/Ag-9= 83;<br>FGO/Ag-10 = 64;<br>FGO/Ag-11 = 24;<br>FGO/Ag-12 = 38 | *E. coli* | (4 h, 37ºC, 80 rpm)<br>FGO: no growth inhibition<br>FGO/Ag-9 and FGO/Ag-10 reduced growth<br>FGO/Ag-11 and FGO/Ag-12<br>completely inhibited growth | - | - |
| 131 | Ag-rGO | GO (HM + 1h sonication) and $AgNO_3$ reduction under a mild condition using L-AA as redutor | d (Ag) = 100 nm–1 µm | *E. coli* | (24 h, 37ºC)<br>GO: no inhibition<br>Ag-rGO: disk of inhibition | - | - |
| 132 | $Ag_xO_y$-rGO | GO (MHM + 1h sonication ) reduced under light irradiation without any reductant and $AgNO_3$ decomposed under light irradiation or heating | $Ag_xO_y$-rGO<br>Single layer<br>l =5 - 30 nm | *E. coli*<br>*S. aureus* | GO and rGO:<br>slight growth inhibition<br>$Ag_xO_y$-rGO (37ºC , 160 rpm, 4.5h): 125.0 µg/mL =0%; 62.5 µg/mL =0%; 31.3µg/mL E.coli = 3.3% and S. aureus = 26,7%<br>MIC = 62,5 µg/mL | - | - |
| 114 | Ag NP/GO paper and suspension | GO (MHM + 2h sonication)<br>Mix GO and AgNO3 in citrate buffer solution + reduction with hydroquinone + vacuum filtration-induced directional flow | GO: single layer<br>Ag NPs average size ≈80nm | *E. coli*<br>*S.aureus* | Inhibition zone of Ag NP ≈ 100% larger than with GO<br>In aquatic media, 37ºC, 4 h:<br>GO: *S. aureus* = 38.7%; *E. coli* = 48.1%<br>Ag NP/GO: *S. aureus* = 12.4%; *E. coli* = 0% | - | - |
| 154 | poly(N-vinylcarbazole) (PVK) /graphene nanoplatelets dispersions and films | G (commercial product + 2h sonication)<br>Solvent mixing + PVK/G composites electrodeposition at indium tin oxide (ITO) surfaces<br>Spin coating of ITO surfaces with pristine GNP (control) | G: t= 1.8 nm<br>l= 10–20µm.<br>PVK-GNP film: t=150 nm | *E. coli*<br>*B. subtilis* | PVK–G at 1000 and 500 µg/ml presents higher toxicity≈80-97%<br>1000 µg/ml, 1h: G≈20%; PVK≈90%; PVK/G≈10%<br>PVK–G films: biofilm growth inhibition | - | - |
| 134 | Ag-G | G: hydrate- (AGC-1) or ammonia- assisted (AGC-2) quenching process of low-cost expandable graphite (EG) + Mix G and $AgNO_3$ with sodium citrate and SDS | G: diameter= 7-9 µm<br>Ag NPs: average diameter≈45-50 nm | *E. coli* | Inhibition zone (24h, 37ºC)<br>≈18,7nm | - | - |
| 89 | rGO–Ag | GO: MHM+3h sonication<br>Mix GO and AgNO3 with ethylene glycol and KOH | Ag NPs mean size=4.7 nm | *S. aureus E. coli* | MIC (µg/mL)<br>rGO: *S. aureus* = 1200; *E. coli*= 1300<br>Ag: *S. aureus* = 50; *E. coli*= 30<br>rGO–Ag: *S. aureus* = 20; *E. coli*= 10 | - | - |
| | rGO–Ag over an electrically conducting carbon foam substrate (rGO–Ag–CF electrode) | rGO–Ag and PTFE dispersed in EtOH through sonication + Carbon foam strip dipped in the solution | | | rGO–Ag–CF (1.5V, 5min) ≈ 0%<br>For *S. aureus* the device is slightly less effective compared to *E. coli*. | | |
| 149 | rGO/chitosan dispersion | GO: MHM + 30min sonication<br>GO mixed with chitosan in acetic acid solution + Hr | GO: t<1 nm<br>rGO/chitosan: t≈2.5nm | *E. coli* | GO: no inhibition zone<br>rGO/chitosan: inhibition zone<br>Viable cell counts for 6h<br>GO: no significant retardation of bacterial growth<br>rGO/chitosan: retardation of bacterial growth | - | - |
| 151 | carboxylated graphene oxide (GO-COOH) complexes with lanthanum(III) (GO–La) | GO: MHM + sonication<br>GO-COOH: GO sonicated for 2h with chloroacetic acid<br>GO-La: GO–COOH mixed with lanthanum chloride | G: t=0.34 nm<br>GO–COOH: t=1 nm<br>GO–La: l=0.2-1.0 µm | *E. coli*<br>*S. aureus* | Zone of inhibition<br>GO–La: *E. coli*= 2.0cm; *S. aureus*= 1.5 cm<br>GO–COOH: no inhibition zone<br>MIC (GO–La) = 1.0 mg/mL | - | - |

| | | | | | | | |
|---|---|---|---|---|---|---|---|
| | | solution + 2h sonication | | | | | |
| 139 | Ag-GO | GO: MHM + ultrasonication bath<br>AgNPs: modified Tollens' process<br>AgNPs mixed with GO suspension +glucose solution + 60s microwave oven | AgNPs average size=40.7nm | *Salmonella typhi*<br>*E.coli*<br>*S.aureus*<br>*S.epidermidis* | MIC<br>*S. typhi* and *E.coli* = 6.25 μg/ml;<br>*S.aureus* and *S.epidermidis* = no inhibition even at 100 μg/ml<br>Stronger against Gram-negative than against Gram-positive bacteria. | - | - |
| 133 | Ag-rGO | GO reduction with $NaBH_4$ + dispersion in sodium citrate aqueous solution with 2h sonication + $AgNO_3$ solution addition+ 30min sonication | Ag NPs average size = 10nm | *Pseudomonas aeruginosa* | Inhibition zone = 5 mm<br>MBC= 15 μg/ml (for 5 hours, in PBS) | - | - |
| 128 | chloro phenyl grafted graphene (CBG) | G:commercial product<br>Grafting chlorophenyl pendants on G via diazotization reaction of 4-chloro aniline | n/s | *E. coli*<br><br>*S. aureus* | *E.Coli*<br>CFU/mL (x$10^8$): G-25 mg= 30; G-50 mg=19; CBG-25 mg= 12; CBG-50 mg =5<br>Zone of inhibition (mm): G-25 mg= 8; G-50 mg=11; CBG-25 mg= 17; CBG-50 mg =23<br>*S.aureus*<br>Zone of inhibition: G=not measurable; CBG-50 mg = 22mm | - | - |
| 158 | graphene oxide–benzylpenicillin (BP) anion intercalated Mg–Al layered double hydroxide (GO–BP-LDH) hybrid films | GO and BP-LDH colloidal suspensions directly mixed by vigorous stirring + 2h utrasonication + transferred to a Petri dish and dried + ammonia immersion | GO: disordered single layer<br>Thickness=1.6nm | Micrococcus lysodeikticus<br>sulfate-reducing bacteria (SRB) | GLF-1, GLF-2, GLF-3, and GLF-4 have BP-LDH mass contents of: 0.00%, 21.81%, 32.43%, and 52.52%.<br>The inhibition rate (IR%) increased as the GO/BP-LDH mass ratio decreased.<br>M. lysodeikticus: GLF-1≈40%; GLF-2≈65%; GLF-3≈80%; GLF-4≈97%<br>SRB: GLF-1≈38%; GLF-2≈58%; GLF-3≈75%; GLF-4≈98% | - | - |
| 152 | graphene derivative-Poly(L-lysine) (PLL) composites:<br>GO-PLL<br>rGO-PLL<br>GO-DS-PLL<br>rGO-DS-PLL<br><br>dispersions and films | GO and rGO: HM+30min sonication<br>GO-DS and rGO-DS: GO and rGO treated with DS<br>rGO-PLL: reacting GO and PLL under KOH, 70ºC 24h.<br>Physical absorption of PLL onto the surface of GO and GO/rGO-DS composites using electrostatic interactions 4ºC, 24 h.<br>Pre-plasma-treated PET film coated with the GO-DS-PLL composite by spin-casting GO-DS-PLL composite solution | rGO-DS: smaller sheets than rGO | *E. coli* | GO-PLL, GO-DS-PLL, rGO-DS-PLL: no growth after 3h and 12h<br>GO,rGO, GO-DS, rGO-DS: bacterial growth<br>rGO-PLL: no growth after 3h and then growth after 6h<br><br>Surfaces: GO = thick bacterial biofilm; rGO-PLL = no biofilm formation.<br>Bacterial growth inhibition: GO-DS-PLL and rGO-DS-PLL > GO-PLL > +PLL and rGO-PLL<br><br>GO-DS-PLL(25 μg/mL)=3%<br><br>PET film = Large bacterial colonies around the edges<br>GO-DS-PLL coated PET = no bacterial growth | - | - |
| 129 | zinc oxide-graphene hybrids (ZnO–G) | in situ thermal decomposition of zinc benzoate dihydrazinate complex on the surface of G, 200ºC for 2h. | ZnO NPs average size =22 nm | E. coli | ZnO-G (0.003 g/ml, 12h,37º) = 0% | - | - |
| 120 | oxide nanoparticles (IONPs) and silver nanoparticles (AgNPs) on the surface of graphene oxide (GO) (GO-IONP-Ag) | GO-IONP: dispersion of GO,$FeCl_3{\cdot}6H_2O$, $CH_2$=CHCOONa and NaOAc in a mixture of EG and DEG<br>GO-IONP-Ag: GO-IONP solution mixed with $AgNO_3$ aqueous solution under stirring in oil bath. Addition of sodium citrate +1h boiling. | n/s | *E. coli*<br>*S. aureus* | GO-IONP-Ag 8 μg/mL (Ag content): *E. coli* =6.1%; *S. aureus* =14.7%<br>GO-IONP= no growth inhibition<br><br>MIC = 8 μg/mL<br><br>Photothermal effect (808 nm, 1.5 W/$cm^2$, 7min)<br>↑antibacterial ability, allowing effective killing of *S. aureus* under a rather low Ag concentrations (4 μg/mL, 7.2 μg/mL). | *E. coli* =Yes, pits<br><br>*S. aureus* = No damage but rough surface and covered by nanomaterial | - |
| 124 | Ag nanoparticles | GO: HM + 60min sonication | GO average thickness ≈ 0.9 nm | E. coli<br>B. subtils | Ag-PDA-GO-50 (50mg $AgNO_3$) (LB plate, 24h) = 0% | - | - |

| | | | | | | | |
|---|---|---|---|---|---|---|---|
| | (Ag NPs) on functionalized polydopamine (PDA)-graphene nanosheets (Ag-PDA-GO) | PDA-GNS: polymerizing dopamine on GO at RT, 24h<br>Ag-PDA-GNS: PDA-GNS mixed with Milli-Q water and $NH_3$ solution + $AgNO_3$ aqueous solution + DA aqueous solution | PDA thickness = 3.8 nm<br><br>Ag-PDA-GO thickness ≈15 nm | | Ag-PDA-GO 1% (v/v) (48h) = 0% | | |
| 156 | rGO/Au NP/Ag NW films | GO, Ag NW, and GO/Au NP films: spin coating the corresponding dispersions.<br>GO/Ag NW and Au NP/Ag NW films: 2 sequential spin coating processes.<br>rGO/Au NP/Ag NW films: Ag NWs were spin coated on glass slides + covered with GO/Au NP film by spin coating + hydrazine vapour, 100ºC for 24 h. | Average length and diameter of the Ag NWs = 20-40 µm and 100-130 nm, respectively. | *E. coli* | Adhesion assay: remains of *E. coli* disrupted by interacting with the hybrid film.<br>Viability=0% (no bacterial colonies) | - | - |
| 140 | Poly (diallyldimethyl ammonium chloride) (PDDA)-protected Ag–rGO | Part A: GO (MHM) + $AgNO_3$ + 30min stirring<br>Part B: GO(MHM) + 30min sonication + 1h high-speed stiring + PDDA as both a reducing and a stabilizing agent<br>Hydrothermal process: Mix Part A + Part B and heat at 160ºC for 4h. | Deposited Ag NP average size = 5 nm<br><br>GO: t= 1.0 nm<br><br>rGO: t = 2.8 nm | *E.coli* | Ag-rGO 50 µg/mL =0% | - | - |
| 153 | poly-l-lysine/reduced graphene oxide/copper nanoparticles hybrid (PLL–rGO–CuNPs) | GO: MHM<br>GO (20 mg/mL) + PLL solution (20 mg/mL), 400 mg EDC·HCl and 240 mg NHS, 24h at RT<br>+<br>100 mg copper nitrate + 0.5h ultrasonication + reduction by hydrazine | CuNPs sizes = 10–50 nm. | *E. coli*<br>*S. aureus* | *E. coli*<br>PLL–rGO: Killing rate=8.230 ±2.056%; MIC= 2500 µg/mL<br>PLL–rGO–CuNPs: Killing rate= 99.990±0.002%; MIC= 300 µg/mL<br><br>*S. aureus*<br>PLL–rGO: Killing rate= 6.977±1.163%; MIC= 1600 µg/mL<br>PLL–rGO–CuNPs: Killing rate= 99.581±0.012%; MIC= 200 µg/mL<br><br>Increasing soaking time MIC increases:<br>*E.coli*= 300, 300, 325, 325, 350, 375 and 400<br>*S.aureus*= 200, 200, 200, 200, 250, 250 and 275 for 0, 0.5, 1, 2, 4, 8 and 16 days respectively. | - | The extracellular fluid contained higher $K^+$, $Ca^{2+}$ and $Mg^{2+}$, and $Cu^{2+}$ was gradually reduced. |
| 142 | rGO–Ag composites | rGO: HM+ fast thermal exfoliation under argon at 1050ºC for 30 s + hydrogen reduction at 400ºC, for 2 h<br>rGO-Ag: hydrogen reduction of (1,5-Cyclooctadiene)(hexafluoroacetylacetonato) silver(I) precursor in supercritical $CO_2$ | GO and RGO = thin sheets<br><br>Ag NPs diameters =10–40 nm | *E. coli*<br>*Listonella anguillarum*<br><br>*Bacillus cereus*<br>*S. aureus* | rGO–Ag composites prepared using:<br>50 mg Ag precursor: MICs (24h) = 0.04, 0.08, 0.16, and 0.16 µg ml−1 against B. cereus, L. anguillarum, E. coli, and S.aureus, respectively;<br>30 mg Ag precursor: MICs (24h)= 0.16 µg ml−1 against all bacteria. | - | - |
| 100 | Ag–GO suspension | GO: MHM<br>+ glucose solution + $AgNO_3$ with ammonia at RT + 5min ultrasonication | n/s | *E. coli* | (Suspension mixed for some time and agar plate,18h)<br>5min = some colonies<br>10min = no colonies | Outer and inner membranes damaged. Cell wrapping. | - |
| 123 | silver-coated GO@Au nanosheets GO@Au@Ag | GO: MHM + 20min sonication<br>BSA-GO: aqueous solution of GO+BSA with TBE buffer at RT for 24 h<br>GO@Au: BSA-GO with an excess amount of 5 nm | n/s | E. coli | For complete growth inhibition, 60h (in terms of Ag mass)<br><br>GO@Au@Ag = 3.2 mg/l<br>Au@Ag = 26.0 mg/l<br>citrate-capped AgNPs = 48.6 mg/l<br>$Ag^+$ = 50 mg/l | With BSA-GO and GO@Au = no effect<br><br>With GO@Au@Ag = bacteria | - |

| | | | | | | | |
|---|---|---|---|---|---|---|---|
| | | AuNPs in a TBE buffer in the presence of NaCl for 12h<br>GO@Au@Ag: GO@Au combined with $AgNO_3$ solution, with PVP as a stabilizer and L-ascorbic acid as a reductant. | | | BSA-coated GO and<br>GO@Au at 3.2 mg/l = no inhibition | seriously aggregated, cell membrane shrink and separate from the cell wall. | |
| 143 | water-soluble polyethyleneimine-rGO–AgNP (PEI-rGO–AgNP) hybrid | GO: MHM + ultrasonication in water bath<br>GO dispersion + PEI solution, EDCÆHCl and NHS, reaction for 24h at RT + $AgNO_3$ + 2h ultrasonication + Hr | PEI-GO: t ≈ 0.6 nm<br><br>AgNPs diameters = 5–15 nm | *E.coli*<br>*S.aureus* | *E.coli*<br>PEI-rGO: 95.8µg/mL=100%; 958µg/mL=85.2%<br>PVP-AgNP: 4.2µg/mL[Ag]=13.6%<br>PEI-rGO–AgNP: 4.2µg/mL[Ag] and 95.8µg/mL[PEI-rGO] =6.3%<br>*S.aureus*<br>PEI-rGO: 95.8µg/mL=100%; 958µg/mL=79.5%<br>PVP-AgNP: 4.2µg/mL[Ag]=10.8%<br>PEI-rGO–AgNP: 4.2µg/mL[Ag] and 95.8µg/mL[PEI-rGO] =3.9% | - | - |
| 101 | polyvinyl-N-carbazole (PVK)–GO nanocomposite (PVK–GO) Dispersions and films | GO: GNPs mixed with $KMnO_4$ + $H_2SO_4$–$H_3PO_4$ addition,50ºC, 12h + poured into ice with 30% $H_2O_2$ + filtration + centrifuged at 4000 rpm, 4 h.<br>Solution mixing + 30min sonication<br>Films: spin coating of PVK–GO solution onto ITO surfaces + cyclic voltammetry experiments | n/s | *E.coli*<br><br>*Cupriavidus metallidurans*<br><br>*B. subtilis*<br>*Rhodococcus opacus* | Toxicity in suspension is time-dependent<br>PVK-GO 1000 µg/mL ([GO] =30 µg/mL)<br>1h: *E.coli* = 89.1%; *C.metallidurans* = 92.3%; *B. subtilis* = 89.4%; *R.opacus* = 90.5%; 3h = 100% for all<br>GO (1000 µg/mL)<br>1h: *E.coli* = 62.0%; *C.metallidurans* = 62.3%; *B. subtilis* = 75.3%;*R.opacus* = 78.6%; 3h: *E.coli* = 100%; *C.metallidurans* = 85%;*B. subtilis* = 92%; *R.opacus* = 89%<br><br>Metabolic activity,1 h, 1000 µg/mL<br>PVK: *E.coli* and *B.subtillis* ≈ 100%<br>GO: *E.coli* ≈30% *B.subtillis* ≈ 12%<br>PVK-GO: *E.coli* and *B.subtillis* ≈ 10%<br><br>Biofilm formation, 48h, 1000 µg/mL: 73-94% inhibited at PVK-GO and 43-68% at GO suspensions<br>Biofilm inactivity on surfaces:<br>GO: *E.coli* ≈19.6%; *B.subtillis* ≈ 20.8%<br>PVK-GO: *E.coli* ≈42.1%; *B.subtillis* ≈ 53.6% | Cell wrapping, while maintaining rod shape and cell integrity. | - |
| 110 | PVK-GO composites films | Mixing TBAH in acetonitrile with PVK-GO + electrodeposition at indium tin oxide (ITO) surfaces | average grain size ≈160 nm | *E.coli* | Cell growth inhibition 1000 µg/ml, 1h:<br>GO-PVK > GO > PVK<br>Live-dead staining: PVK-GO film = 10%; GO film = 16%<br>Biofilm formation: inhibited at PVK/GNP and GNP films surfaces | - | - |
| 125 | GO/RGO with anchoring materials: native lactoferrin (NLf), NLf protected Au clusters (Au@NLf) and chitosan (Ch) rGO/GO-Ch-NLf and rGO/GO-Au@NLf-Ch | GO: MHM+ 45min sonication<br>rGO: GO + hydrothermal reduction<br>rGO/GO-NLf and rGO/GO-Au@NLf: NLf or Au@NLf anchored through a electrostatic interaction and stirred for 2h.<br>rGO/GO-Ch-NLf and rGO/GO-Au@NLf-Ch: GO/RGO-NLf composites mixed with Ch solution and stirred for 2h. | n/s | *E.coli* | Antibacterial activity of the composites was found to be several folds higher than the parent GO/rGO | - | - |
| 102 | Ag–GO | Raw-GO: HM<br>H-GO: HM + $H_2$ treatment +<br>Mix with $AgNO_3$ solution and 12h ultrasonication + in situ reduction using low-temperature plasma | AgNPs size on:<br>rGO = 2 nm<br>H-GO = 10nm | *E.coli* | Radius of inhibition zone: GO = 0cm; GO/Ag = 5.2cm; H-GO/Ag = 3.1cm<br>Disinfection rate: GO/Ag > H-GO/Ag<br><br>GO/Ag 100µg/mL, 3h = complete killing<br>GO ≈ no antibacterial activity | - | - |
| 103 | Tetradecyl triphenyl phosphonium bromide (TTP) functionalized few-layered | GtO: Brodie method<br>TTP-GtO: TTP slowly added to GtO solution stirring at 60ºC for 6 h<br>TTP-FGt: $NaBH_4$ reduction of TTP-GtO | FGt ≈ 4 layers | *E. coli*<br>*S. aureus* | TTP–FGt-1 (13.8%wt TTP),TTP–FGt-2 (23.9%wt TTP), TTP–FGt-3 (33.7%wt TTP)<br>MIC (µg/mL) (24h, 37ºC):<br>*E. coli*: FGt > 10 000; TTP–FGt-1 = 750; TTP–FGt-2 = 250; TTP–FGt-3 = 200<br>*S. aureus*: FGt > 10 000; TTP–FGt-1 = 450; TTP–FGt-2 = | - | - |

| | | | | | | | |
|---|---|---|---|---|---|---|---|
| | graphite (FGt) TTP–FGt | FGt: $NaBH_4$ reduction of GtO | | | 150; TTP–FGt-3 = 125<br><br>MIC (μg/mL) after 72 h TTP–FGt-3 soaking: *E.coli* = 580; *S.aureus* = 280 | | |
| 144 | rGO– β-cyclodextrin (CD)–Ag | GO (MHM) + $AgNO_3$ addition + in situ reduction by hydrazine hydrate and $NH_4OH$ with the presentation of β-CD + high-speed stirring for 1 h at 90 °C | Ag NPs size = 50–70 nm | *E.coli*<br>*B.subtillis* | Inhibition zone<br><br>rGO–CD–Ag > Ag–CD > rGO–Ag > Ag > rGO–CD | - | - |
| 135 | Ag-GO | GO: MHM + 30min ultrasonic bath<br>+<br>Mix with $AgNO_3$<br>+ 30min ultrasonic bath + sodium citrate as the stabilizing agent, 30 min at 130ºC. | GO: Thickness = 0.7-1.2 nm Size distribution = 300–800 nm<br><br>Ag NPs average size = 7.5 nm | *P. aeruginosa* | GO (from 0.1 to 5.0 μg/mL) = no antibacterial activity<br><br>GO–Ag (0.1, 0.5, 1.0 and 1.5 μg/mL) = no antibacterial activity<br><br>MIC<br>Ag-GO = 2.5 - 5.0 μg/mL (30-60min)<br><br>Anti-biofilm activity<br>(2.5 μg/mL,1h)<br>= 100% inhibition rate | - | - |
| 109 | Polyoxyethylene sorbitan laurate (TWEEN)/ rGO "paper-like" material | MHM + reduction of aqueous colloidal suspension of GO and TWEEN using hydrazine monohydrate | t ≈ 30 μm | Bacillus cereus | TWEEN/rGO paper = no bacterial attachment nor growth (37ºC,16h)<br><br>rGO paper = bacterial attachment and growth (37ºC,16h) | - | - |
| 104 | sulfur nanoparticles decorated RGO (SRGO) | thiosulfate solution + GO (MHM+ultrasonication) solution + 30min sonication + lemon juice and 60min stirring + 10min sonication | n/s | *E.coli*<br>*S.aureus*<br>*Candida albicans* | MIC (μg/mL)<br>RGO: *E.coli* = 31; *S.aureus* = 22.7; *C.albicans* = 47<br>SRGO: *E.coli* = 19.3; *S.aureus* = 13.7; *C.albicans* = 29<br>Sulfur NPs: *E.coli* = 21.7; *S.aureus* = 18.3; *C.albicans* = 33.7 | - | - |
| 136 | Ag-rGO | HM + dispersion in sodium citrate aqueous solution + 2h sonication + $AgNO_3$ solution + 30min sonication + $NaBH_4$ reduction + stirring with pH 11 at RT for 70 min | AgNPs average size = 10 nm | *E.coli* | Inhibition zone: 10 μg/mL = 8 mm; 50 μg/mL = 24 mm<br><br>rGO 50 μg/mL = no detectable inhibition<br><br>MIC: 8h < 20 μg/mL; 5h = 5 μg/mL; 3h = 10 μg/mL | Yes | - |
| 145 | Ag@dsDNA@GO | GO: commercial product<br>+<br>$AgNO_3$ solution + dsDNA solution + reduction with $NaBH_4$ | Different sizes of AgNPs: 18, 8 and 5 nm | Xanthomonas perforans | 20h<br>50ppm Ag NPs = 55%<br>100 ppm and 200 ppm Ag NPs = 1%<br>GO = no effect<br>20ppm Ag(18nm)@dsDNA@GO <5%<br>20 ppm Ag(8nm)@GO =50%<br>100 and 200 ppm Ag(8nm)@GO ≈ 0%<br>Ag(5nm)@dsDNA@GO: 1ppm = 73%; 4ppm = 54%; 8ppm = 48%; 12ppm = 40%; 16ppm = 0%; 20 ppm = 0% | Yes | - |
| 150 | polyethylene glycol (PEG) and polyhexamethylene guanidine hydrochloride (PHGC) dual-polymer-functionalized GO (GO-PEG-PHGC) | GO: MHM + dialysis + sonication<br>PHGC: melt polymerization of guanidine hydrochloride with hexamethylenediamine<br>GO-PEG-PHGC: GO dispersion mixed with PEG + sonication + PHGC addition under sonication | GO: smooth surface, large thickness, and small wrinkles at the edges<br><br>GO-PEG-PHGC: much rougher surface | *E.coli*<br>*S.aureus* | LB agar plates, 60min<br>GO, GO-PEG and GO-PHGC: plenty of bacteria colonies survive<br>GO-PEG-PHGC: completely kill *E. coli* and *S. aureus*<br><br>Antibacterial activity:<br>GO-PEG<GO<GO-PHGC< GO-PEG-PHGC<br><br>Nº of bacterial colonies (*E. coli*) on GO-PEG-PHGC decreases 74.42% after only 30 min incubation. | - | - |

t=thickness; l=length, n/s= not studied, MIC= minimum inhibitory concentration, HM = Hummers method, MHM = modified Hummers method, Hr = hydrazine reduction; NRs = nanorods; NRCs = nanorod composites; NPCs = nanoparticle composites; NW = nanowalls.

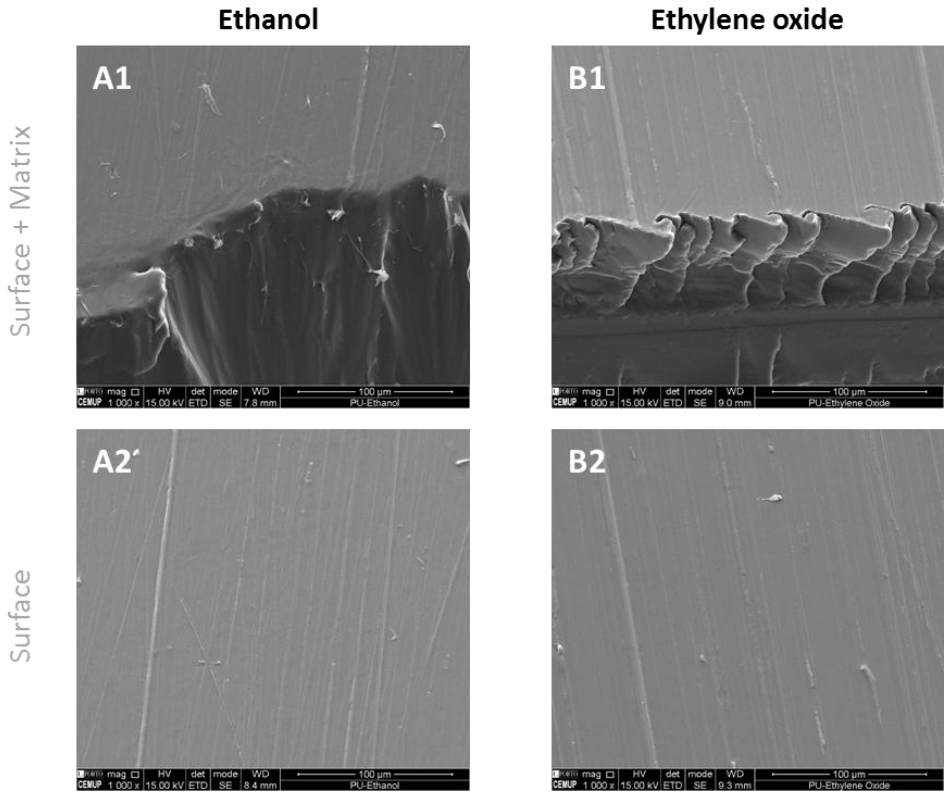


**Figure A 1.** Testing different sterilization methods on neat PU samples obtained by melt-blending. The surface of the sample sterilized by ethanol (A) and sample sterilized by ethylene oxide (B) show no differences at the surface. Magnification of 1000×, scale bar = 100 µm.

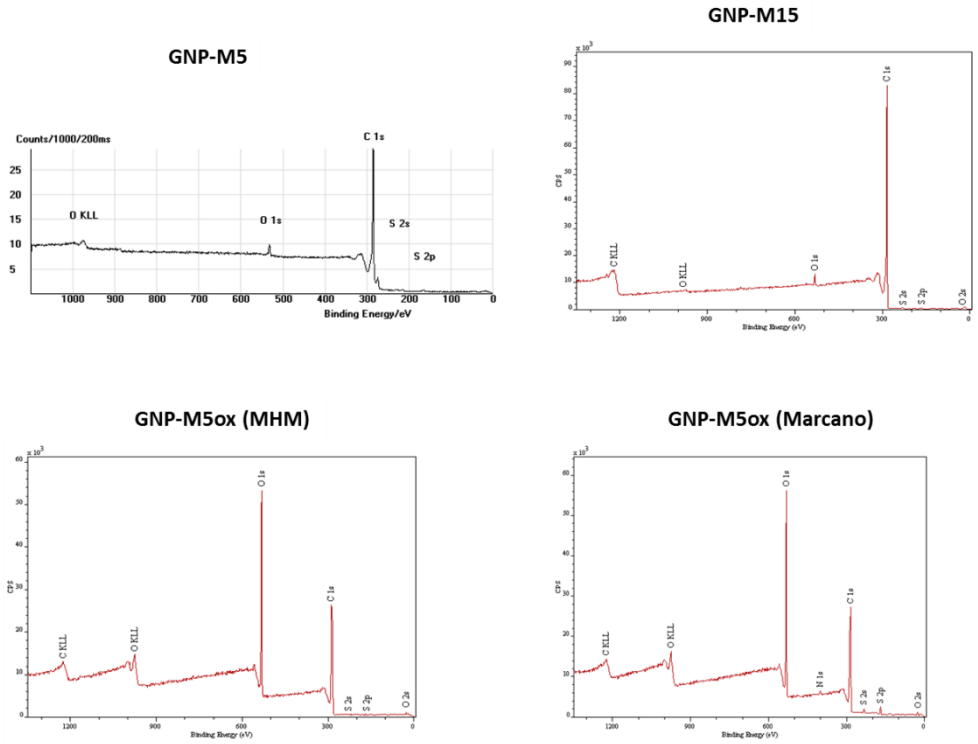


**Figure A 2.** XPS survey spectra of GNP-M5, GNP-M15, GNP-M5 oxidized by MHM and GNP-M5 oxidized by Marcano's method.

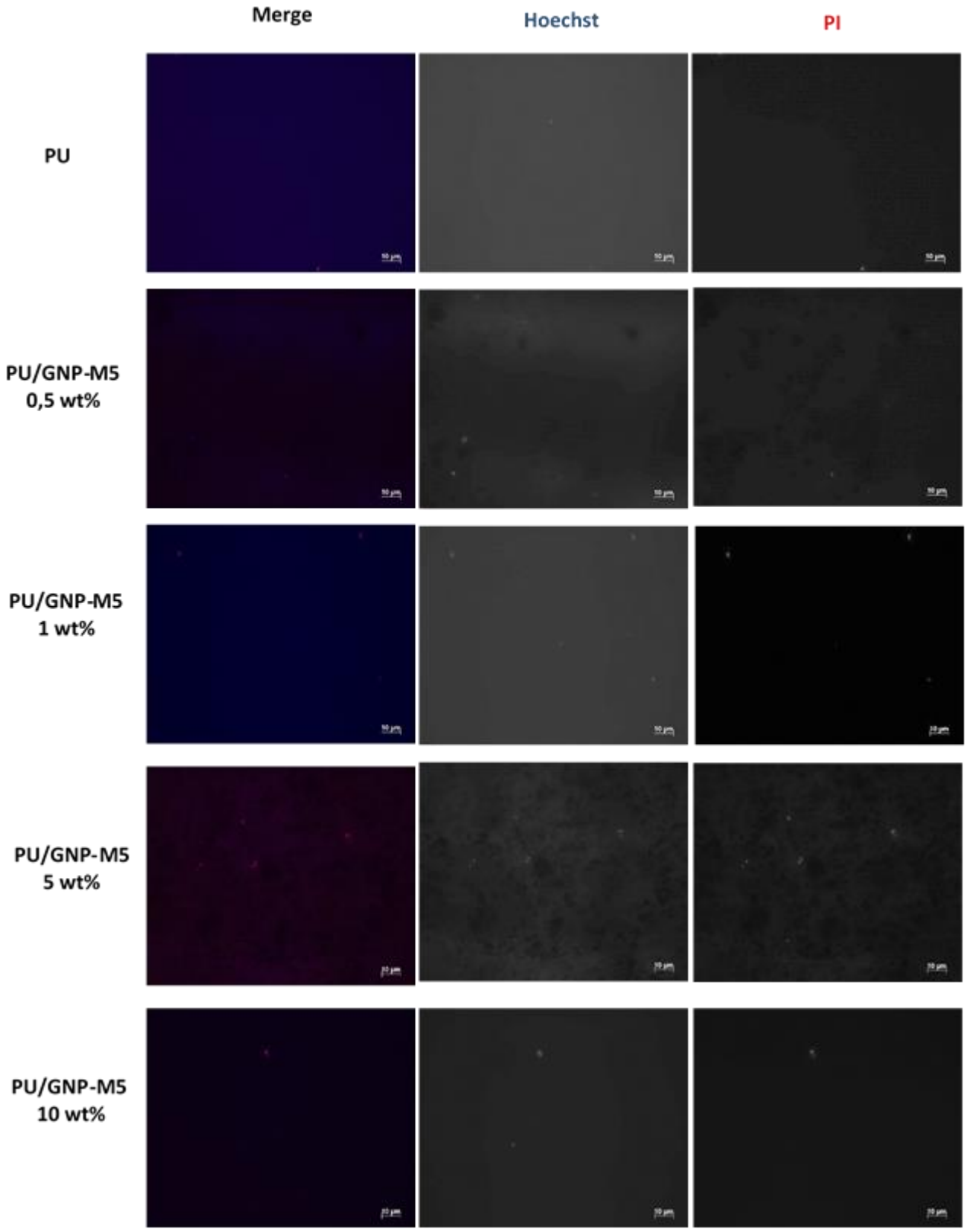


**Figure A 3.** Representative images of the PU/GNP-M5 samples obtained by melt-blending cultured with *S.epidermidis* for 24h in contact. Live and dead bacteria are stained blue (Hoechst) and dead bacteria are stained (red). Scale bar corresponds to 10 µm.

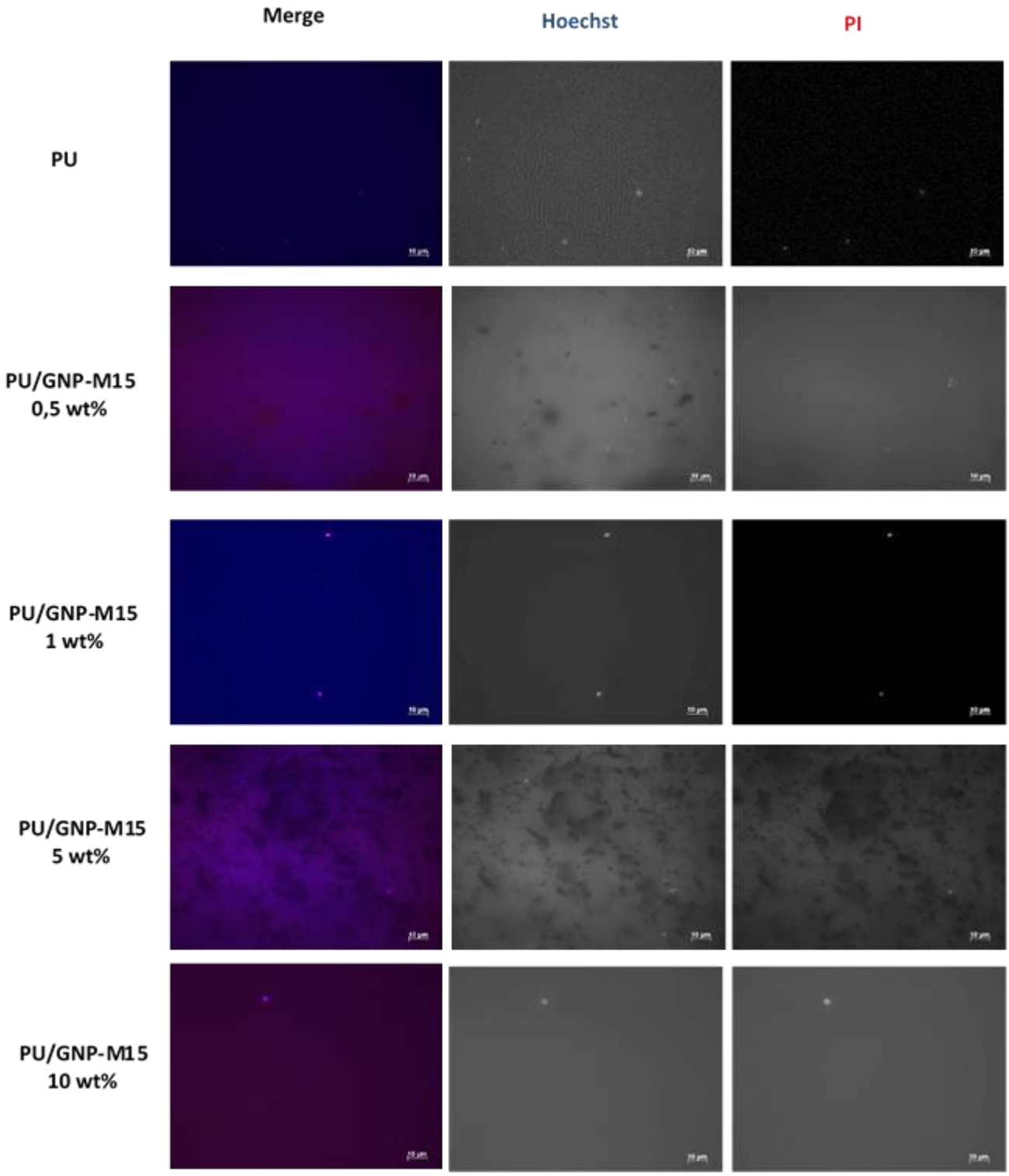


**Figure A 4.** Representative images of the PU/GNP-M15 samples obtained by melt-blending cultured with *S.epidermidis* for 24h in contact. Live and dead bacteria are stained blue (Hoechst) and dead bacteria are stained (red). Scale bar corresponds to 10 µm.

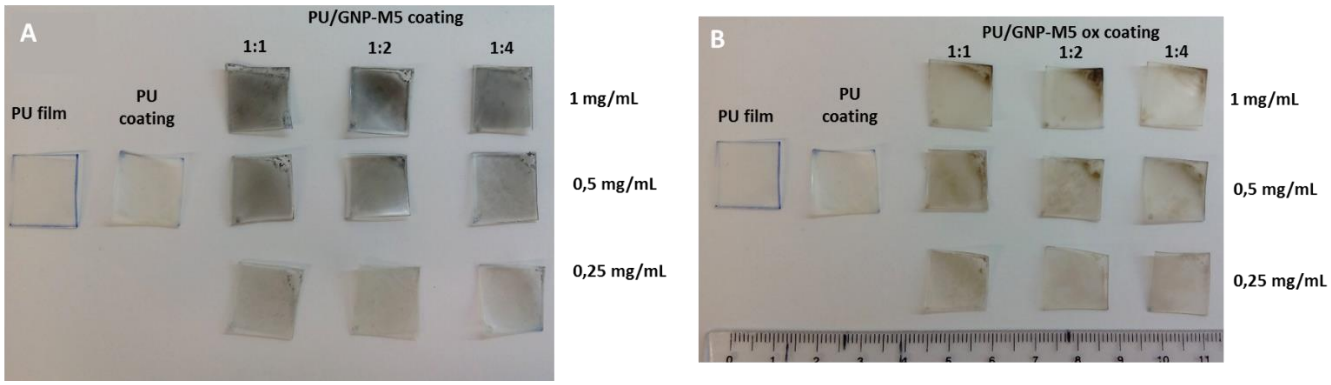


**Figure A 5.** Images of the different samples obtained: PU film produced by casting and PU coating on PU film (control), PU/GNP-M5 (A) and PU/GNP-M5 ox coatings (B) on PU film after the rubbing test (3 passages with eraser).

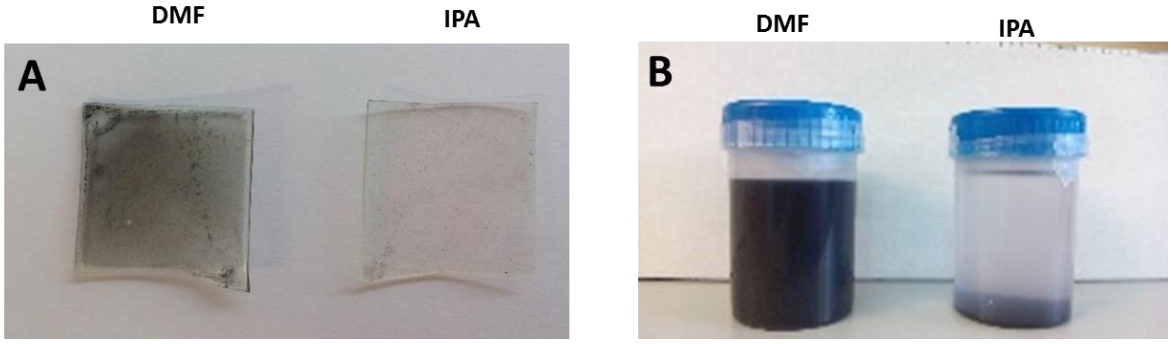


**Figure A 6.** Comparison between PU/GNP-M5 1mg/mL 1:1 coatings obtained using DMF and IPA solvents (A) and the dispersions used after setting for 1 day (B).

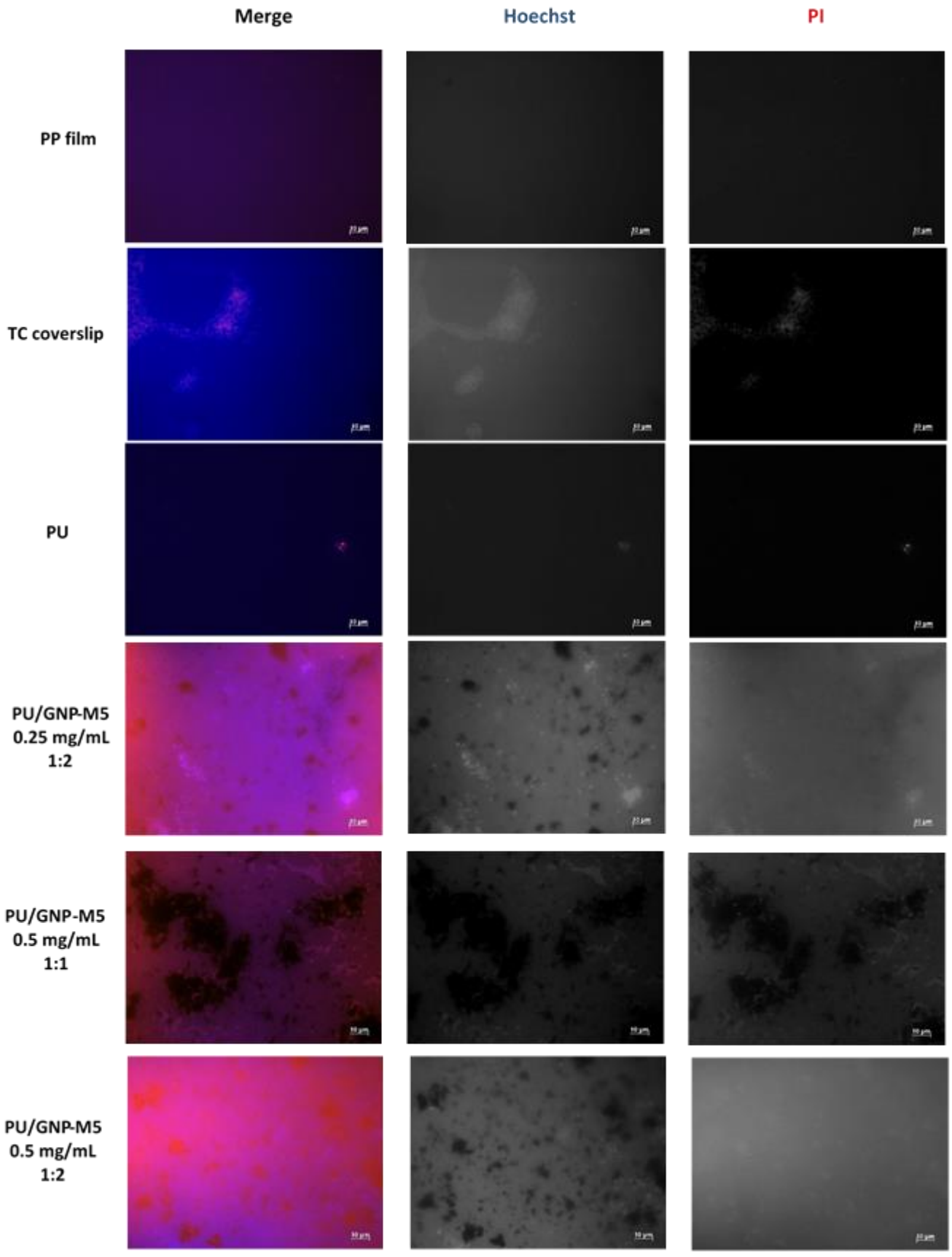
Merge
Hoechst
PI
PP film
TC coverslip
PU
PU/GNP-M5
0.25 mg/mL
1:2
PU/GNP-M5
0.5 mg/mL
1:1
PU/GNP-M5
0.5 mg/mL
1:2

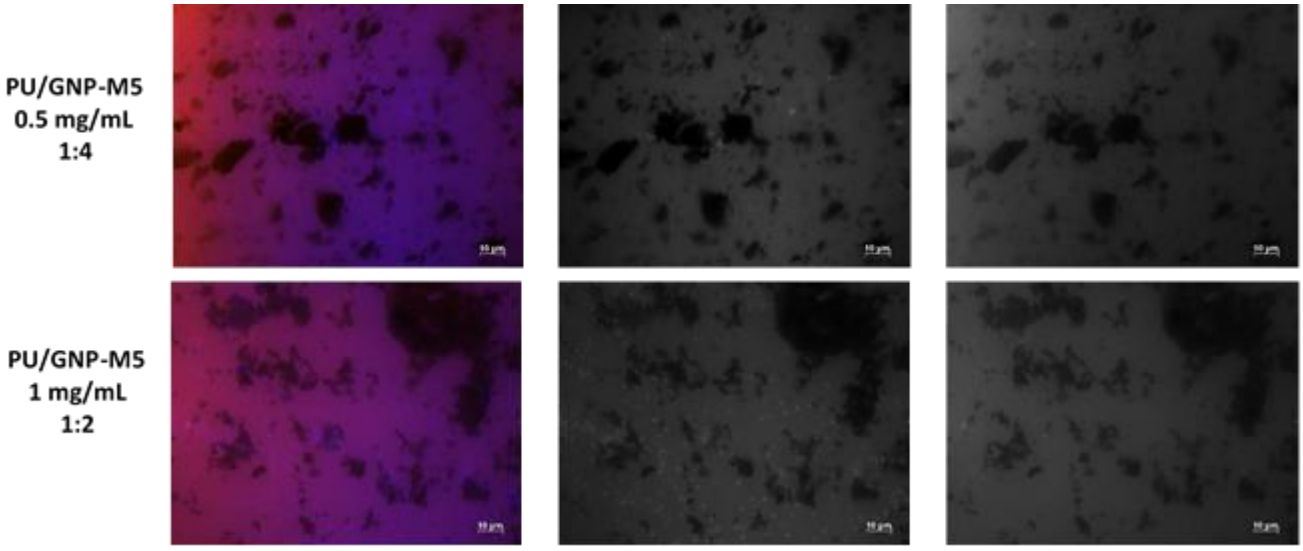


**Figure A 7.** Representative fluorescence images showing the viability of the *S.epidermidis* bacteria on the different PU/GNP-M5 coatings after 24 h incubation in direct contact assay. Bacteria were stained with Hoechst (live and dead bacteria) blue stain and propidium iodide (dead bacteria) red stain. Magnification at 100×, scale bar represents 10 µm.

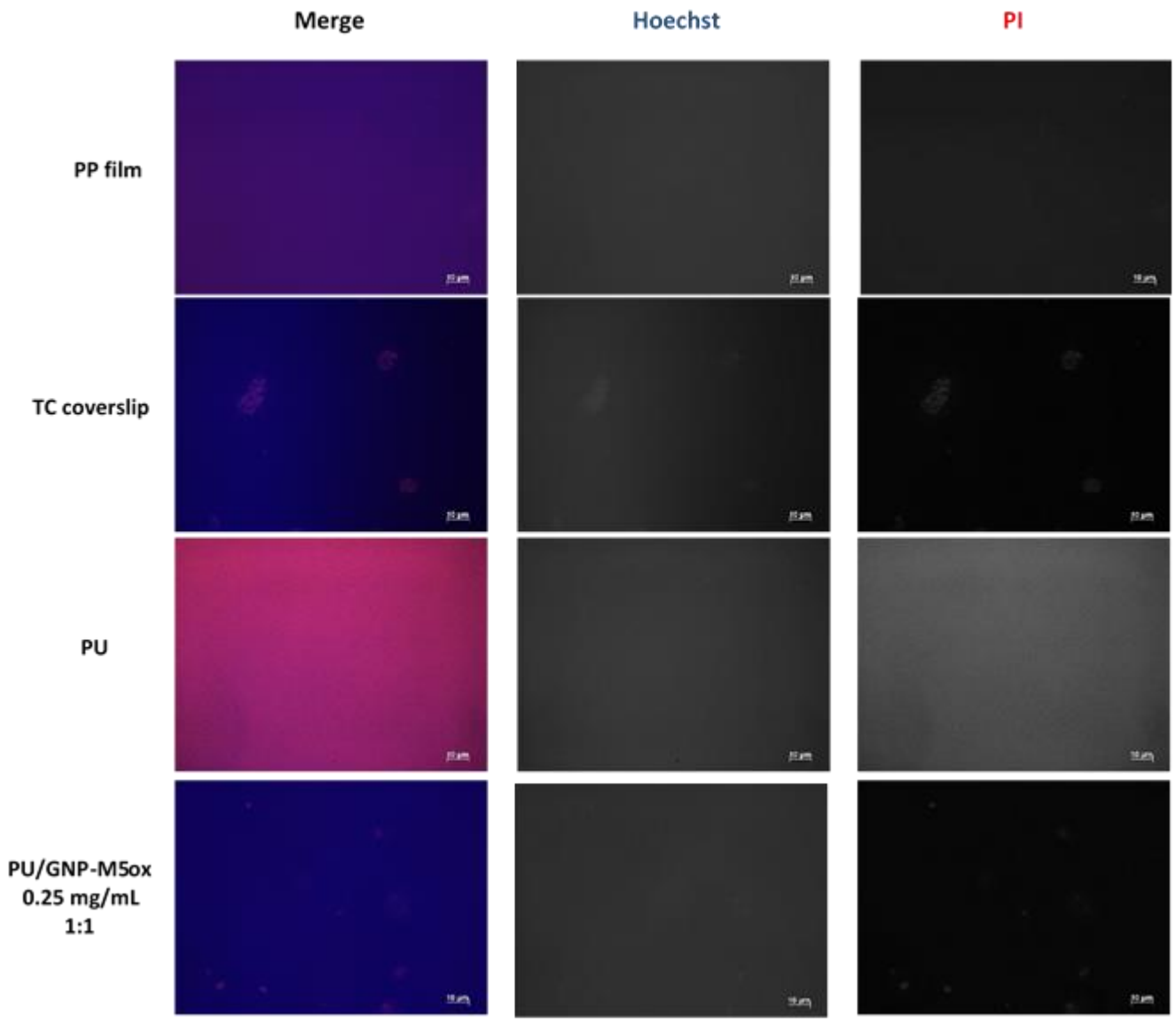
Merge
Hoechst
PI
PP film
TC coverslip
PU
PU/GNP-M5ox
0.25 mg/mL
1:1

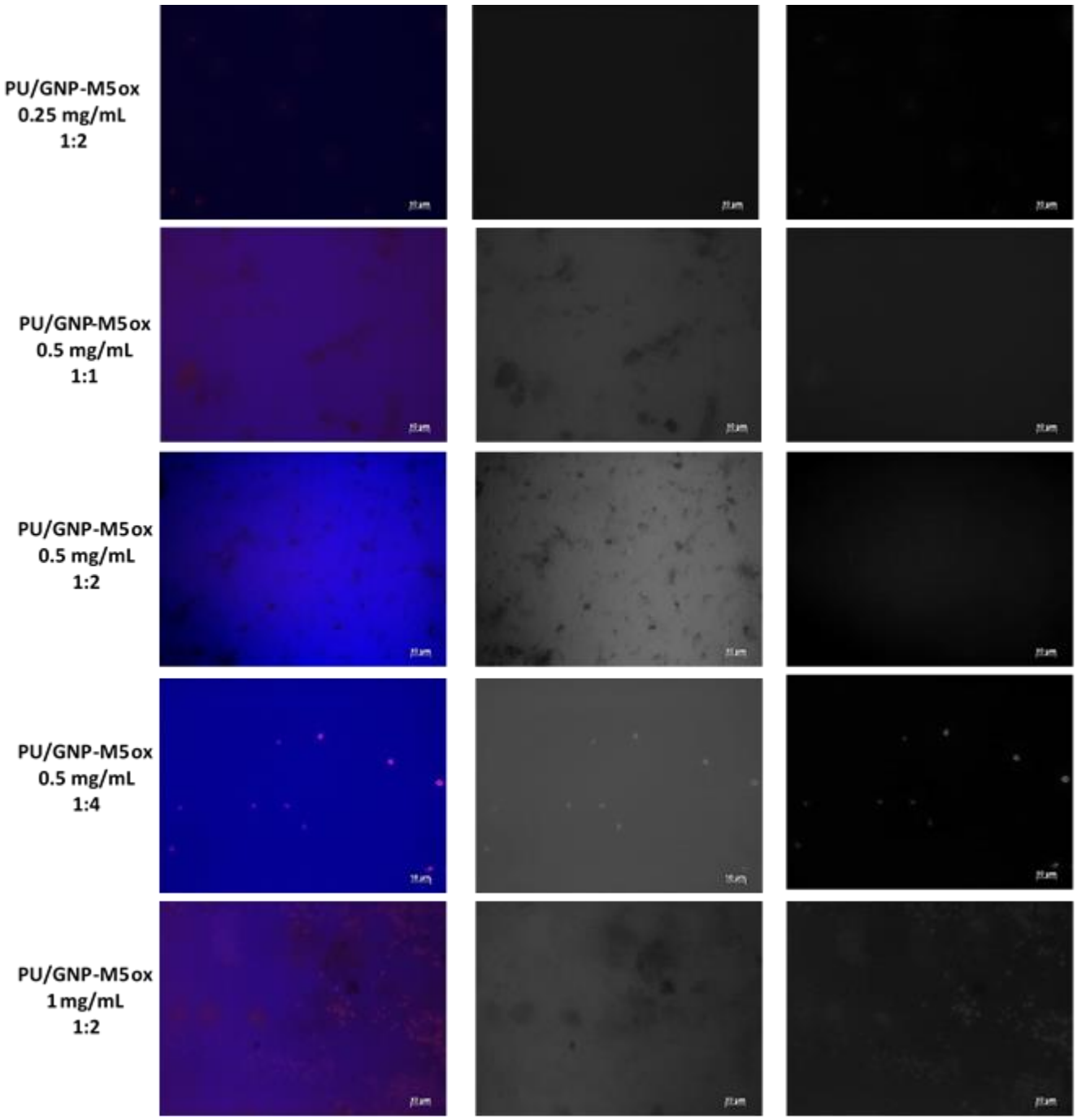


**Figure A 8.** Representative fluorescence images showing the viability of the *S.epidermidis* bacteria on the different PU/GNP-M5 coatings after 24 h incubation in direct contact assay. Bacteria were stained with Hoechst (live and dead bacteria) blue stain and propidium iodide (dead bacteria) red stain. Magnification at 100×, scale bar represents 10 µm.

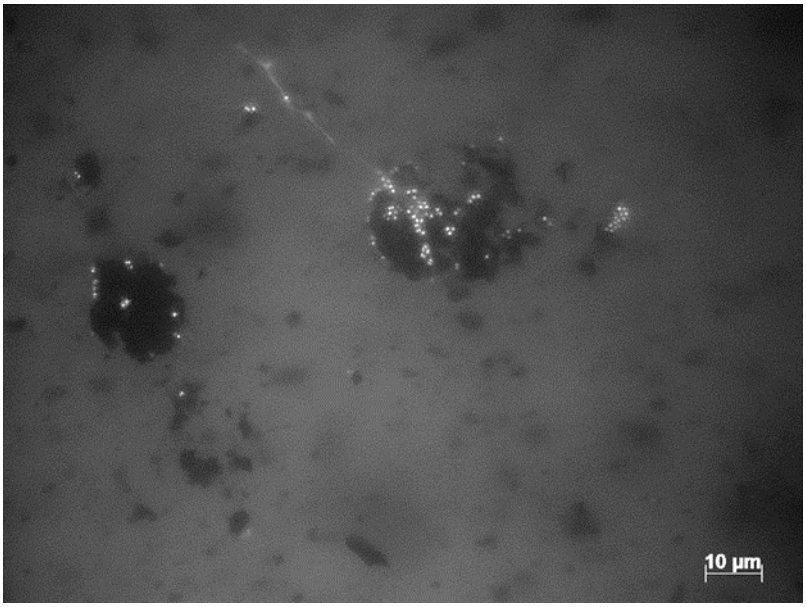


**Figure A 9.** Fluorescence microscope image of *Staphylococcus epidermidis* stained with DAPI after 24h incubation on PU/GNP-M5 0.5 wt% composite obtained by melt-blending. Magnification of 100×.